

ANALYSIS OF EX-VESSEL STEAM EXPLOSIONS FOR THE COMBUSTION ENGINEERING SYSTEM 80+

March 1994

H. Esmaili and M. Khatib-Rahbar

**Energy Research, Inc.
P.O. Box 2034
Rockville, Maryland 20847**

**Work Performed Under the Auspices of the
United States Nuclear Regulatory Commission
Office of Nuclear Regulatory Research
Washington, D. C. 20555
Contract No. 92-04-045, FIN L-25422**

**9412140075 941209
PDR ADOCK 05200002
A PDR**

Enclosure 5

ACKNOWLEDGEMENTS

We wish to thank Professors M. L. Corradini of the University of Wisconsin and S. I. Abdel-Khalik of the Georgia Institute of Technology for reviewing the draft version of this manuscript and providing numerous useful comments. We also wish to thank Dr. A. Behbahani of the United States Nuclear Regulatory Commission, Office of Nuclear Regulatory Research, for his comments and for providing the necessary technical information.

EXECUTIVE SUMMARY

This report contains an assessment of consequences of an ex-vessel energetic fuel-coolant interaction in the reactor cavity of CE System 80+ containment. Two mechanistic computer codes, TEXAS and IFCI, have been used to estimate the dynamic pressures and the resulting impulsive loads on the containment cavity boundaries resulting from the interaction of core debris material relocating into the pre-existing reactor cavity water following core melt accidents. The main objectives of the present report were to characterize the initial and boundary conditions, provide a perspective on the predictive capability of TEXAS and IFCI, and estimate the dynamic pressures and impulsive loads on the cavity boundaries.

TEXAS is a one-dimensional computer code while IFCI is two-dimensional. There are also a number of other modelling differences between the codes. The effect of the variations in the modelling parameters and their impacts on the prediction of explosion pressures have been investigated by a limited comparison of TEXAS predictions to the KROTOS experiments. The simulation of KROTOS-26 using IFCI was not successful due to problems with the premixing phase of the interaction. The explosion model parameters in TEXAS for the CE System 80+ plant calculations were based on the simulations of a few KROTOS experiments.

Prediction of the ex-vessel fuel-coolant interaction energetics for CE System 80+ required specification of the relevant initial conditions. The most important initial conditions for the present analysis were the melt mass, composition, and temperature in the lower head prior to vessel breach; the size and location of the vessel breach, the depth of the water pool in the cavity and the conditions in the primary system and containment. The initial conditions proposed here were based on the recent results of SCDAP/RELAP5 calculations for station blackout accidents in Surry scaled to CE System 80+. A comparison between thermal hydraulic features of Surry and CE System 80+ is also provided. Two scenarios corresponding to a single penetration failure (scenario A) and a rupture (scenario B) are proposed, given the uncertainties in the mode of lower head failure; also a number of sensitivity calculations have been performed to envelope the range of expected impulsive loads on the cavity boundaries.

Based on the range of impulse loads estimated for scenario A involving a single instrument tube penetration failure near the center of the lower head, the failure likelihood of the corbel supports is low, however, for the cavity wall, the likelihood of failure is expected to be higher. If an instrument tube penetration fails near the corbel supports, the loads on the cavity boundaries are expected to be higher (due to the close proximity of the corbel supports and the cavity wall to the explosion zone), and the likelihood of the corbel supports failure, as well as the cavity wall, become relatively high. For scenario A, involving failure of multiple instrument tube penetrations, the failure likelihood of both the cavity wall and the corbel supports are expected

to be high. For scenario B, the high impulsive loads on the cavity boundaries indicate a high likelihood of failure for all cases considered. Scenario B was considered based on the uncertainties regarding the mode and size of the lower head failure, and given these uncertainties, conditions in scenario B cannot be ruled out at the present time. However, to obtain an estimate of the probability of failure for the corbel supports and the cavity wall, the impulsive load uncertainties must also be considered. The present analyses did not attempt to provide probabilistic distributions for the FCI-induced loads. Furthermore, it should also be noted that the failure of the cavity does not automatically lead to containment failure and CE assigns a conditional probability of 0.05 for containment failure given cavity failure.

It is important to note that the underlying phenomena associated with the steam explosion issue are still not well understood and the current hypotheses remain technically controversial. Therefore, the present study is not intended to provide the NRC with a definitive quantitative estimate of the ex-vessel steam explosion energetics for the CE System 80+ containment, rather, it is directed at providing a calculational method and/or framework for exploring the possible range of impulsive loads based on our current understanding of these complex phenomena.

TABLE OF CONTENTS

1.	INTRODUCTION	1
1.1	FCI Modeling Approach and Methodology	2
1.2	Objectives of the Present Study	4
2.	BRIEF DESCRIPTION OF FUEL-COOLANT INTERACTION MODELS	5
2.1	TEXAS Fuel-Coolant Interaction Model	5
2.2	IFCI Fuel-Coolant Interaction Model	6
2.3	Comparison of Code Predictions with Recent Experiments	7
3.	COMBUSTION ENGINEERING SYSTEM 80+ DESIGN	16
4.	SPECIFICATION OF THE INITIAL AND BOUNDARY CONDITIONS	20
4.1	Containment and Primary System Pressures at Vessel Breach	20
4.2	Melt Initial Conditions in the Lower Plenum at Vessel Breach	22
4.3	Mode, Size and Location of Vessel Breach	27
4.4	Cavity Condition at Vessel Breach	32
4.5	Base Case Conditions for Ex-Vessel FCI in CE System 80+	32
5.	ASSESSMENT OF FCI ENERGETICS FOR CE SYSTEM 80+	36
5.1	Scenario A	36
5.1.1	Base Case Calculations	36
5.1.2	Sensitivity Calculations	49
5.1.2.1	Sensitivity to the Water Pool Depth of 3 m (S-1)	49
5.1.2.2	Sensitivity to the Water Pool Depth of 4.5 m (S-2)	57
5.1.2.3	Sensitivity to Melt Superheat of 200 K (S-3)	60
5.1.2.4	Sensitivity to the Number of Failed Penetrations (S-4)	63
5.1.2.5	Sensitivity to Initial Melt Velocity (S-5)	66
5.1.2.6	Sensitivity to the Saturated Water Pool (S-7)	69
5.2	Scenario B	72
5.2.1	Base Case Calculations	72
5.2.2	Sensitivity Calculations	80
5.2.2.1	Sensitivity to Water Pool Depth of 3 m (S-1)	80
5.2.2.2	Sensitivity to the Initial Melt Velocity and Saturated Water Pool (S-6 and S-7)	85

6.	SUMMARY AND CONCLUDING REMARKS	93
6.1	Summary and Insights	93
6.2	Concluding Remarks	97
7.	REFERENCES	100
	APPENDIX: THERMODYNAMIC ANALYSIS OF STEAM EXPLOSIONS	103

LIST OF FIGURES

Figure 1	KROTOS test section and pressure vessel	10
Figure 2	Local vapor void fraction in the coolant pool for the KROTOS-26 simulation using TEXAS at the end of premixing calculation (1.5 s)	13
Figure 3	Comparison of the predicted and measured explosion pressures in KROTOS-26 experiment using TEXAS (ERI represents the present simulation, while UW represents the analysis by Tang [13]).	14
Figure 4	Fragility curves for the concrete cavity wall and corbel supports [17]	18
Figure 5	Schematic of the CE System 80+ cavity region and corbel supports	19
Figure 6	Schematic of the CE System 80+ lower head	31
Figure 7	Predicted vapor void fraction and melt volume fraction at the end of the premixing calculation using IFCI computer code with nonuniform radial nodalization for the base case in Scenario A	37
Figure 8	Predicted vapor void fraction at the end of premixing calculation (1 second) using TEXAS computer code (scenario A, base case)	40
Figure 9	Predicted explosion pressure history at different axial locations using TEXAS computer code after 1 second of premixing (scenario A, base case)	41
Figure 10	Predicted vapor void fraction at the end of premixing calculation (2 seconds) using TEXAS computer code (scenario A, base case)	42
Figure 11	Predicted explosion pressure history at different axial locations using TEXAS computer code after 2 seconds of premixing (scenario A, base case)	43
Figure 12	Predicted vapor void fraction and melt volume fraction at the end of the premixing calculation using IFCI computer code (scenario A, base case)	46

Figure 13	Predicted explosion pressure history at different axial locations in the inner radial node using IFCI computer code (scenario A, base case)	47
Figure 14	Predicted explosion pressure history at different axial locations in the outer radial node (wall) using IFCI computer code (scenario A, base case)	48
Figure 15	Predicted vapor void fraction at the end of premixing calculation (1 second) using TEXAS computer code (scenario A, 3 m pool depth) . . .	52
Figure 16	Predicted explosion pressure history at different axial locations using TEXAS computer code (scenario A, 3 m pool depth)	53
Figure 17	Predicted vapor void fraction and melt volume fraction at the end of the premixing calculation using IFCI computer code (scenario A, 3 m pool depth)	54
Figure 18	Predicted explosion pressure history at different axial locations in the inner radial node using IFCI computer code (scenario A, 3 m pool depth)	55
Figure 19	Predicted explosion pressure history at different axial locations in the outer radial node (wall) using IFCI computer code (scenario A, 3 m pool depth)	56
Figure 20	Predicted vapor void fraction at the end of premixing calculation (1 second) using TEXAS computer code (scenario A, 4.5 m pool depth) . .	58
Figure 21	Predicted explosion pressure history at different axial locations using TEXAS computer code (scenario A, 4.5 m pool depth)	59
Figure 22	Predicted vapor void fraction at the end of premixing calculation (1 second) using TEXAS computer code (scenario A, melt superheat of 200 K)	61
Figure 23	Predicted explosion pressure history at different axial locations using TEXAS computer code (scenario A, melt superheat of 200 K)	62
Figure 24	Predicted vapor void fraction at the end of premixing calculation (1 second) using TEXAS computer code (scenario A, simultaneous failure of eight penetrations)	64

Figure 25	Predicted explosion pressure history at different axial locations using TEXAS computer code (scenario A, simultaneous failure of eight penetrations)	65
Figure 26	Predicted vapor void fraction at the end of premixing calculation (1 second) using TEXAS computer code (scenario A, initial melt velocity of 8 m/s)	67
Figure 27	Predicted explosion pressure history at different axial locations using TEXAS computer code (scenario A, initial melt velocity of 8 m/s)	68
Figure 28	Predicted vapor void fraction at the end of premixing calculation (1 second) using TEXAS computer code (scenario A, saturated water pool)	70
Figure 29	Predicted explosion pressure history at different axial locations using TEXAS computer code (scenario A, saturated water pool)	71
Figure 30	Predicted vapor void fraction and melt volume fraction at the end of the premixing calculation using IFCI computer code (scenario B, base case)	74
Figure 31	Predicted explosion pressure history at different axial locations in the inner radial node using IFCI computer code (scenario B, base case)	75
Figure 32	Predicted explosion pressure history at different axial locations in the outer radial node (wall) using IFCI computer code (scenario B, base case)	76
Figure 33	Predicted vapor void fraction at the end of the premixing calculation using TEXAS computer code (scenario B, base case)	78
Figure 34	Predicted explosion pressure history at different axial locations using TEXAS computer code (scenario B, base case)	79
Figure 35	Predicted vapor void fraction and melt volume fraction at the end of the premixing calculation using IFCI computer code (scenario B, 3 m pool depth)	82
Figure 36	Predicted explosion pressure history at different axial locations in the inner radial node using IFCI computer code (scenario B, 3 m pool depth)	83

Figure 37	Predicted explosion pressure history at different axial locations in the outer radial node (wall) using IFCI computer code (scenario B, 3 m pool depth)	84
Figure 38	Predicted vapor void fraction for scenario B using TEXAS computer code (3 m pool depth)	87
Figure 39	Predicted explosion pressure history at different axial locations using TEXAS computer code (scenario B, 3 m pool depth)	88
Figure 40	Predicted vapor void fraction for scenario B using TEXAS computer code (initial melt velocity of 15 m/s)	89
Figure 41	Predicted explosion pressure history at different axial locations using TEXAS computer code (scenario B, initial melt velocity of 15 m/s)	90
Figure 42	Predicted vapor void fraction for scenario B using TEXAS computer code (saturated water pool)	91
Figure 43	Predicted explosion pressure history at different axial locations using TEXAS computer code (scenario B, saturated water pool)	92
Figure 44	Comparison of the TEXAS estimated impulsive loads on the cavity boundaries with the CE System 80+ containment capacity for scenario A	98
Figure 45	Comparison of the TEXAS estimated impulsive loads on the cavity boundaries with the CE System 80+ containment capacity for scenario B	99

LIST OF TABLES

Table 1	Results of the thermodynamic model parametric study	3
Table 2	Maximum explosion pressures predicted using TEXAS computer code for KROTOS-26	11
Table 3	Comparison of the CE System 80+ core design to Surry	16
Table 4	Comparison of the hot leg/surge line and bypass configurations between CE System 80+ [15] and Surry [16,20]	22
Table 5	Debris initial conditions at vessel breach for CE System 80+ based on Reference [17]	24
Table 6	Estimate of debris initial conditions in CE System 80+ scaled from Surry DCH study [16]	26
Table 7	Postulated debris initial conditions in the lower plenum at vessel breach for CE System 80+ FCI analysis	28
Table 8	Summary of initial conditions for the base case	34
Table 9	Summary of the sensitivity calculations	35
Table 10	Predicted pressure impulse for the base case in scenario A	39
Table 11	Comparison of the pressure impulse for the base case condition in scenario A	45
Table 12	Comparison of the pressure impulse in scenario A (3 m pool)	51
Table 13	Predicted pressure impulse in scenario A using TEXAS computer code (3 m pool)	57
Table 14	Predicted pressure impulse in scenario A using TEXAS computer code (200 K melt superheat)	60

Table 15	Predicted pressure impulse in scenario A using TEXAS computer code (simultaneous failure of eight penetrations)	63
Table 16	Predicted pressure impulse in scenario A using TEXAS computer code (melt velocity of 8 m/s)	66
Table 17	Predicted pressure impulse in scenario A using TEXAS computer code (saturated water pool)	69
Table 18	Predicted pressure impulse for the base case condition in scenario B using IFCI computer code (particle fragment size of 1 mm)	73
Table 19	Predicted pressure impulse for the base case condition in scenario B using TEXAS computer code	77
Table 20	Predicted pressure impulse for the 3 m pool sensitivity calculation using IFCI computer code (scenario B; particle fragment size of 1 mm)	81
Table 21	Predicted pressure impulse for the 3 m Pool sensitivity calculation using TEXAS computer code (scenario B)	85
Table 22	Predicted pressure impulse for sensitivity cases S-6 (melt velocity) and S-7 (saturated water pool) using TEXAS computer code (scenario B)	86
Table 23	Maximum predicted pressure impulses: comparison of codes	94
Table 24	Summary of the maximum impulse loads at the cavity boundaries for the CE System 80+	96

NOMENCLATURE

CR	Conversion ratio (see Equation A.6)
C_{fr}	Proportionality constant in the fuel fragmentation rate
c_p	Specific heat at constant pressure
c_v	Specific heat at constant volume
D	Diameter
g	Gravitational acceleration
h	Specific enthalpy
h_{fg}	Enthalpy of vaporization
m	Mass
N_p	Number of fuel particles
P	Pressure
R_c	Gas constant
r	Radial distance from the center of the cavity
s	Specific entropy
T	Temperature
u	Specific internal energy
U	Velocity; Total internal energy
U_o	Melt discharge velocity at vessel breach
v	Specific volume
V	Volume
W	Explosion expansion work
We	Weber number defined as $\rho_c U_r D_f / \sigma$
x	vapor quality
z	Axial distance from the bottom of the cavity

Greek Symbols

α	Vapor void fraction
Δ	Difference operator
ρ	Density
σ	Surface tension
τ	Time scale

Subscripts

c	Coolant
e	Equilibrium
f	Fuel
fr	Fragmentation
j	Jet
l	Liquid coolant
m	Melt; Mixture
o	Initial condition
p	Particle
r	Relative
w	Water

1. INTRODUCTION

During postulated core meltdown accidents in a Light Water Reactor (LWR), the molten core material will ultimately relocate to the lower plenum of the Reactor Pressure Vessel (RPV). Following the structural failure of the RPV lower head, the molten core debris will pour into the reactor cavity where the potential for interactions with any water present exists. There is a high likelihood for energetic Fuel-Coolant Interaction (FCI) when the molten core debris is dispersed in the cavity water. This energetic FCI is initiated by the transfer of energy from the hot liquid (fuel) to the colder liquid (coolant) during liquid-liquid contact resulting in rapid steam generation which could lead to a high local pressure. In an energetic FCI, the pressurization time scale is short compared to the time scale for the inertial pressure release and a shock wave is generated that propagates spatially through the fuel-coolant medium.

The processes leading to an energetic FCI can be characterized by the following four phases:

- (1) premixing of fuel and coolant
- (2) triggering
- (3) propagation
- (4) expansion

The premixing phase of the interaction is complex. However, experiments and numerical simulations/analyses continue to obtain a better understanding of this phenomenon. The premixing phase describes the interval during which a hot liquid material, initially as a coherent glob or as a stream pour, penetrates a cooler liquid, breaks up into small particles and is dispersed into the volume of the cooler liquid. This 'premixing' is believed to aid in increasing the energetics of an explosion. This phase could be described qualitatively by the condition that the two liquids disperse into one another. The phenomena that characterize this mixing process consist of (1) heat transfer from the hot liquid to the coolant due to film boiling, (2) evolution of steam and hydrogen and (3) fuel breakup by the relative-velocity-induced fragmentation.

Triggering is a local small-scale phenomenon which initiates the fragmentation of the fuel. Most fuel-coolant-interactions appear to be initiated by the collapse of the vapor film layer or bubble in a localized region which may arise spontaneously or can be triggered by an external pressure pulse. The fuel-coolant mixture can produce high pressure vapor when undergoing an explosion and do work against its surroundings. Once the explosion trigger is initiated, the pressure pulse propagates through the mixture. The explosion propagates spatially with a velocity which is greater than the speed of sound in the region ahead of the shock front in a fashion somewhat similar to a chemical detonation wave. Also, during the explosion expansion, mechanical work is done on the surroundings. Either these dynamic pressures or the explosion work could cause damage to the structures.

It has been established that the necessary initial condition for a steam explosion in an LWR is the formation of a coarse mixture of fuel and coolant. Also, the explosive fragmentation will eventually decide the hazard of FCI processes during a severe accident. In this work we focus on the hazard potential from the dynamic pressures.

1.1 FCI Modeling Approach and Methodology

There are basically three FCI modeling approaches and these can be used for assessing the dynamic pressures generated by an FCI:

- (1) Thermodynamic models (i.e., Hicks-Menzies ideal equilibrium model)
- (2) FCI parametric models
- (3) Direct simulations of the FCI based on more mechanistic models

The first approach is conservative because it provides the upper bound pressure loads from a steam explosion. The mathematical details of this approach are provided the Appendix. The limitation of this approach is that one is required to provide the global values of the fuel involved in the explosion, the vapor void fraction, and the amount of coolant participating in the explosion. The result from such analysis indicates that, for a reasonable range of fuel to coolant volume or mass ratios ($V_c/V_f=1$ to $m_c/m_f=1$) and global void fractions (5% to 40%) as predicted by mixing calculations or other estimates, the explosion pressures are quite large and the structural integrity of the containment may be compromised. This suggests that upper bound analyses do not provide an appropriate answer; therefore, more mechanistic estimates are desirable. Only if the pressures predicted by the thermodynamic equilibrium model are below the failure limits of the structure, is there no need to perform the more mechanistic calculations. Table 1 presents typical peak pressures and conversion ratios (the conversion ratio is defined as the ratio of the work potential during the expansion phase of the FCI to the initial fuel energy) using the thermodynamic model.

The second approach is more mechanistic because it would employ an energetic FCI model that allows for kinetics between the fuel and the coolant liquids to more realistically estimate the fuel energy transfer rate. However, such explosion models are still somewhat parametric [1] because one is still required to specify the amount of coolant and fuel participating in the explosion; for example, this is not known *a priori* unless more mechanistic mixing analysis is performed. Also, these models are lumped parameter models that require estimates of the global mixture vapor void fractions. Thus, as in the thermodynamic model, the fuel to coolant liquid ratio in the explosion mixture and the global void fraction are the key determinants for the explosion pressure history.

Table 1 Results of the thermodynamic model parametric study

$V_c/V_f = 1$ ($m_c/m_f \sim 0.1$)			$m_c/m_f = 1$ ($V_c/V_f \sim 10$)		
α	P (MPa)	CR	α	P (MPa)	CR
0.05	2368	0.43	0.05	680	0.32
0.1	2145	0.43	0.1	531	0.31
0.2	1734	0.42	0.2	301	0.29
0.3	1371	0.41	0.3	151	0.28
0.4	1060	0.40	0.4	68	0.27

The results from these parametric calculations would provide not only the peak pressure (as would the thermodynamic models), but also the time history of the pressure. These estimates are not as conservative as the thermodynamic approach, however, they still suffer from being parametric and lack any dimensionality.

The final approach is to mechanistically consider the different phases of the FCI (i.e., mixing, triggering, propagation, and expansion). Several computer codes (i.e., TEXAS [2], PM-ALPHA/ESPROSE [3], and IFCI [4]) have been developed in the United States to predict the fuel-coolant interaction process. In the present analysis, the TEXAS and IFCI computer codes have been used. A brief description of these computer codes is provided in Section 2. TEXAS is a one-dimensional code whereas both IFCI and PM-ALPHA/ESPROSE are two dimensional. The extent of radial spreading of melt in the coolant during the mixing phase of the interaction and the spatial propagation of the explosion after the mixture has been triggered requires at least a two-dimensional calculation.

The explosion escalation and propagation process and its associated energetics are controlled by the rate of fuel fragmentation. One should be aware that the rate of fuel fragmentation and the mechanisms involved are still not well-known, however, experimental and modelling studies continue to shed light on this aspect of the interaction. The KROTOS experiments [5,6] to-date, provide the most definitive data to compare the explosion model to simulate the process in a one-dimensional experimental setup. More experimental work is required to provide data for the validation of two dimensional propagation models and the explosive interactions involving prototypic reactor materials as discussed in Reference [7].

1.2

Objectives of the Present Study

The objective of this report is to investigate the potential dynamic pressure loads resulting from ex-vessel fuel-coolant-interactions on the Combustion Engineering (CE) System 80+ Pressurized Water Reactor (PWR) containment. Specifically,

- (1) Establish the initial and boundary conditions that have an impact on the resulting impulsive (dynamic) loads in the event of a steam explosion,
- (2) Provide a perspective on the predictive capability of the existing mechanistic computer codes by a limited comparison to the KROTOS test data, and
- (3) Calculate the dynamic pressures on the cavity boundaries as a result of energetic interactions. To this end, the TEXAS and IFCI computer codes will be used to assess the potential magnitudes of the impulsive pressure loads following ex-vessel steam explosions.

It should be recognized that given the current state of the art, it is difficult to expect anything more than a prediction of the trends of explosive fuel-coolant interactions following severe accidents. Therefore, the present study is not intended to provide the NRC with a definitive quantitative estimate of the ex-vessel steam explosion energetics for the CE System 80+ containment, rather, it is directed at providing a calculational method and/or framework for exploring the possible range of impulsive loads based on our current understanding of these complex phenomena.

2. BRIEF DESCRIPTION OF FUEL-COOLANT INTERACTION MODELS

In this section brief descriptions of the two mechanistic computer codes, TEXAS and IFCI, used in the assessment of ex-vessel steam explosion energetics for the CE System 80+ are presented. The detonation phase of the FCI is still not well-understood, and modeling differences exist in the various computer codes examined as part of this study. Therefore, it is desirable to consider the impact of the uncertainties in the modelling of particle fragmentation kinetics during the detonation phase which are due largely to a lack of sufficient experimental validations of the existing models.

2.1 TEXAS Fuel-Coolant Interaction Model

The TEXAS computer code is based on a one-dimensional transient model for hydrodynamic calculations developed at Sandia National Laboratories (SNL) and modified for fuel-coolant-interactions by Chu [2]. TEXAS solves the one-dimensional, three-field equations describing the fuel-coolant-interaction and its hydrodynamics. Two fields represent the coolant as liquid and vapor; one field represents the discrete fuel particles. The liquid and vapor fields are solved using the Eulerian technique and the particle phase is treated using the Lagrangian formulation. In this model, the governing conservation equations for each phase (i.e., liquid, vapor and particle) are written separately, which allows thermal and mechanical nonequilibrium between the phases to exist. The effects of condensation, evaporation, and interfacial momentum transport are included as source terms in the partial differential equations. A hydrodynamic particle breakup model based on the Rayleigh-Taylor instability mechanism is implemented in TEXAS. It is postulated that this mode of instability is dominant in FCIs [2]. The dynamic particle breakup model implemented in TEXAS predicts the Lagrangian particle size at a new time ($n+1$) using the field variables at the old time level (n) without any reference to the history of the particle. The particle diameter at the new time level is then given by the expression

$$D^{n+1} = D^n (1 - C_0 \Delta T^* We^{C_1}) \quad (1)$$

where ΔT^* is the dimensionless time step and We is the Weber number evaluated by the relative velocity and density of the coolant phase at the old time level. The empirically determined coefficients C_0 and C_1 in Equation (1) are $0.1093 - 0.0785 (\rho_c/\rho_f)^{1/2}$ and 0.246, respectively [2]. This linear fuel breakup model is developed from a complete theoretical model for multi-stage droplet breakup [2].

During the propagation phase of the FCI, the fuel fragmentation is due to vapor film collapse and coolant liquid jet impingement and entrapment below the fuel surface. This process results in rapid liquid coolant vaporization leading to the fragmentation of the fuel particle. This fragmentation process would terminate once this fuel-coolant microscale interaction achieves

pressure equilibration in a time τ_{fr} . The total fuel fragmentation rate model in TEXAS is given by:

$$\begin{aligned} \dot{m}_f &= C_{fr} \rho_p \pi D_p^2 N_p U_{fr} F(\alpha) \\ U_{fr} &= \sqrt{(P - P_o) / \rho_l} \end{aligned} \quad (2)$$

where the function $F(\alpha)$ is used to drive the fragmentation rate to zero when the void fraction approaches unity, P is the local fluid pressure at any time near the fuel mass and P_o is the initial ambient pressure. The proportionality constant C_{fr} in the fuel fragmentation model and the fragmentation time τ_{fr} are empirically determined constants. These parameters can strongly impact the rate of fuel fragmentation and thus the peak explosion pressures (the values of these constants and comparison to the KROTOS experiments are given in subsection 2.3).

The TEXAS model requires the user to define the system geometry, the initial and the boundary conditions. The fuel entry mode into the pool can be modelled as a coherent jet or in the form of discrete 'blobs' or particles. To prescribe the initial conditions in the TEXAS simulation of a FCI, the radius of the particle/coherent jet along with the fuel initial velocity and thermophysical properties must be established. In addition, the water pool conditions and initial vapor void fraction are also required.

2.2 IFCI Fuel-Coolant Interaction Model

IFCI [4] is a two-dimensional, Eulerian, four-field computer code that is intended to be used in the prediction of fuel-coolant-interaction for nuclear reactors and other industrial applications. The four fields consist of water vapor (steam), liquid water, solid fuel and liquid fuel. A set of conservation equations (mass, momentum, and energy) are solved for each field which allows for non-equilibrium between different fields to exist.

The phenomenological models in IFCI include:

- (1) Dynamic particle breakup based on local hydrodynamic conditions (this model is based on that proposed by Pilch [8]).
- (2) Melt surface area convection model (the convected quantity is the melt surface area per unit volume).
- (3) Melt surface area tracking model (this algorithm is used in IFCI for cases where the size scale of the melt is greater than the finite difference length scale).
- (4) Trigger model to initiate the explosion in the mixture.

- (5) Particle fragmentation model to calculate the rate of particle breakup during propagation of the explosion in the mixture.
- (6) Constitutive relations for heat and momentum transfer between the fluids (different flow regime maps based on the local volume fraction of the mixture components).

IFCI requires the user to specify the two-dimensional (cylindrical) problem domain into a number of axial and radial nodes along with the initial and boundary conditions (the melt and coolant conditions in the problem domain and specification of the inflow and outflow boundaries). There are currently three user-specified detonation models in IFCI which include a purely parametric detonation model initiated in a particular cell, a pressure threshold model where detonation is triggered when the pressure in a cell exceeds the threshold value, and a pressure/pressure rise rate threshold model (in this case the detonation is triggered when both the pressure and pressure rise in a cell exceed the specified values). Once detonation is activated in a computational cell, the fuel particles are assumed to fragment to a predetermined (user input) size, and the detonation model requires information regarding the diameter of the fine fragments and the fragmentation time. A complete description of the input parameters is provided in Reference [4].

2.3 Comparison of Code Predictions with Recent Experiments

A number of experiments have been performed recently to obtain a better understanding of the fuel-coolant interaction mechanisms and to provide data for computer code modelling. A more complete review of the previous fuel-coolant interaction experiments is provided in Reference [9]. The recent experiments include:

1. KROTOS - These experiments were performed at the KROTOS facility at the Joint Research Center (JRC)-Ispra [5] to study the fuel-coolant premixing under different initial conditions and propagation and energetics of the triggered fuel-coolant interaction in a one dimensional geometry (the axial length of the test tube was approximately 1 m as compared to the inner diameter of 0.095 m). In KROTOS-21, 7.5 kg of tin at an initial temperature of 1350 K was used. The system pressure was 0.1 MPa and the water temperature and height were 360 K and 1.1 m, respectively. In KROTOS-26 to KROTOS-30 experiments, the melt (aluminum oxide) mass was approximately 1.5 kg with a temperature of 2573-2673 K. The depth of the water pool was approximately 1.1 m and the water subcooling was varied from 10 K to 80 K (the initial system pressure was 0.1 MPa). The melt delivery nozzle was 0.03 m which was positioned approximately 0.455 m above the pool surface. Five pressure transducers (K1 to K5) provided the explosion pressure at various axial locations in the test tube. The trigger device was attached to the lower end of the test tube. The trigger gas chamber volume was 15 cm³ and could be charged to a maximum pressure of 15 MPa.

2. FARO - The FARO scoping test and quenching test were also performed at the JRC-Ispra FARO plant [10,11]. The objectives of these tests were to examine the fuel melt quenching at high pressures, and the thermal loading of the bottom vessel structure under typical accident conditions. The melt composition in both tests were 80 % UO_2 and 20 % ZrO_2 and the melt mass varied between 18 kg in the scoping test to 44 kg in the quenching test. The initial melt temperatures were 2900 K and 3000 K. The water depth was 0.87 m in the scoping test and 1 m in the quenching test, and the system pressures were 5 MPa and 5.8 MPa, respectively. The amount of water subcooling at melt contact varied from 2 K in the scoping test to 12 K in the quenching test. No explosions were observed in these tests.
3. IET - The IET experiments were performed in the Surtsey facility at Sandia National Laboratories in support of Direct Containment Heating (DCH) program [12]. This facility is a 1:10 scale of the Zion nuclear reactor cavity. IET-8A experiment in the test series has provided data on energetic FCI with a depressurized primary system, while IET-8B was performed under high pressure melt ejection. In these experiments, 43 kg of thermite charge was injected into a half-filled (with water) scale model of Zion cavity. The driving steam pressure was 1.06 MPa in the IET-8A experiment and the corresponding value for the IET-8B was 6.2 MPa. The interaction of the melt with the water in the cavity resulted in explosive FCI.

The KROTOS experiments are most relevant to the present study as they provide direct measurements of the explosion pressures in the test vessel. A comparison of TEXAS simulations with several KROTOS experiments is given in Reference [13]. To match the experimental data with the TEXAS simulation of KROTOS-21, the proportionality constant C_{fr} in the fuel fragmentation model (see Equation 2) was set to 0.001, and the fragmentation time τ_{fr} was set to 2 msec. For KROTOS-26 and KROTOS-28 tests [13], the proportionality constant and fragmentation time were selected to be 0.002 and 0.5 ms, respectively. Even though the KROTOS-26 simulation showed good agreement with the experimental data both in terms of the magnitudes of the dynamic pressures and the duration of the pressure pulse, the maximum pressures in the KROTOS-28 simulation were much smaller than the experimental data [13].

The operational assessment of the IFCI code (stand-alone version 6.0) is provided in Reference [14]. A number of parametric calculations using the experimental conditions in FARO quenching test (no explosions) and IET-8 experiments have been performed. The predicted pressures and temperatures in the FARO quenching test were within 10 % of the experimental values. The simulations included parametric variations of the user input constants (e.g., convergence criteria, effect of nodalization, etc.) and the effect of such variations is documented in Reference [14]. A number of numerical difficulties have also been reported in the operational assessment [14] of the IFCI code which will be discussed later. In the IET-8A simulations, no

direct comparison with the experimental data was performed since the simulations were merely performed to demonstrate the capability of IFCI in producing energetic steam explosions.

The IFCI simulations have produced the qualitative characteristics of the FARO and IET-8A experiments and the trigger models have successfully predicted the explosive phenomena [14]. However, a quantitative comparison to the IET-8A experimental data and the IFCI trigger models have not yet been performed. Therefore, additional work is required to increase the level of confidence in the predictive capabilities of the IFCI computer code. On the other hand, the TEXAS model has produced relatively good agreement with the one-dimensional experimental data [13].

In KROTOS-26 experiment, the depth of the coolant water was 112 cm with a system pressure of 0.1 MPa and a water temperature of 333 K. The melt mass was 1.43 kg (aluminum oxide) at an initial temperature of 2573 K. The trigger device had a volume of $15 \times 10^{-6} \text{ m}^3$ at an initial pressure of 11.2 MPa located at the bottom of the test tube. The mechanical destruction of the trigger device membrane delivered a pressure pulse that propagated vertically upwards through the fuel-coolant mixture. There was incomplete melt delivery from the crucible and post-test examination of the debris collected at several axial locations indicated that approximately 0.5 kg of the melt remained in the crucible. The total post-test weight was 1.589 kg which included the tin disc separating the melt from the delivery nozzle in the crucible. Therefore, it is estimated in the present calculations that approximately 1 kg of melt was dropped into the water pool. The debris size varied from less than 0.1 mm to greater than 4 mm (for a more complete description of the post-test debris distribution, see Reference [5]). The maximum recorded explosion pressure was approximately 24 MPa and the pressure wave caused considerable damage to the upper water container and the level meter. It should be mentioned that the explosion pressures exceeded the upper limit of the pressure transducers which were set at 24 MPa, and the actual pressures were expected to be higher. Thus, the recorded pressures were truncated at 24 MPa. Figure 1 shows the experimental setup in the KROTOS-26.

In the present TEXAS model of the KROTOS-26 experiment, the test section was nodalized into eleven axial cells (0.1 m) in the water pool and nine cells in the vapor space which was similar to the nodalization employed in the KROTOS-21 [13]. The trigger device during the explosion phase was modelled as a steam filled cell in the bottom of the pool with an initial pressure of 11.2 MPa corresponding to the experimental value. The initial particle diameter was set equal to the nozzle diameter (0.03 m) and the initial particle velocity was estimated to be 2.3 m/s (based on the gravity head) at a distance of 0.15 m above the pool surface. In the present TEXAS simulation, it took approximately 1.5 seconds for the melt to penetrate to the bottom of the pool. Figure 2 shows the vapor void fraction distribution in the coolant pool. The maximum vapor void fraction of 50% occurs approximately 0.8 m from the bottom of the pool. During the mixing calculation, the fuel particles broke up into smaller diameter particles (see

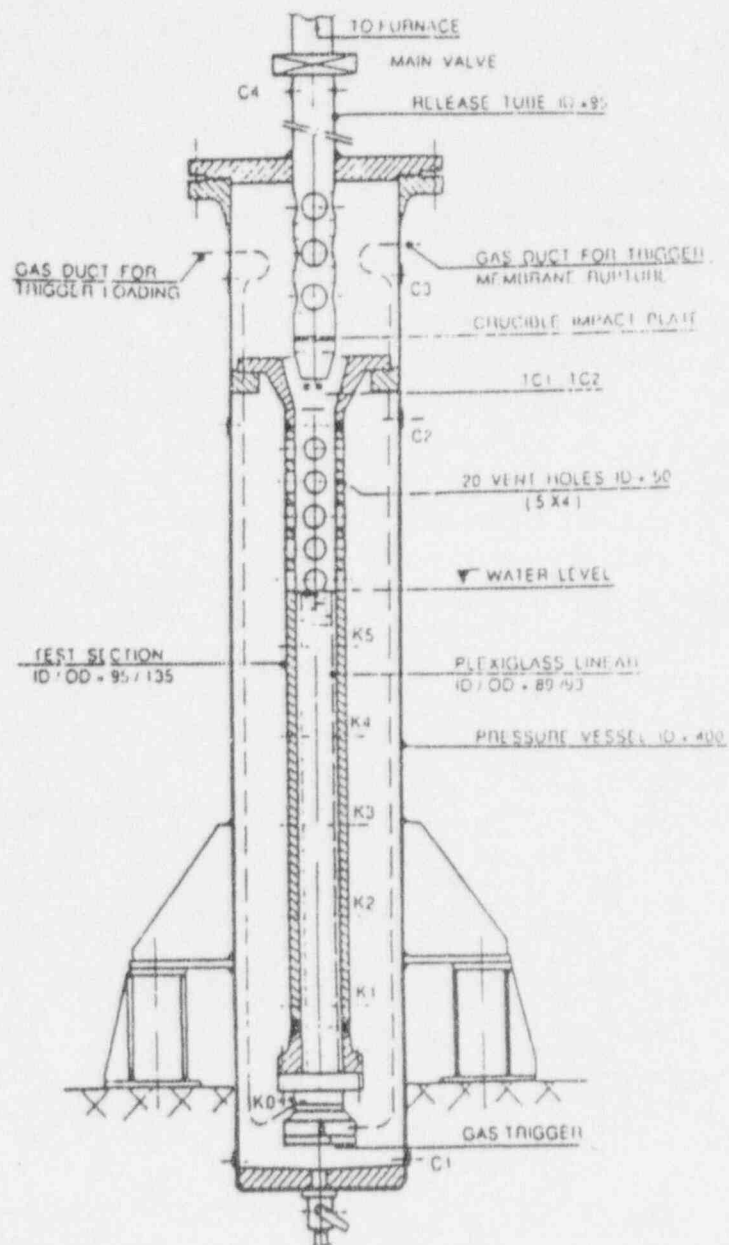


Figure 1 KROTOS test section and pressure vessel

Equation 1) as they travelled in the coolant pool. The minimum particle diameter was found to be approximately 12 mm. It should be mentioned that the experimental setup did not allow for the assessment of the premixing conditions, i.e., the vapor void fraction and the characteristic particle size.

The explosion was triggered at the bottom of the pool and the pressure pulse propagated upwards through the mixture. The fuel fragmentation rate is given by Equation (2), where C_{fr} and τ_{fr} are the empirically determined parameters. The fragmented fuel then instantaneously transfers all its thermal energy to the liquid coolant in vaporizing the liquid to vapor. Figure 3 shows the explosion pressures at the axial locations corresponding to the pressure transducer positions of K1 through K5 (20 cm apart). The reason for the low explosion pressure at the K4 location has not been discussed in Reference [5], however, it appears that this transducer was unreliable because its pressure signal was too low compared with those of the other transducers [13].

The proportionality constant and the fragmentation time in this calculation were assigned values of 0.001 and 2 ms, respectively. With a higher proportionality constant of $C_{fr}=0.0015$, the maximum explosion pressure of 50 MPa occurred at the K5 pressure transducer which was approximately twice the value recorded experimentally (recall that the pressure transducers were set at 24 MPa). If the value of the proportionality constant was decreased below 0.001 (keeping the fragmentation time constant) or the fragmentation time was decreased below 2 ms (keeping the proportionality constant), the maximum explosion pressures would be lower. Table 2 presents a comparison of the maximum explosion pressures between the experiment and the simulation using various values of the proportionality constant and fragmentation time.

Table 2 Maximum explosion pressures predicted using TEXAS computer code for KROTOS-26

Pressure transducer	Maximum Explosion Pressure (MPa)			
	$C_{fr}=0.0005$ $\tau_{fr} = 1 \text{ ms}$	$C_{fr}=0.001$ $\tau_{fr} = 1 \text{ ms}$	$C_{fr}=0.001$ $\tau_{fr} = 2 \text{ ms}$	$C_{fr}=0.0015$ $\tau_{fr} = 2 \text{ ms}$
K1	10.0	16.4	22.5	37.7
K2	12.7	19.4	24.8	37.4
K3	12.8	21.3	24.1	37.8
K4	5.4	9.8	24.9	38.0
K5	4.8	8.9	27.0	50.5

In the KROTOS-26 test the melt delivery was incomplete. The analysis by Tang [13] indicated that the melt remained in the upper portion of the pool before the explosion was triggered and the premixing time was estimated to be approximately 0.65 second. Based on these analysis, the values of C_{fr} and τ_{fr} were chosen to be 0.002 and 0.5 ms and the pressure pulse duration showed good agreement with the experimental data. In the present KROTOS-26 simulation, the premixing time was 1.5 second and during this time the melt penetrated all the way down towards the bottom of the pool. Therefore, our initial conditions at the end of premixing calculations (before the onset of explosion) were different from those of Tang (the results of analysis by Tang are also shown in Figure 3).

It was hypothesized by Tang [13] that the values of C_{fr} and τ_{fr} were mainly affected by the melt thermal energy, e.g., in the KROTOS-21 (with tin as the fuel), these constants were 0.001 and 2 ms, while for the KROTOS-26 (with alumina as the fuel) the corresponding values were 0.002 and 0.5 ms (even though the magnitudes of the pressures in the KROTOS-28 simulation were much smaller than the experimental data as mentioned earlier). Since corium has a thermal energy between those of tin and alumina, the estimated values of the proportionality constant and the fragmentation time were found to be 0.0015 and 1 ms for uranium dioxide based on a simple interpolation. In the plant calculations for CE System 80+, we have chosen the values of 0.0015 and 2 ms for these constants. Of course, no conclusive relationship between the fuel thermal energy and these constants could be drawn at the present time. The experimentally determined values of the proportionality constant and fragmentation time obtained from the one-dimensional experiments does not automatically assure that these values would be universal (i.e., the effects of scaleup to reactor conditions and multi-dimensionality effects cannot be addressed within the one dimensional experimental framework). However, these empirically determined parameters represent the current assessment of the TEXAS model as compared with the KROTOS experiments.

A similar experimental benchmarking exercise was also attempted with the IFCI code. As mentioned before, the detonation model in IFCI is parametric. For example, given a trigger pressure threshold and a characteristic size of the fragmented fuel drops, IFCI would predict the rate of pressurization during the explosion phase of the interaction. In the current version of IFCI, using the pressure threshold detonation model, once the pressure in a particular computational cell exceeds the input pressure threshold value, the fuel drops are assumed to fragment into a predetermined size during a prescribed fine fragmentation time (10 μ s in the present simulations) thereby increasing the fuel surface area and heat transfer to the coolant. The computational domain for the KROTOS-26 simulation consisted of a cylindrical geometry with a height of 1.26 m and diameter of 0.095 m. The computational domain was divided into 2 radial nodes (0.024 mesh size) and 63 axial nodes (0.02 m mesh size) with 56 axial nodes in the water. The melt was delivered in the inner node at the top of the computational domain, and a constant pressure boundary condition was prescribed at the top of the outer node. The initial melt velocity and particle size were similar to the TEXAS input.

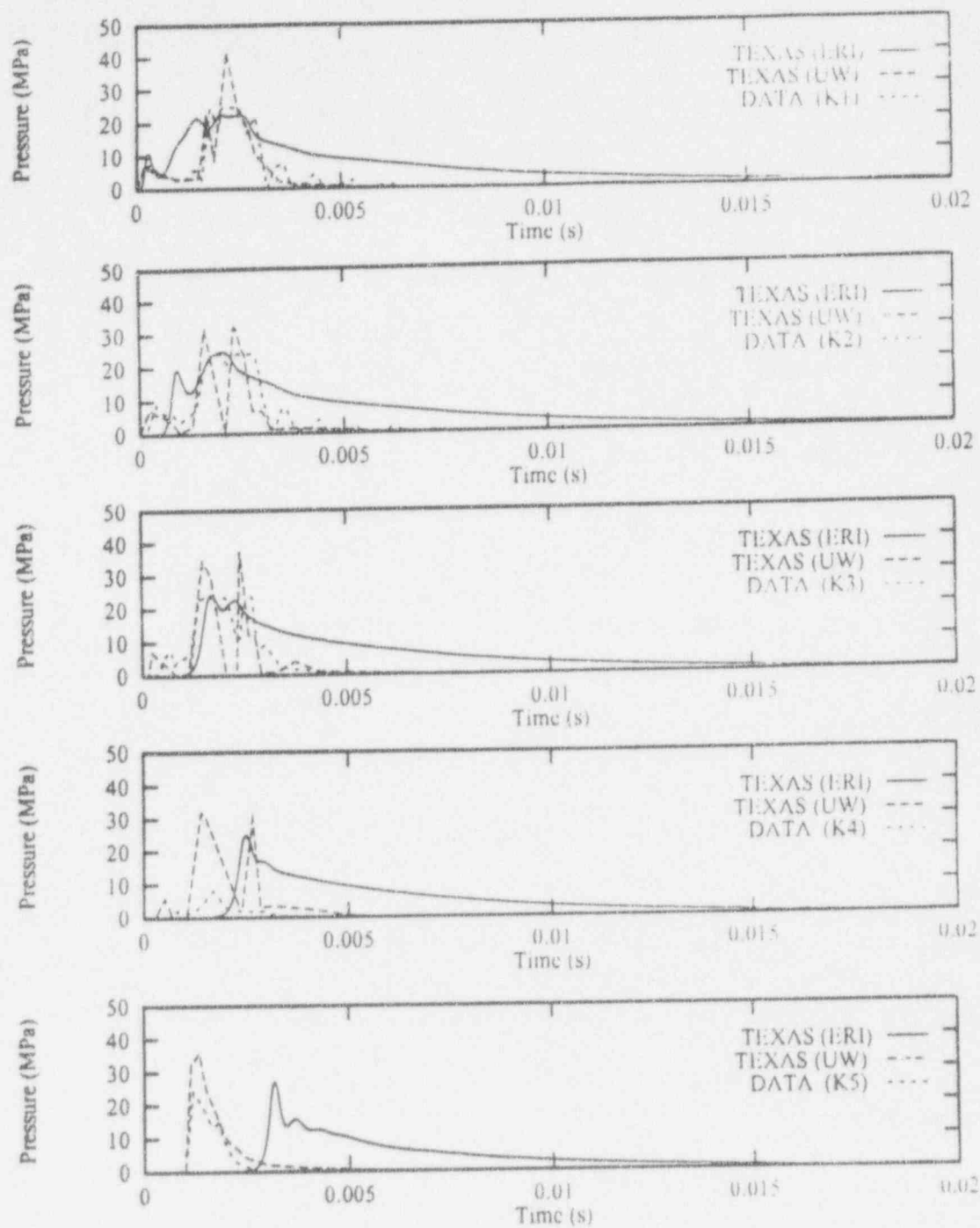


Figure 3 Comparison of the predicted and measured explosion pressures in KROTOS-26 experiment using TEXAS (ERI represents the present simulation, while UW represents the analysis by Tang [13]).

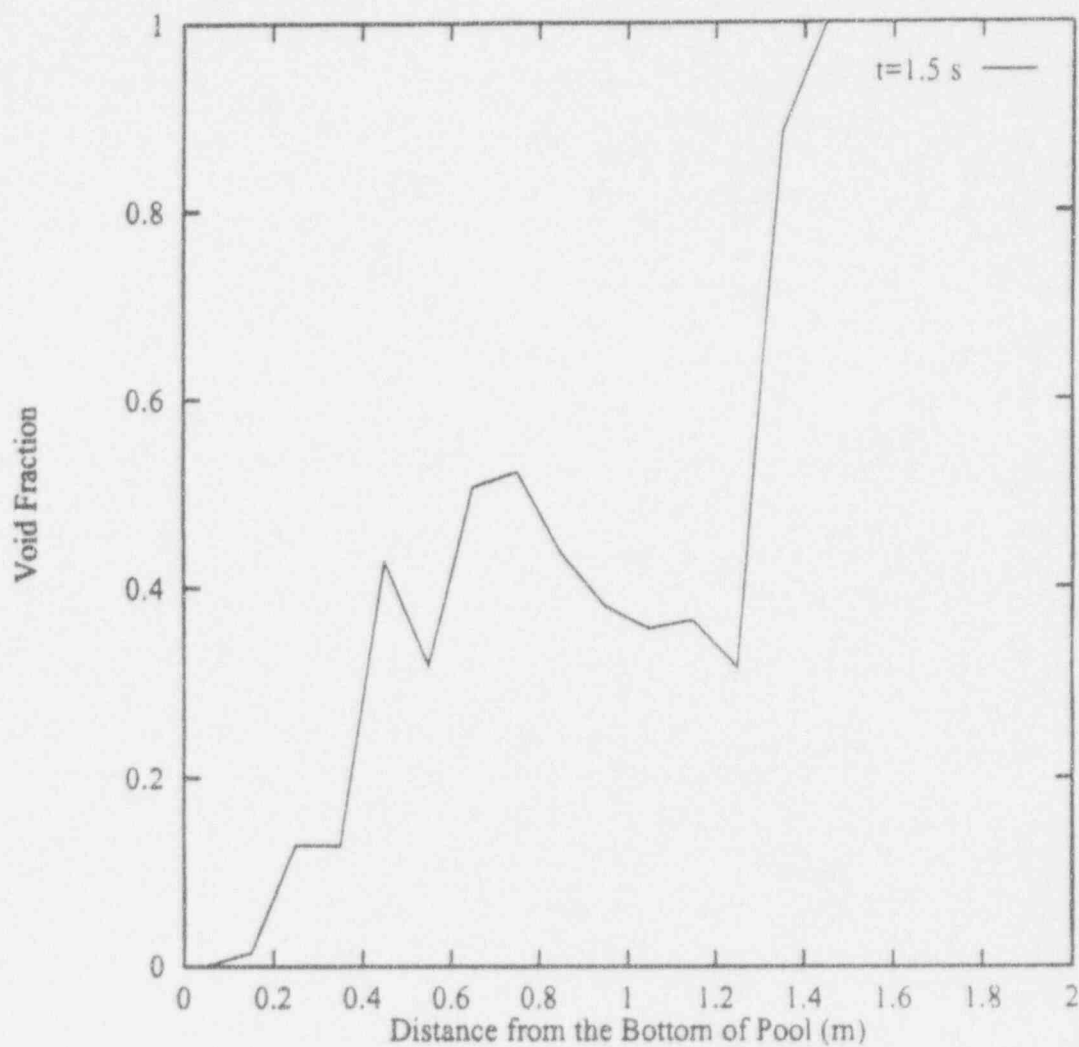


Figure 2 Local vapor void fraction in the coolant pool for the KROTOS-26 simulation using TEXAS at the end of premixing calculation (1.5 s)

During the premixing phase of the interaction, it took the melt approximately 2 seconds to penetrate to the bottom of the water pool. Even though the melt mass delivered was 1 kg corresponding to the value used in TEXAS, by the end of the premixing run, approximately half the melt appeared to have exited the computational domain through the constant pressure outflow boundary. Increasing the melt delivery rate was also not successful, and therefore this simulation was abandoned.

Several problems exist in the current version of IFCI code as documented in Reference [14] and require further investigation (e.g., flow regime map, surface tracking algorithm, coarse breakup, etc.). IFCI also shows strong sensitivity to the nodalization of the computational domain. Increasing the radial resolution seems to be a major problem, for example, numerical errors and unphysical results were observed for finer radial nodalization (e.g., doubling of the radial nodes in the FARO experiment resulted in numerical errors). The resolution of computational domain becomes more important during the explosion phase of the interaction since finer nodes are required to track the propagation of the explosion in a two-dimensional geometry. The radial nodalization restriction could also become a serious limitation in the case of scaleup to reactor geometries, e.g., in the CE System 80+ in the lower cavity (below the corbel support region), the radial distance to the cavity wall is approximately 3.7 m and even with a 0.1 m radial mesh 37 radial nodes are required. Therefore, given the current status of the IFCI code, at least we can expect a qualitative assessment of the trends associated with the propagation of the explosion. TEXAS computer code will be used to perform sensitivity calculations and predict the local explosion pressures. In the IFCI simulations presented for the CE System 80+, a nominal fragmented particle size of 0.1 mm will be used unless otherwise noted.

3.

COMBUSTION ENGINEERING SYSTEM 80+ DESIGN

The CE System 80+ design consists of a 1300 MW(e) pressurized water reactor in a spherical, large, dry, steel containment. The CE System 80+ Reactor Coolant System (RCS) has a two-loop configuration with each loop having one hot leg and two cold legs. The containment vessel has a spherical steel shell 61 m in diameter and a free volume of 94,578 m³. A large cavity floor area is provided for assuring adequate area for spreading and coolability of core debris on the cavity floor. During the course of a severe accident, the cavity can be flooded by operator action through the use of the Cavity Flooding System (CFS). Table 3 shows a limited comparison of the core design for the CE System 80+ [15] and Surry (a Westinghouse design) [16]. CE System 80+ has a higher power density and Zr content compared to Surry. The higher power density and Zr oxidation can result in higher thermal loads on the RCS pressure boundary.

Table 3 Comparison of the CE System 80+ core design to Surry

	CE System 80+	Surry
Power level, MW _e	3914	2441
Core inventory (mt)		
UO ₂	120.5	79.8
Zr	33.6	16.5
Steel	0	3.8
Control Rod Material	7.5	2.7
Thin upper plenum steel	NA	16
Thin lower plenum steel	29	10
Power/UO ₂ Mass (MW _e /mt)	33	31
Power/Zr Mass (MW _e /mt)	116	148

The CFS consists of an In-Containment Refueling Water Storage Tank (IRWST), the Holdup Volume Tank (HVT), the reactor cavity itself, and a number of connecting pipes, valves, and power sources. The system is designed to provide cooling water to the reactor cavity in the event of a postulated severe accident. Water flows by gravity driving head from the IRWST to the HVT through four 12" diameter spillways, and it is then directed to the reactor cavity through two 10" diameter cavity spillways. The valves in the connecting pipes and spillways are motor operated. In the event of loss of offsite power, diesel generators and alternative AC power supplies can actuate the CFS valves. However, due to the concern for potential ex-vessel

steam explosions, the reactor cavity flooding can be delayed. It is stated in Reference [17] (page 3-21) that "....it is presently the intent of the accident management guidance to ensure that at least 5 feet of water is within the reactor cavity prior to vessel breach. To accomplish this goal, the operator must actuate the CFS prior to, or during the early phase of the severe accident progression." In addition, based on the information provided by the Nuclear Regulatory Commission (NRC) [18], the cavity water height can reach as high as 5.5 m above the cavity floor or approximately 0.46 m below the RPV.

The RPV is partially supported by the concrete corbels. Even though the cavity and the containment wall are not directly connected, there is a concern that a steam explosion-induced failure of the corbel supports and the cavity wall could ultimately lead to containment failure.

A structural analysis of the cavity region has been performed by CE [17] to estimate the structural capacity of the cavity wall and the corbel supports. This analysis shows that the corbel supports have a higher dynamic capacity compared to the cavity wall. It is asserted that the corbel supports can withstand a dynamic loading of at least 32 kPa-s (corresponding to zero probability of failure), whereas the corresponding value for the cavity wall is approximately 5 kPa-s as shown in Figure 4 (reproduced from Figure 3.6-3 of Reference [17]). The calculated median impulse capacity of the cavity wall is 22.6 kPa-s; however, the median capacity of the corbel supports which appears to be much higher is not provided in Reference [17].

Figure 5 shows a schematic of the cavity and the corbel supports for the CE System 80+. The radial distance from the center of the cavity to the corbel supports is approximately 1.5 m and the distance to the cavity wall is approximately 3.7 m. The corbel supports terminate at an elevation of 73+6 which is approximately 3.5 m above the cavity floor.

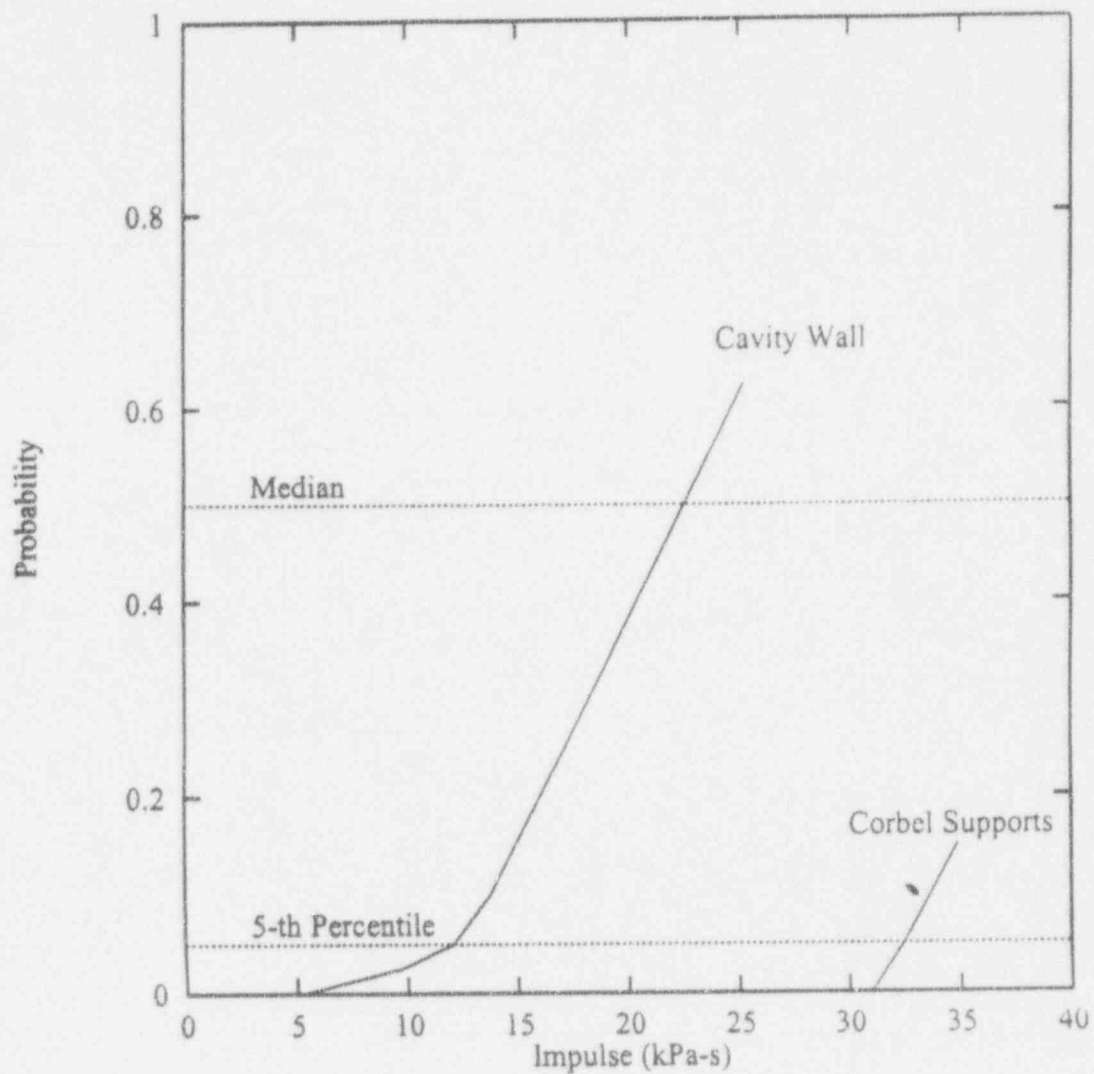


Figure 4 Fragility curves for the concrete cavity wall and corbel supports [17]

4. SPECIFICATION OF THE INITIAL AND BOUNDARY CONDITIONS

The delineation of the initial and boundary conditions involves the specification of the quantity, composition, and temperature of the molten debris in the lower plenum at the time of vessel breach, the mode, size, and the location of the lower head failure, the primary and containment system pressures at vessel breach, and the depth and temperature of the water pool in the lower cavity.

4.1 Containment and Primary System Pressures at Vessel Breach

A number of CE System 80+ specific MAAP calculations have been performed and are documented in Reference [17] for various transients including station blackout scenarios, large break LOCAs, small break LOCAs, total loss of feed water, steam generator tube ruptures and the V sequence. The containment pressure at the time of vessel breach based on these calculations can vary between approximately 0.1 MPa to 0.28 MPa depending on the scenario considered. In the present analysis, the containment pressure at the time of vessel breach is assumed to be 0.2 MPa. Note that small differences in the containment pressure at the time of vessel breach does not affect the resulting FCI energetics.

Plant-specific MAAP calculations [17] show that the primary system pressure at vessel breach is strongly dependent on the accident scenario. The MAAP-predicted RPV pressure at vessel breach is about ~ 17 MPa (full system pressure) for the station blackout sequences, ~ 2.8 MPa for the small break LOCAs, and < 0.3 MPa for large break LOCA scenarios.

Recent SCDAP/RELAP5 calculations in support of the DCH issue resolution for Surry and Zion plants (both Westinghouse designs) [19,16] have shown that most of severe accident scenarios (which are initially at high pressure) are not expected to progress to core meltdown at full system pressure, without temperature-induced failure of the pressure boundary. Natural circulation of hot steam and hydrogen within the degrading core, upper plenum, hot leg piping and the steam generator tubes could lead to high structural temperatures and ultimately creep-rupture of the pressure boundary at an ex-vessel RCS location. The failure of the pressure boundary could lead to primary system depressurization before vessel breach. In addition, the operators can intentionally depressurize the primary system before vessel breach thus mitigating the effects of the High Pressure Melt Ejection (HPME).

The SCDAP/RELAP5 results show a low probability for HPME in Zion during station blackout scenarios that progress without recovery and operator actions at full system pressure [16]. Most likely scenarios involve depressurization through the leaking pump seal, surge line or hot leg creep rupture-induced failure. Of course, higher probabilities were established for accident sequences involving Reactor Coolant Pump (RCP) seal leakage that progress at lower pressures (TMLB' sequences with 250 and 480 gpm leakage per pump). The results of SCDAP/RELAP5

calculations for Surry indicated that there was a low probability of HPME during TMLB' sequences without leakage and with seal leakage of 250 gpm per pump (higher probabilities are established for TMLB' sequences with pump seal leakage of 480 gpm). It should be noted here that in cases with a higher seal leakage (480 gpm per pump), the primary system pressure at vessel breach was low (1.36 MPa). The differences in the ex-vessel failure probabilities in Zion and Surry were attributed to differences in the bypass geometry and the relatively higher decay power density in Zion [16] (i.e., 33 MW_t/mt UO₂ in Zion versus 31 MW_t/mt UO₂ in Surry).

Table 4 gives a comparison of the design features of Surry [16] and CE System 80+ hot legs and the surge line [15]. The CE System 80+ core bypass geometry is similar to Surry, i.e., there are holes in the top of the core baffle plates below the upper core plate. The flow direction between the core barrel and core baffle is dependent on the geometry of the bypass (Zion has a downcomer bypass geometry which has holes in the core barrel below the upper core plate). This feature has a direct effect on the in-vessel natural circulation and the progression of core damage by providing a relatively cool return flow path for steam for Surry-like bypass geometries. The geometric characteristics of the hot leg and surge line in CE System 80+ are similar to Surry and given the higher power density in CE System 80+, the lower L/D in the hot leg, the potential for ex-vessel failure before lower head failure is expected to be at least as high as in Surry (it should be mentioned that the thermal diffusivity of carbon steel is approximately four times that of stainless steel and given the higher thickness of the hot leg in CE System 80+ and associated uncertainties in the temperature-induced failure of the hot leg, the results of the present assessment would not be greatly influenced by the different material).

Given the expected high failure probabilities in the hot leg/surge line for CE System 80+ (based on the comparison with Surry in the absence of any plant specific calculations), in the present analysis the primary system is assumed to be depressurized at the time of vessel breach, and the discharge of molten core debris from the R/FV into the reactor cavity is assumed to be primarily gravity driven. A sensitivity calculation under HPME will also be performed to assess the FCI energetics following vessel breach at higher system pressures.

Table 4 Comparison of the hot leg/surge line and bypass configurations between CE System 80+ [15] and Surry [16,20]

Design Parameter	CE System 80+	Surry
Bypass geometry	Surry-like	Holes in the top of the core baffle plates below the upper core plate
Hot Leg Design	Length (L) = 3.96 m Diameter (D) = 1.07 m L/D = 3.7 Thickness (t) = 0.112 m Material = Carbon steel	Length (L) = 7.7 m Diameter (D) = 0.74 m L/D = 10.4 Thickness (t) = 0.081 m Material = Stainless steel
Surge Line Design & Configuration	Length (L) = 22.1 m Diameter (D) = 0.257 m Thickness (t) = 0.033 m Material = Stainless Steel	Length (L) = 23.2 m Diameter (D) = 0.2668 m Thickness (t) = 0.0287 m Material = Stainless steel

4.2 Melt Initial Conditions in the Lower Plenum at Vessel Breach

The quantification of molten debris mass, composition and temperature in the lower plenum at vessel breach depends primarily on the accident scenario. Calculations performed to date using state-of-the-art severe accident analysis codes have shown large variations in the predicted quantity, composition, and temperature of the relocating core debris into the lower plenum.

Melt relocation to the lower plenum may be different under various accident sequences. In certain low pressure sequences, such as a loop seal LOCA, melt progression involves fuel clogging, limited in-core blockage formation, and failure of the grid plate below the core [21]. This sequence of events has been predicted to occur following a station blackout accident accompanied by a seal failure, using the MELPROG computer code [21]. Melt progression in high pressure sequences involves the formation of a melt crucible surrounded by a metallic crust that extends radially and axially in the core [21]. The failure of the crust leads to melt relocation to the lower plenum. Such a melt progression scenario is of interest, especially when the high pressure sequences turn into low pressure sequences after intentional or thermally-induced depressurization. However, a comparison of the results for the masses of solid and molten corium between the high and low pressure scenarios obtained from MELPROG simulations of these accident sequences [21] do not indicate large differences in the accumulating debris quantity in the lower plenum or in the quantity of ejected material following reactor vessel breach.

A survey by Levy [21] of the existing plant calculations revealed that the total amount of ejected material would be between 40 to 70% of the core weight. The ejected metallic content of the melt based on an early MELPROG calculation was estimated to be in the range of 30% to 70%; however, as suggested by Levy [21], a metallic content of 30% to 50% may be more realistic (due to the fact that in the MELPROG, the crust and lower grid plate took a very long time to fail thus involving a large amount of structural steel). The average temperature of the ejected material was assumed to be 2500 K.

The quantity and composition of corium in the lower plenum for the CE System 80+ are shown in Table 5. Table 5 is reproduced here from Table 4.1.1-1 of Reference [17] in which the debris masses were scaled based on the survey by Levy [21], with some minor adjustments (e.g., the mass distributions were conservatively assumed to reflect the higher content of zircaloy in CE System 80+). The total ejected mass range from 34 to 63 percent of the core inventory.

Recent analysis [16] have identified two accident sequences; namely, the Small Break Loss of Cooling Accident (SBLOCA) under wet core conditions, and a station blackout accident (TMLB') under dry core conditions, to envelope the range of initial conditions for DCH in Surry nuclear power plant. To arrive at a bounding estimate for the melt initial conditions, these two accident sequences were further divided into two additional scenarios giving a total of four scenarios as outlined below:

- Scenario I: SBLOCA sequences under wet core conditions (crucible formation and massive relocation to the lower plenum) with early penetration failure,
- Scenario II: SBLOCA sequences under wet core conditions (crucible formation and massive relocation to the lower plenum) with early rupture,
- Scenario III: TMLB' sequences under dry core conditions (temporary crust formation and gradual relocation to the lower plenum) with delayed penetration failure,
- Scenario IV: TMLB' sequences under dry core conditions (temporary crust formation and gradual relocation to the lower plenum) with late rupture,

Probability distributions were assigned to the masses of UO_2 and steel in the lower plenum, and fraction of Zr oxidized in-vessel using Risk Oriented Accident Analysis Methodology (ROAAM) by employing a physically-based probability scale [22]. The mass of ZrO_2 in the lower plenum was estimated based on the core wide fraction of Zr oxidized and the assumption that the amount of ZrO_2 in the melt was proportional to the ratio of the mass of molten UO_2 to the core inventory (79,800 kg of UO_2 in Surry). The total steel inventory including the upper and lower plenum steel structures was approximately 32,500 kg in Surry [16] (the upper and lower plenum steel inventory only involved the thin structures that are expected to melt).

Table 5 Debris initial conditions at vessel breach for CE System 80+ based on Reference [17]

Parameter	High Pressure (creep rupture failure)	High Pressure (Penetration failure)	Low Pressure (creep rupture failure)
Total Mass Ejected* (%)	40	34	63
Molten Fraction	0.815	1.0	0.445
Average Debris Temperature (K)	2500	2500	2500
Molten Mass Composition			
Steel (kg)	16,000	8,500	28,700
Zr (kg)	15,000	15,000	13,000
UO ₂ (kg)	24,000	34,300	5,000
ZrO ₂ (kg)	0	0	0
Solid Mass Composition			
Steel	0	0	0
UO ₂	12,200	0	59,100
ZrO ₂	0	0	0

* Based on the total core mass of 168,000 kg including lower support structure [17].

In ROAAM, a process likelihood of 1/10 was associated with behavior that is within known trends but was obtainable only at the edge-of-spectrum parameters, a process likelihood of 1/100 was associated with behavior which cannot be positively excluded but was outside the spectrum of reason, and a 1/1000 process likelihood was associated with physically unreasonable behavior (best estimate was assigned a process likelihood of 1). Therefore, given this probability scale, the lower bound, the best estimate, and upper bound ranges were expressed with uniform distributions. For example, in scenario I for Surry, the lower bound range for UO₂ mass was between 0 to 4,000 kg (i.e., values between 0 and 4,000 were given the same probabilities) with process likelihood of 1/100, the best estimate range was between 12,000 to 20,000 (based on the TMI-II accident) with process likelihood of 1, and the upper bound range was between 28,000 kg to 36,000 kg with process likelihood of 1/100 (note also that the assignment of these

probability distributions is purely subjective and Reference [16] is still undergoing peer review and will not be used as a basis for the present FCI analysis).

The debris temperature in the lower plenum at vessel breach for the different scenarios varied between 1900 K to 2800 K depending on the melt composition, and the maximum melt superheat was assumed to be approximately 200 K during relocation.

Table 6 shows the point estimates of the lower bound, the best estimate, and upper bound ranges for the melt mass in CE System 80+ scaled from Surry (i.e., the point estimate lower bound is the minimum value in the lower bound range, the point estimate value of the best estimate range is the average value of the range, and the point estimate value of the upper bound range is the maximum value in the upper bound range).

SCDAP/RELAP5 calculations [19] for a station blackout transient in Surry indicated that the debris composition at lower head failure would be mainly oxidic. The average composition of the debris in the lower plenum for all scenarios considered (TMLB' sequences with and without pump seal leakage) was primarily a mixture of UO_2 and ZrO_2 with weight fractions of 0.85 and 0.15, respectively. The molten fraction at vessel breach varied between 0 and 0.22. The fraction of UO_2 in the lower plenum varied between 7% to 70% of the core inventory. These calculations further indicated that melt superheat can be as high as 200 K at vessel breach. The current version of SCDAP/RELAP5 allows the user to parametrically control the heat transfer between the molten core and the coolant during relocation to the lower head (only two extremes of minimum and maximum debris/coolant heat transfer are allowed in SCDAP/RELAP5). The maximum superheat value of 200 K at lower head failure was predicted based on minimum debris/coolant heat transfer during relocation. A parametric variation of the debris/coolant heat transfer resulting in maximum debris/coolant heat transfer indicated a superheat value of 30 K.

Based on the aforementioned discussions and considering the uncertainties in the modeling of melt progression in the severe accident codes (e.g., MELPROG and SCDAP/RELAP5), the debris initial conditions for the current FCI analysis are presented in Table 7. The lower and upper bound debris masses are based on the results of the SCDAP/RELAP5 calculations for Surry [19] which showed large variations in the amount of accumulating debris in the lower plenum at vessel breach. In the present analysis, the lower bound corresponds to 10% of the core UO_2 inventory whereas the upper bound corresponds to 70% of the core UO_2 inventory and our best estimate for UO_2 mass in the lower plenum at vessel breach is 40% of the core inventory. The mass of ZrO_2 in the melt is based on the weight fractions of 0.85 (UO_2) and 0.15 (ZrO_2) in the mixture mentioned previously. The debris temperature in the lower plenum is estimated based on an average debris temperature in the SCDAP/RELAP5 parametric calculations [19] assuming a superheat value of 100 K based on the melting temperature of 2800 K.

Table 6 Estimate of debris initial conditions in CE System 80+ scaled from Surry DCH study [16]

	Scenario I			Scenario II		
	Lower Bound	Best Estimate	Upper Bound	Lower Bound	Best Estimate	Upper Bound
UO ₂ (kg)	0	24,000	54,000	0	13,500	43,600
ZrO ₂ (kg)	0	3,600	13,000	0	2,000	10,500
Zr (kg)	-	-	-	1,200	2,000	2,800
Steel (kg)	-	-	-	740	3,400	6,800
Total mass (kg)	0	27,600	67,000	1,940	20,900	63,700
Temperature (K)	2800			2500		

Table 6 Continued

	Scenario III			Scenario IV		
	Lower Bound	Best Estimate	Upper Bound	Lower Bound	Best Estimate	Upper Bound
UO ₂ (kg)	-	-	-	-	0	24,000
ZrO ₂ (kg)	-	-	-	-	0	7,100
Zr (kg)	-	-	-	-	0	4,600
Steel (kg) ^(a)	0	38,000	58,000	0	38,000	58,000
Total mass (kg)	0	38,000	58,000	0	38,000	93,700
Temperature (K)	1900			2350		

- (a) Since the mass of the thin upper plenum steel was unavailable, the current estimates are scaled from the lower plenum steel in CE System 80+ (29 mt) and Surry (10 mt), i.e., the point estimates of Surry are simply multiplied by 2.9.

In the initial conditions postulated here, the debris composition in the lower plenum is assumed to be mainly oxidic (in the Surry calculations [19], only small amounts of Zr and steel were

present in the debris pool). However, the metallic content of the debris can have a substantial impact on hydrogen generation and combustion. The hydrogen generation and combustion are important in the assessment of containment failure by DCH induced loads during HPME. However, in the present analysis of ex-vessel FCI, this phenomenon is not considered important in the assessment of dynamic pressure impulses since the variations in the melt thermophysical properties is considered to be of secondary importance given the uncertainties in the detonation models (it should be mentioned that experimental evidence suggest that noncondensable gas generation tends to stabilize the vapor film around the particle and mitigate the effects of coolant jet penetration and steam explosion).

Even though the core melt progression between the Zion/Surry plants and CE System 80+ is expected to be different in many details, the overall timing of the melt progression is similar according to Reference [17] (Reference [17] does not provide a validation of the assertion). For ex-vessel FCI analysis, the total mass and composition of the debris in the lower plenum is of secondary importance, since the time scale for FCI (a few seconds) is much shorter than DCH. The mass and thereby the height of the debris bed in the lower plenum can only affect the melt discharge velocity. Considering best estimate and upper bound values, the height of debris pool varies between 0.87 m to 1.17 m and thus, the melt discharge velocity varies between 4.1 m/s to 4.8 m/s assuming a melt density of $10,000 \text{ kg/m}^3$. Therefore, the difference in the melt discharge velocity is approximately 15% and this variation is not expected to impact the melt discharge time and the particle break up in the coolant pool. Therefore, for the purposes of calculating a characteristic point estimate melt discharge velocity, a velocity of 4.8 m/s corresponding to the upper bound value is assumed.

The melt temperature at vessel breach is also based on the temperatures for different scenarios in the SCDAP/RELAP5 calculations. The average melt temperature from these calculations is approximately 2900 K, and the debris is assumed to be superheated by 100 K based on a debris melting temperature of 2800 K.

4.3 Mode, Size and Location of Vessel Breach

An important consideration in the assessment of ex-vessel FCI energetics is the mode and size of the bottom head failure. There are two limiting conditions in the size of the bottom head failure, the first is the failure of instrument tube penetrations, and the second is the local rupture of the vessel bottom structure. Another consideration involves the location of the lower head failure.

Table 7 Postulated debris initial conditions in the lower plenum at vessel breach for CE System 80+ FCI analysis

	Lower Bound	Best Estimate	Upper Bound
UO ₂ (kg)	12,000	49,000	85,000
ZrO ₂ (kg)	2,000	9,000	15,000
Zr (kg)	0	100	260
Steel (kg)	0	0	0
Total mass (kg)	14,000	58,100	100,260
Temperature (K)	2900		

Rempe et al. [23] have analyzed the possibility of the lower head failure in a light water reactor based on three accident scenarios. Three debris conditions in the lower plenum were considered in their analysis. Case I involved a metallic slurry with an initial temperature of 2400 K and a constant heat flux of 0.015 MW/m² to the vessel. Case II involved a ceramic slurry with an initial temperature of 2800 K and a constant heat flux of 0.05 MW/m² to the vessel. Case III involved a ceramic molten pool with an initial temperature of 3113 K and a constant heat flux of 0.2 MW/m² to the vessel. The results of this investigation [23] indicated that for Case I (metallic slurry), neither penetration tube nor vessel failure was predicted. For Case II and III, vessel failure was predicted between 2 to 4 hours, and 30 minutes, respectively.

Pilch et al. [22] have quantified a range of hole sizes for determination of initial conditions towards DCH issue resolution in the Zion nuclear power plant. Two different hole sizes corresponding to a penetration failure (0.0254 m) and a creep rupture (0.4 m) were identified in their analysis. The creep rupture occurs from formation of hot spots in the lower head as a result of jet impingement or nonuniform heating of the lower head. According to Reference [22], the spacing between the lower head penetrations at Zion is approximately 0.5 m, and the maximum rupture size is not expected to exceed 0.4 m based on the assumption that the hot spot does not interact with the stress concentration field near the penetrations.

It should also be noted that during melt discharge, the failure area is expected to ablate and the final failure area would be larger. The DCH time scale is of the order of tens of seconds, whereas, for steam explosions the time scale is much shorter (of the order of 1 second). Thus, ablation is not expected to play a major role (also note that the rate of ablation is considerably lower in low pressure discharge of melt through the ablating hole). For the present analysis, hole ablation during melt discharge can be safely neglected without any loss of conservatism.

The size of an instrument tube penetration is 3 cm (see Appendix F of Reference [17]), and there are 61 such penetrations in the lower head of the reactor vessel in CE System 80+ as shown in Figure 6. The minimum spacing between the instrument tubes is approximately 0.2 m in the CE design and based on the rationale given by Pilch et al. [22], the initial rupture size in CE System 80+ would be approximately 0.2 m. However, to account for the uncertainties in the rupture size, a hole size of 0.4 m has been conservatively assumed for the present study. Based on this analysis, two scenarios are proposed to provide a limiting estimate of the dynamic pressures within the cavity. Scenario A represents an instrument tube penetration failure (0.03 m) while scenario B corresponds to a rupture size of 0.4 m.

Another uncertainty is the location of lower head failure. The failure location is important in the determination of the dynamics pressures and impulsive loads on the cavity boundaries especially if the failure location is close to the cavity wall and corbel supports. It is of less importance in the case of failure of multiple instrument tube penetrations and local rupture since the explosion zone is much larger compared to a single instrument tube penetration failure and a significant decay of pressure wave at the cavity wall and corbel supports is not expected. The location of the instrument tube penetration failure is dependent on the melt progression, volume of the melt on the lower head and method of melt delivery to the lower head.

If a crucible blockage forms in the central region of the core surrounded by lower and upper crusts (like in the TMI-II accident), the subsequent failure of the crust leads to melt delivery to the lower plenum. The location of failure of this crust can be either at the core support plate (bottom breach) or near the side at the core barrel. The latter is considered to be more probable at this time since the natural convection currents in a hemispherical molten pool are expected to transfer more heat to the lateral boundaries [22]. The one available piece of experimental evidence, i.e., the TMI-II accident, also indicates that lateral failure of the crust is more probable. If this is the case, only a small fraction of the molten pool will relocate to the lower plenum initially which is expected to collect at the center of the bottom head. Once a molten pool accumulates on the lower head, failure of the instrument tube(s) at the central region of the bottom head is expected to occur within a short time. It should also be mentioned that during melt relocation to the central region of the lower head, some limited ablation of the lower head may occur at any location where the melt first contacts the lower head.

If however, breach of the crucible occurs at the bottom, a massive pour is expected to occur and the entire contents of the crucible will quickly relocate to the lower head. Hence several instrument tube penetrations even farther away from the center will be submerged by the molten pool. In addition, even for the case of the side failure (of the crucible), if the central instrument tube penetrations do not fail before significant amount of debris has been formed in the lower plenum, the molten debris would accumulate covering the outermost instrument tube penetrations. Thus, although the failure of penetration tubes at the center is more probable than

failure of the penetrations away from the center, the latter case cannot be completely ruled out at the present time.

The outer instrument tube penetrations in the CE System 80+ lower vessel head are located approximately 1.5 m away from the central penetrations. The axial distance between the outer and the central penetrations in CE System 80+ is estimated to be approximately 0.45 m. Given the best estimate and upper bound melt masses in the lower plenum, the heights of the debris pool were approximately 0.87 m and 1.17 m, respectively. It was estimated that the outer instrument tube penetrations are expected to be submerged in the debris pool. Once the molten pool forms in the lower head, the natural convection within the molten pool would preferentially transfer heat to locations away from the bottom. Hence, heat up of the outer instrument tube penetrations are also probable and the failure of these penetrations are expected to be as likely as the central penetrations. However, for reasons outlined earlier (smaller melt pool relocation to the lower head due to side crust failure), failure of the central penetrations is expected to be more likely than the failure of the side penetrations. It should also be mentioned that if an outer instrument tube fails, the discharge velocity is expected to be lower compared to the central penetration (lower gravity head), however, the melt would accelerate covering this additional distance (0.45 m) and the melt jet velocity at the pool surface would be similar to the central penetration case.

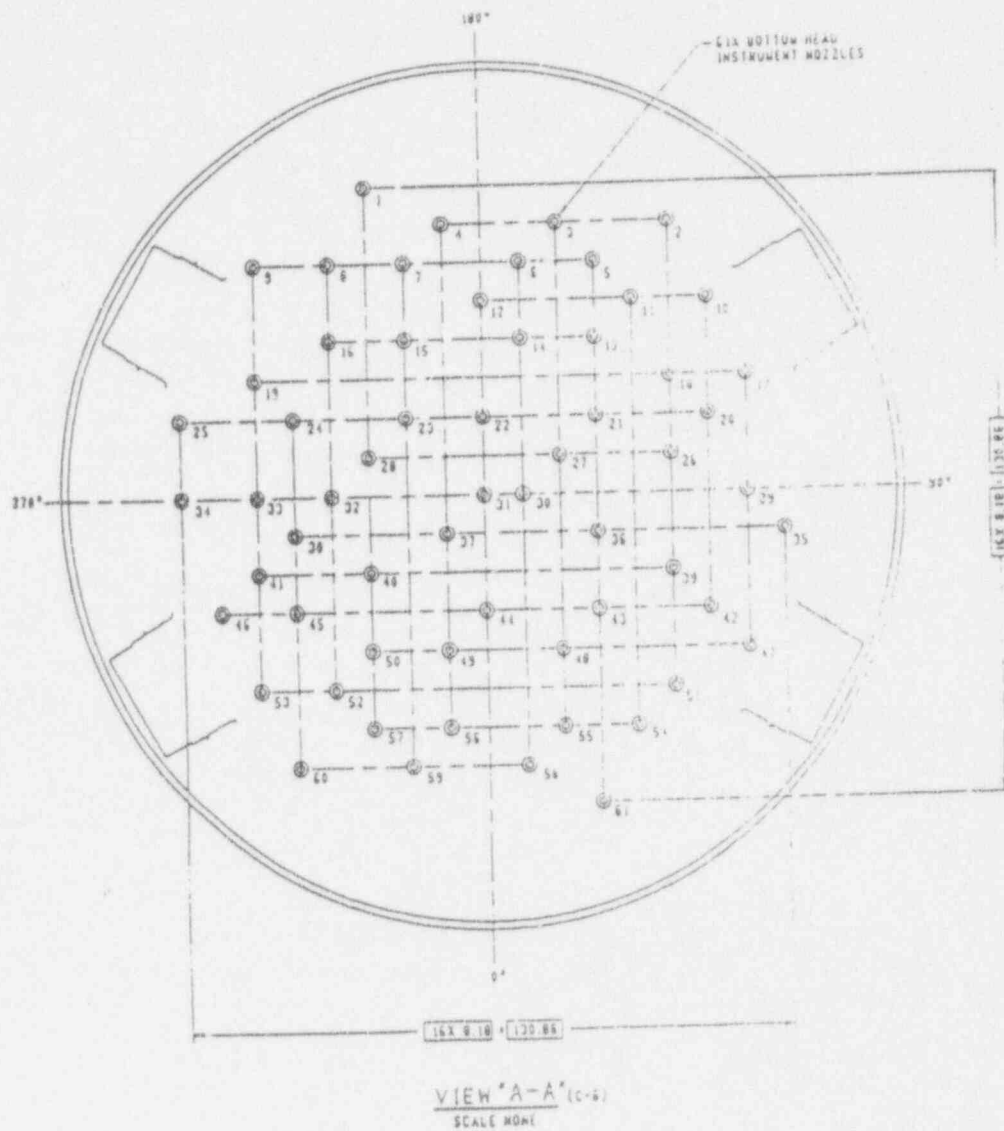


Figure 6 Schematic of the CE System 80+ lower head

The depth of the water pool in the cavity may be different under various accident sequences, i.e., the amount of the water in the cavity may be at condensate level or the cavity may be deeply flooded. The source of deeply flooded cavities is through CFS that is initiated by operator action to cool the debris and mitigate the effects of fission product release. As mentioned previously, the height of the water pool in the cavity can reach as high as 5.5 m which is taken as the base case. In addition, a water pool height of 3 m is also chosen to study the fuel-coolant interaction that occur primarily below the corbel region.

The source of cavity water in the case of deeply flooded condition is the water inventory in the IRWST, and the water temperature is expected to be subcooled. For a containment pressure of 0.2 MPa at vessel failure, the partial pressure of steam is approximately 0.08 MPa and the saturation temperature corresponding to this partial pressure is 367 K. The water pool in the IRWST and the steam-air mixture above it are assumed to be at thermal and mechanical equilibrium (i.e., equal temperatures and pressures). Therefore, the temperature of the water pool can be as high as 367 K and including the effect of thermal stratification, the bulk temperature of the water in the IRWST is assumed to be lower. For the present analysis, a pool temperature of 353 K is assumed, and given the containment pressure of 0.2 MPa at vessel breach, the water pool is assumed to be subcooled by approximately 40 K.

Table 8 presents the base case initial conditions for the FCI calculations for the two scenarios corresponding to a penetration failure and a rupture failure. The corium discharge is assumed to be gravity-driven. For the purpose of determining the melt pour rate, even though some of the core debris may be solid, it is assumed that the molten pool volume corresponds to the mass of the entire debris inventory in the lower plenum (it is not known whether the solid materials are stratified or completely mixed within the debris). Assuming a corium mass of 100,000 kg (based on the upper bound value given in Table 7) in the lower plenum and a corium density of 10,000 kg/m³, the height of the corium inventory in the reactor vessel lower plenum (diameter of approximately 5.4 m [17]) is estimated to be 1.17 m. The corium discharge velocity at vessel breach is calculated using:

$$U_o = \left[2g\Delta z + \frac{2\Delta P}{\rho} \right]^{1/2} \quad (3)$$

where Δz is the corium height in the lower plenum, ΔP is the pressure difference between the reactor vessel and the cavity at vessel breach, ρ is the corium density, and g is the acceleration due to gravity (ΔP is zero for the base case). It should also be pointed out that the actual mass

of the debris in the lower plenum has only a small impact on the fuel-coolant interaction (see subsection 4.2).

The melt temperature in the present analysis was taken to be 2900 K (with a superheat value of 100 K) based on the melt composition and temperature from the recent results of SCDAP/RELAP5 calculations for the Surry plant [19].

Although it is known that ablation can occur during the course of melt discharge, it is not possible to include the variations of melt discharge velocity and vessel breach area with time in the calculations since there are no provisions for the inclusion of an ablating penetration failure in the computer code models. For the purpose of the present analysis, the reactor vessel was assumed to be depressurized at the time of vessel breach and the melt discharge is gravity-driven. An estimate of the hole ablation for the CE System 80+ was performed based on the analysis in Reference [21]. For the gravity-driven melt discharge through the ablating penetration (the case considered here), the rate of ablation was much smaller than the high pressure case analyzed in Reference [21]. During the first few seconds of the interaction, the hole radius was estimated to be increased by less than 10%. Since the FCI would most likely occur early in the melt release, a fixed diameter hole size is not a serious limitation.

As mentioned previously, the information provided by CE to the NRC suggests that the depth of the water pool in the reactor cavity during severe accident conditions could be as high as 5.5 m, hence a 5.5 m pool depth is chosen for the base case calculations. However, a water pool depth of 3 m is also included in the present calculations to determine the impact of the fuel-coolant interaction energetics below the corbel region as part of the sensitivity calculation.

Table 9 shows the variations of the initial conditions (from the base case) for the sensitivity calculations in the present assessment using both TEXAS and IFCI computer codes. Note that in the case of IFCI, only the water pool depth of 3 m was considered; it was felt that other sensitivity calculations would not be useful until a complete resolution of the known IFCI computer code numerical deficiencies [14] (e.g., finer radial nodalization) and validation of the explosion model have been performed. The IFCI computer code was used here mainly to assess the radial spreading of the melt in the pool in order to determine the mesh cross-sectional area in the one-dimensional TEXAS calculations, and to estimate the decay of the explosion pressure (and the pressure impulse) away from the explosion zone. A number of sensitivity calculations that were not believed to be important for TEXAS calculations in Scenario B were not performed including the pool depth of 4.5 m and melt superheat of 200 K. The higher number of penetration failures would not be relevant in the case of Scenario B. However, the TEXAS calculations for Scenario B included an additional sensitivity calculation with higher initial melt velocity (15 m/s). This initial velocity corresponds to a pressure difference of approximately 1.2 MPa between the primary system (1.36 MPa) and the containment (0.2 MPa). The primary system pressure was chosen based on the results of the SCDAP/RELAP5 calculations [19] for

Table 9 Summary of the sensitivity calculations

Sensitivity Cases		TEXAS		IFCI	
		Sc-A	Sc-B	Sc-A	Sc-B
S-1	Pool Depth = 3 m	✓	✓	✓	✓
S-2	Pool Depth = 4.5 m	✓			
S-3	Melt Superheat = 200 K	✓			
S-4	Number of Penetration Failures = 8	✓	N/A		N/A
S-5	Initial Melt Velocity = 8 m/s	✓			
S-6	Initial Melt Velocity = 15 m/s		✓		
S-7	Pool Temperature = 393 K, Saturated	✓	✓		

a pump seal leakage of 480 gpm. As mentioned previously, the probability of ex-vessel failure in Surry was high (between 0.98 and 1) for all TMLB' sequences except for the sequence involving the 480 gpm seal leakage. However, for this sequence, the primary system pressure at the time of lower head failure was low (1.36 MPa), and consequently this case was chosen to represent the HPME in the present FCI analysis.

Table 8 Summary of initial conditions for the base case

Properties	Scenario A	Scenario B
Melt discharge velocity (m/s)	4.8	4.8
Melt Release rate (m ³ /min)	0.21	36
Melt Mass Flow Rate (kg/s)	35	6000
Melt Mass in Lower Plenum at Vessel Breach (kg)	100,000	100,000
Debris Temperature (K)	2900	2900
Debris Superheat (K)	100	100
Hole size (m)	0.03	0.4
Water pool height (m)	5.5	5.5
Failure Mode	single instrument tube	creep rupture

5. ASSESSMENT OF FCI ENERGISTICS FOR CE SYSTEM 80+

In this section the results of ex-vessel FCI calculations using the TEXAS and IFCI computer codes are presented. The two cases considered represent a single instrument tube penetration (Scenario A) and a rupture failure (Scenario B) of the RPV lower head.

5.1 Scenario A

5.1.1 Base Case Calculations

Within a one-dimensional simulation framework employed in TEXAS, the extent of particle dispersion and mixing in the surrounding coolant cannot be known *a priori*. Therefore, it was decided to perform a mixing calculation with the two-dimensional IFCI computer code. A cylindrical geometry was considered for the IFCI calculation. In order to obtain an estimate of the radial spreading of the corium jet, it was not necessary to simulate the entire cavity geometry since it was assumed that the melt would pour into the central region. The height of the cylindrical computational domain was 3 m and the depth of the water pool was 2 m (this pool depth was considered based on the observation that after 1 second the melt jet penetrates approximately 2 m into the water pool) and the radius of the cylinder was set to 0.5 m (this radius was based on the judgement that at this radial distance the interaction of the melt jet with cylinder wall was insignificant). The radius of the jet was 0.015 m. The nodalization of the computational domain involved 12 uniform axial nodes ($\Delta z = 0.25$ m), and 6 nonuniform radial nodes ($\Delta r = 0.015, 0.015, 0.02, 0.1, 0.1, 0.25$) which allowed a finer radial nodalization near the melt jet. The melt was poured at the top of the computational domain in the innermost radial node, and a constant pressure boundary condition was specified in the outermost radial node at the top of the computational domain. The initial and boundary conditions represented the base case for this simulation.

Figure 7 shows the vapor void fraction and the melt volume fraction in the water pool at the end of the premixing calculation using the IFCI computer code. It took the melt approximately 1 second to travel the 2 m depth of the pool. It can be observed during this time that the melt primarily remains in the central region of the water pool. The vapor void fraction was highest near the centerline and gradually decreased away from the interaction zone. The maximum radial spreading of the melt in the water pool was approximately 0.15 m. The cross-section of the interaction zone during this time frame is approximately 0.07 m^2 . Therefore, for the purposes of performing one-dimensional TEXAS calculations, a conservative cross-sectional area of 0.2 m^2 was selected (decreasing the mesh cross-sectional area would increase the local void fraction leading to lower dynamic pressures). The two-dimensional IFCI calculation alleviated the need to perform parametric area calculations using TEXAS by providing a more reasonable estimate of the interaction zone.

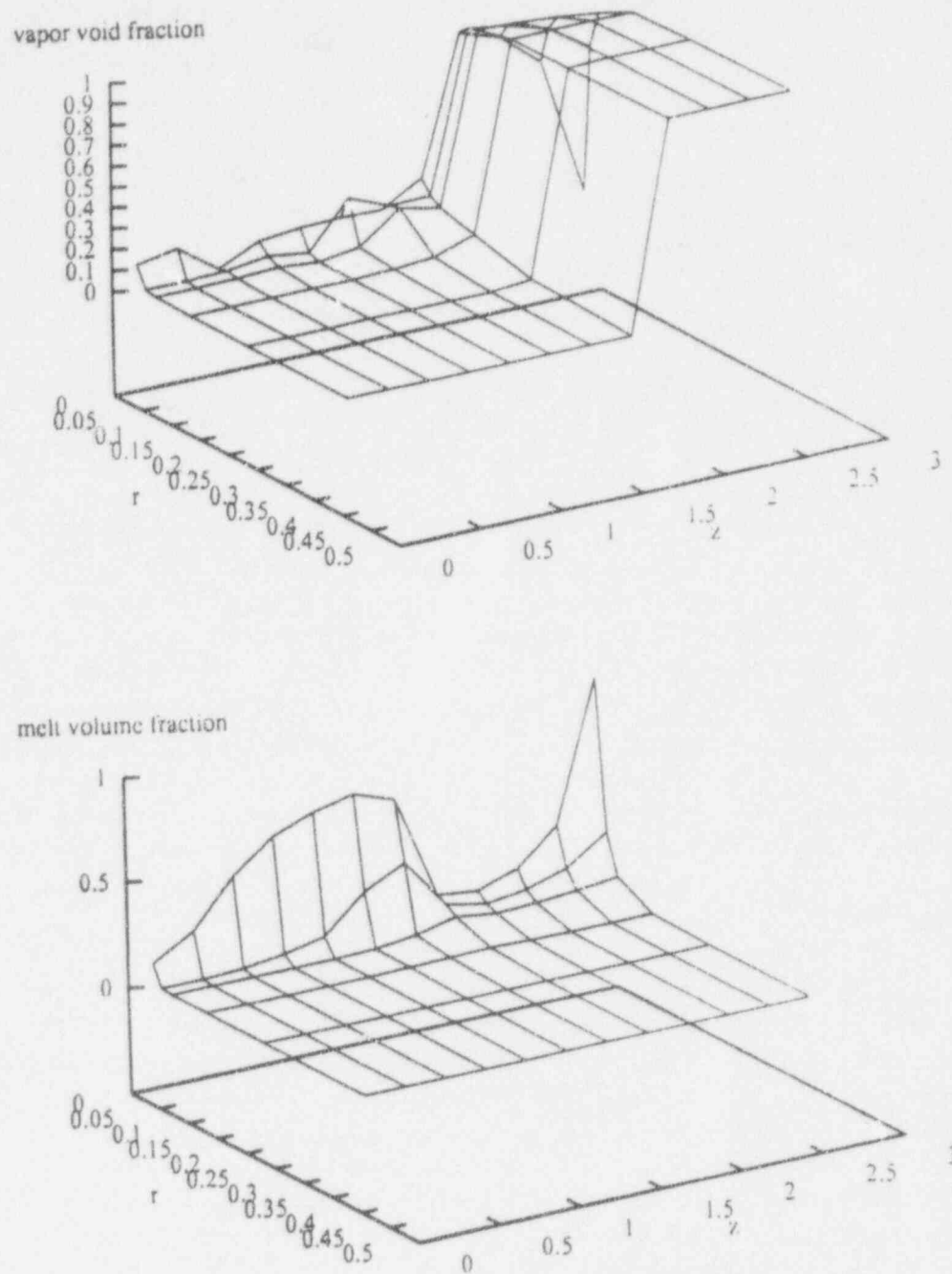


Figure 7 Predicted vapor void fraction and melt volume fraction at the end of the premixing calculation using IFCI computer code with nonuniform radial nodalization for the base case in Scenario A

Comparison of Figures 8 and 10 show that at a later time of 2 seconds the vapor void fraction in the water pool was considerably increased. During this time period, the particles exchanged energy with the coolant and lost some of their thermal energy. Also more particles solidified after 2 seconds of mixing compared with 1 second of mixing. Consequently, these particles did not participate in the explosion process. Even though after 2 seconds of interaction the mass of melt in the water pool was twice the amount after the 1 second interaction period, the pressure impulses were lower (due to the combined effects of particle quenching and higher vapor void fraction). The total mass of fragmented fuel during the propagation phase was approximately 1.6 kg which was lower than the previous case. Table 10 shows the comparison of pressure impulses for the 1 and 2 seconds of premixing calculations. The sensitivity calculations will be performed for 1 second of premixing given the uncertainties in the triggering time (note that for the 1 second premixing calculation, higher impulses were observed).

Table 10 Predicted pressure impulse for the base case in scenario A using TEXAS computer code

Axial Distance, z (m)	Pressure Impulse (kPa-s)	
	1 second of premixing	2 seconds of premixing
4.4	42	26
4.6	37	19
4.9	27	12
5.1	12	4

The corbel supports extend from approximately 3.5 m from the bottom of the cavity to the bottom of the reactor vessel (see Figure 5) which is approximately 6 m above the cavity floor, and with a pool depth of 5.5 m, only the upper 2 m of the pool are in the corbel support region. The TEXAS calculation for Scenario A further indicated that the melt would remain primarily in the upper 2 m of the pool during the premixing phase of the interaction (duration of 1 sec) before the melt particles started to quench. Therefore, in the present FCI model, the pool was modelled as a 2.5 m high cylindrical computational domain with 8 axial nodes (0.25 m) in the water pool to assess the FCI energetics in the corbel support region. The radial size of the computational domain was 1.5 m, and the radial nodalization employed 6 equally-spaced radial cells (0.25 m size). This was in contrast to the previous calculation (Figure 7) where the radial size of the computational domain was 0.5 m, and a finer nodalization was used near the melt jet. Using the same fine nodalization required more radial nodes which would cause numerical difficulties.

In the TEXAS computer model for Scenario A, the axial mesh size was selected to be 0.25 m with a cross-sectional area of 0.2 m². The constant of proportionality, C_{fr} , and particle fragmentation time, τ_{fr} , were chosen to be 0.0015 and 2 ms, respectively. The melt was poured into the water pool and was allowed to mix with the coolant for 1 second before the explosion was triggered. This premixing time was chosen based on the observation that any shorter time would yield smaller pressures due to smaller amount of fuel that could mix with the coolant, and a longer time resulted in the quenching of the fuel particles as they travelled down the water pool. During this time, the particles remained in the upper 2 m of the pool (above the corbel support region). As the particle size became smaller due to particle breakup during the mixing phase of the interaction, they experienced increased drag and would not be able to penetrate to the bottom of the pool before they were quenched.

Figures 8 and 9 show the simulation results for a mixing calculation of 1 second duration. During this time, the coherent jet was broken up into smaller particles. As the particles moved downward in the water pool they began to quench. During the 1 second interaction period, the particles remained in the upper part of the water pool. The time of the explosion trigger was assumed to be 1 second after the corium jet entry into the water pool. This was judged to be appropriate based on the interpretation that the explosion would most likely be triggered at or near the time of contact with the basemat floor or where the fuel debris began to quench in their passage through the water pool. The former limit has been observed empirically in experiments due to the postulated effect of the bottom surface allowing for water entrapment. The latter criterion of fuel debris quench was also empirically observed and was postulated to occur because a spontaneous film boiling collapse would trigger the explosion locally. If the trigger time is decreased, the void fraction in the pool and the corium mass mixed with water will also decrease. The reduction in void fraction tends to increase the local pressures and thus the impulsive loads because a smaller void fraction reduces the mixture compressibility leading to higher pressures. On the other hand, the reduction in participating corium mass tends to decrease the impulse load because there is less fuel available to thermally drive the explosion. If the time at which the explosion is triggered is reduced (thus reducing the premixing time), the local vapor void fraction and the mass of solidified particles would also decrease which could lead to higher explosion pressures.

The maximum vapor void fraction was approximately 0.6 as shown in Figure 8 and the explosion pressures at various axial distances from the bottom of the pool are shown in Figure 9. The total mass of fragmented fuel during the propagation phase was approximately 2.8 kg. The pressure impulses at these axial locations were obtained by time integration of the transient pressure history.

In order to investigate the effects of mixing time (before the explosion is triggered), a TEXAS simulation with a mixing time of 2 seconds was also performed. The results of TEXAS simulation for the premixing time of 2 seconds duration are shown in Figures 10 and 11.

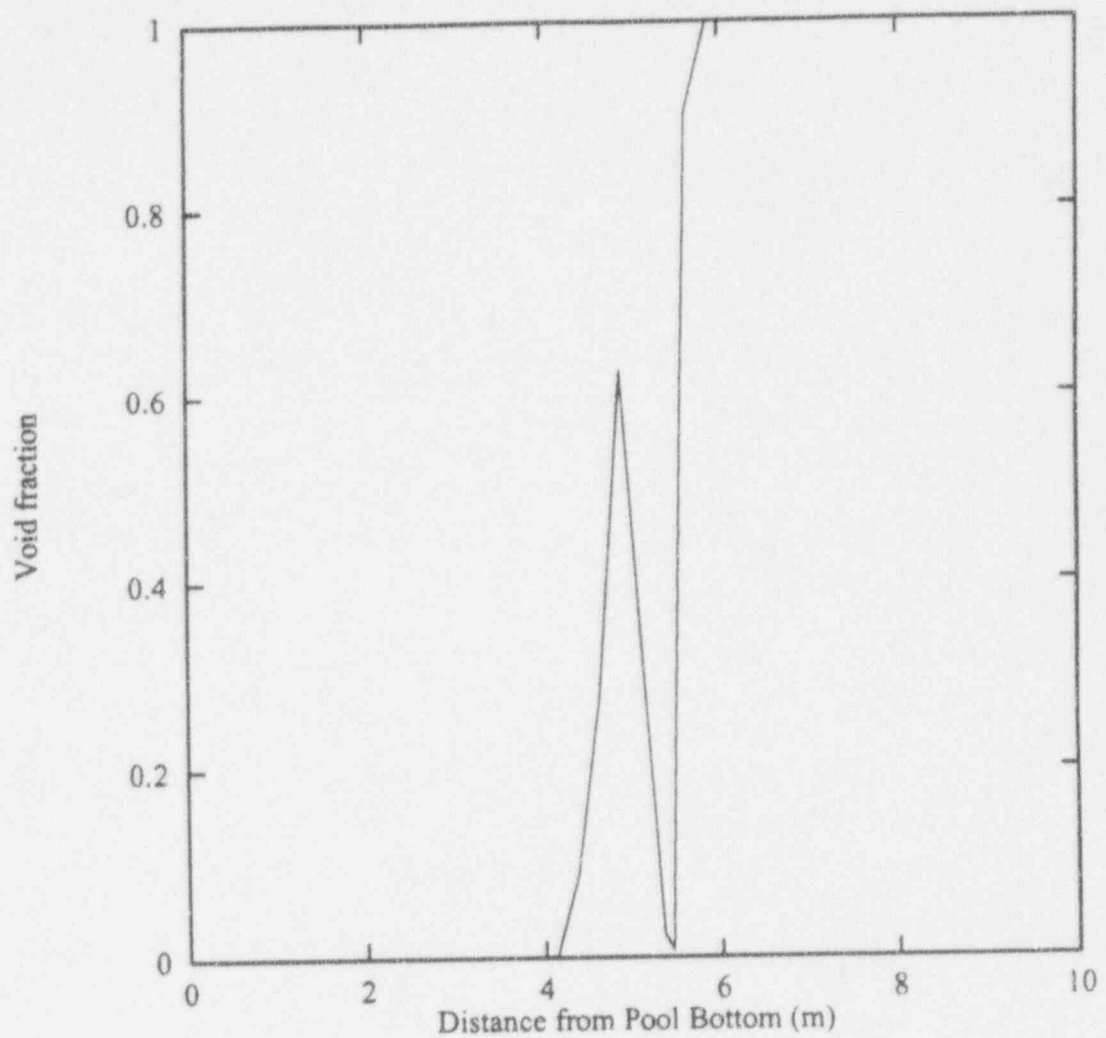


Figure 8 Predicted vapor void fraction at the end of premixing calculation (1 second) using TEXAS computer code (scenario A, base case)

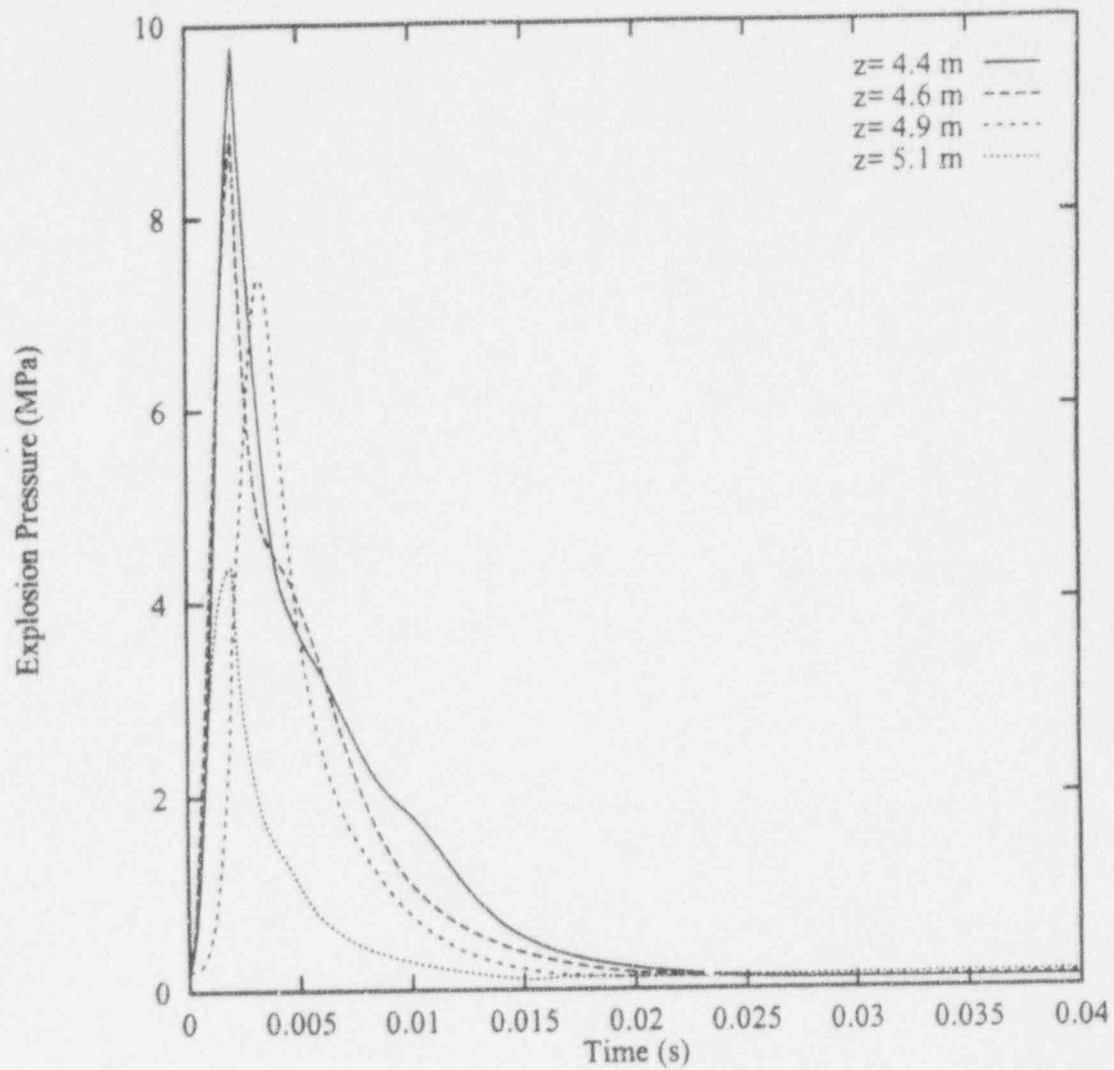


Figure 9 Predicted explosion pressure history at different axial locations using TEXAS computer code after 1 second of premixing (scenario A, base case)

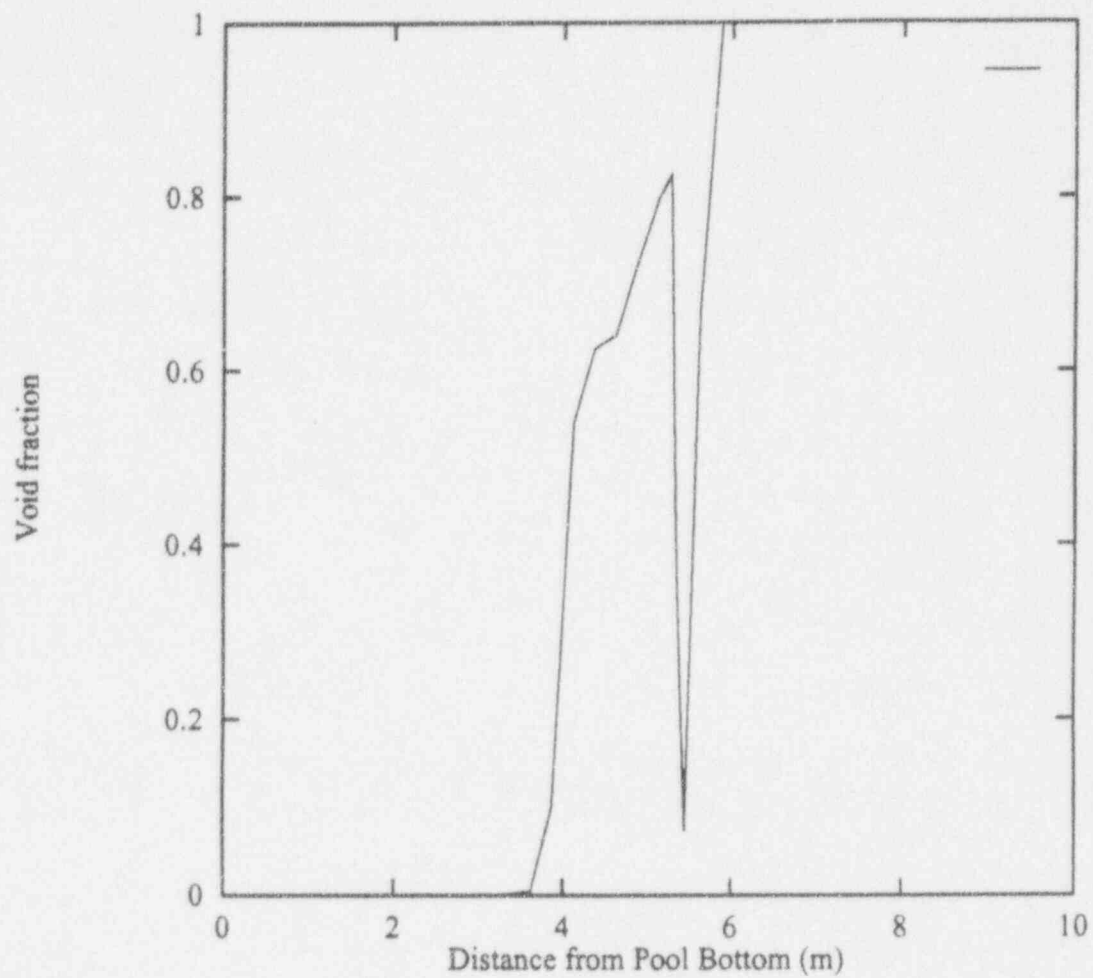


Figure 10 Predicted vapor void fraction at the end of premixing calculation (2 seconds) using TEXAS computer code (scenario A, base case)

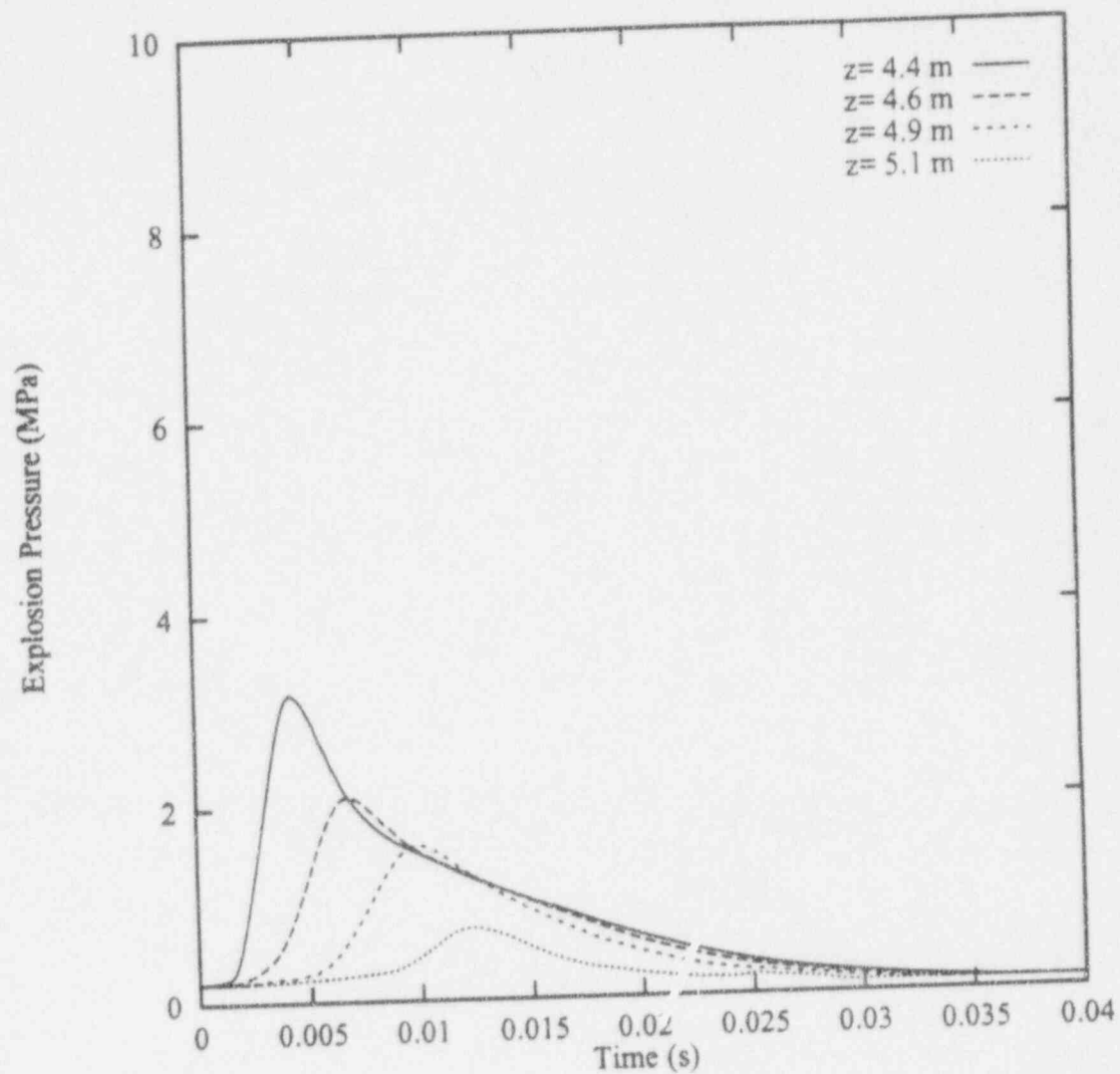


Figure 11 Predicted explosion pressure history at different axial locations using TEXAS computer code after 2 seconds of premixing (scenario A, base case)

In this IFCI simulation, the first radial node corresponded to the same mesh cross-sectional area as in the TEXAS calculation and the axial nodalization were also similar in the two calculations. The melt was poured in the first radial ring at the top of the computational domain and it took the melt approximately 1 second to travel to the bottom of the corbel supports region which was similar to the TEXAS prediction.

Figure 12 shows the vapor void fraction and the melt volume fraction in the coolant pool (the axial coordinate, z , indicates the distance from the bottom of cavity and the radial coordinate, r , indicates the radial distance from the center of the cavity). The maximum vapor void fraction in the TEXAS calculation was 0.6, however, the IFCI predicts a much smaller vapor fraction. In the IFCI calculation for the base case, the minimum melt diameter was approximately 12 mm as compared to 4 mm in the TEXAS calculation, and a smaller melt diameter during particle breakup produces a higher heat transfer surface area between the melt and coolant for the similar melt conditions (melt mass and temperature). Thus, the higher vapor void fraction in the TEXAS simulation can be attributed to the more efficient particle breakup and increased surface area. The melt mass in the computational domain at the end of the premixing run was similar to the TEXAS calculation (~ 35 kg). The melt volume fraction decreases from the top of the pool and extends to 3.5 m above the cavity floor. This figure also indicates that the melt remains primarily in the central ring. The explosion was triggered from this premixing condition by specifying a pressure trigger threshold value of 0.22 MPa and a particle fragment size of 0.1 mm.

Figures 13 and 14 show the explosion pressures at various axial locations. The maximum explosion pressure in the inner node (radius of 0.25 m) was approximately 24 MPa occurring near the top of the coolant pool ($z=5.1$ m), while the maximum explosion pressure at the wall was approximately 9 MPa (radius of 1.5 m) which occurred at $z=4.9$ m. Table 11 lists the comparison of the predicted pressure impulses at various axial locations using TEXAS (1 second of premixing) and IFCI computer codes. A number of observations regarding the comparison of the predicted pressure impulses and radial decay of pressure impulse are in order.

1. The maximum pressure and pressure impulse in the IFCI calculations appeared to decay radially by a factor of approximately 2.5 from the inner node to the outer node (wall).
2. The nodalization in the IFCI calculations may be considered coarse for the prediction of the explosion propagation. Increasing the radial nodalization (which is important for the prediction of radial decay of pressure) would always produce numerical errors (see next section). Ideally, one should explore the effects of nodalization in the prediction of explosion pressure and the maximum pressure, and given the current radial nodalization deficiency in IFCI, it was not possible to perform sensitivity calculations with different number of radial nodes.

3. The maximum local pressure impulses from the IFCI (39 kPa-s) and TEXAS (42 kPa-s) computer codes showed good agreement. However, the axial locations in the two codes were not similar (for example, TEXAS predicted higher pressures and pressure impulses at lower location in the coolant pool, while the IFCI predictions are the opposite which could be due to variations in the local void fractions and differences in the explosion model). The maximum radial decay of pressure and pressure impulse in the IFCI calculations did not occur at the same axial locations, which is not surprising considering the fact that the pressure wave expansion and radial decay would not necessarily occur at the same axial location.

Based on the above discussion, the prediction and quantitative decay of the pressure wave require finer nodalization in IFCI.

Table 11 Comparison of the pressure impulse for the base case condition in scenario A

Axial Distance, z (m)	Pressure Impulse (kPa-s)		
	TEXAS	IFCI	
		Inner Nodes	Wall Nodes
4.4	42	20	15
4.6	37	22	12
4.9	27	26	13
5.1	12	39	9
5.4	-	25	3

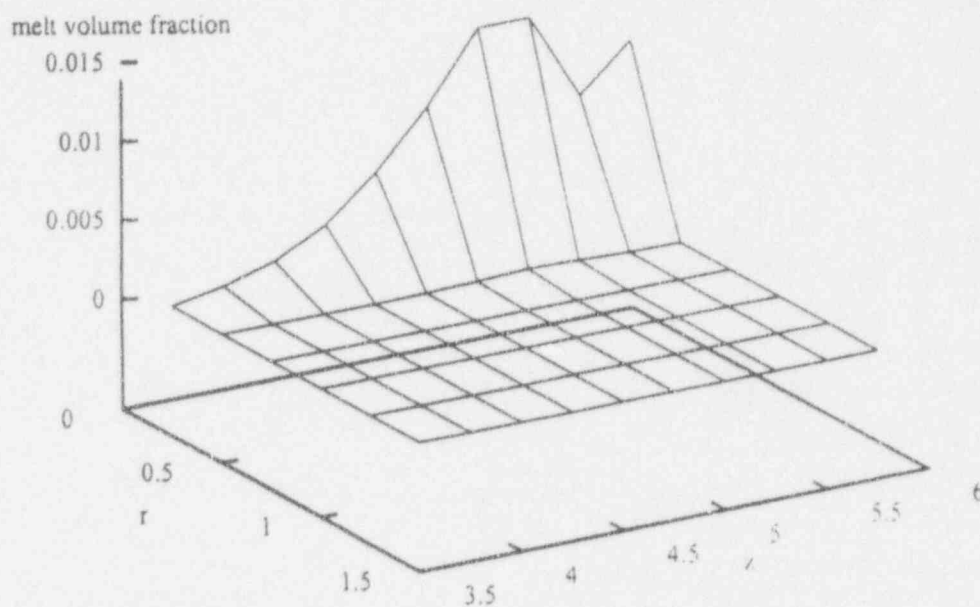
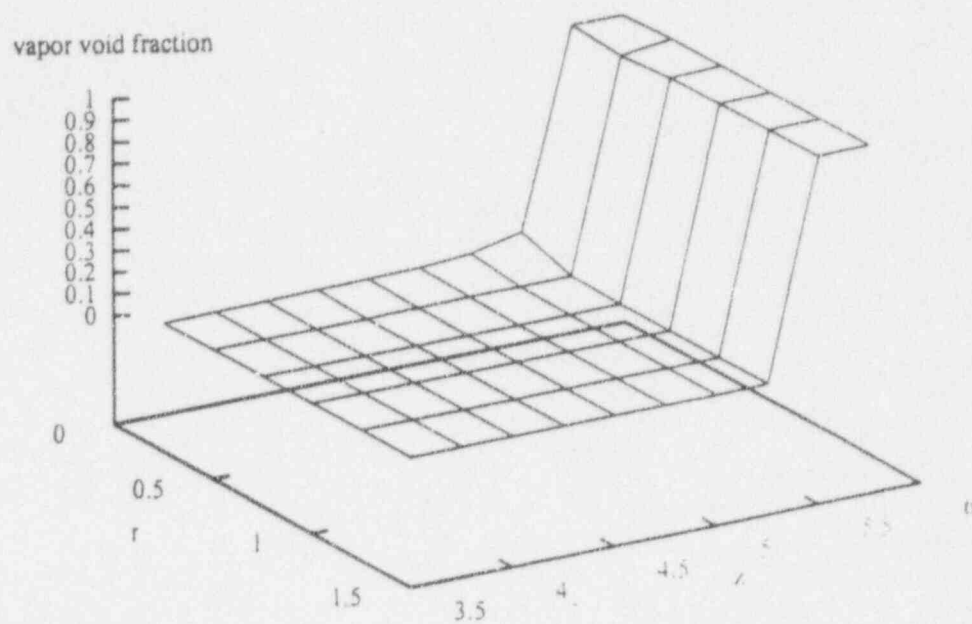


Figure 12 Predicted vapor void fraction and melt volume fraction at the end of the premixing calculation using IFCI computer code (scenario A, base case)

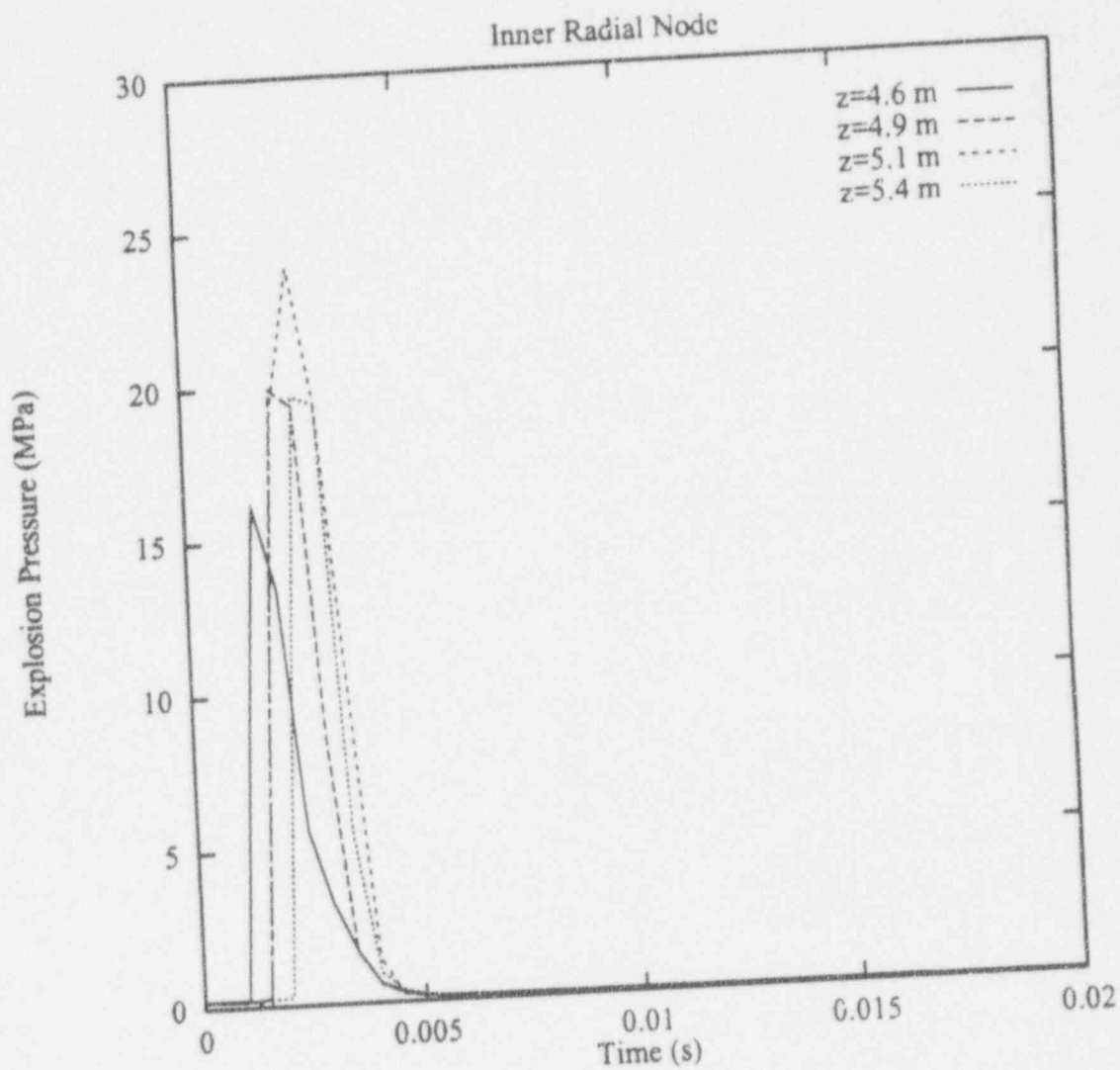


Figure 13 Predicted explosion pressure history at different axial locations in the inner radial node using IFCI computer code (scenario A, base case)

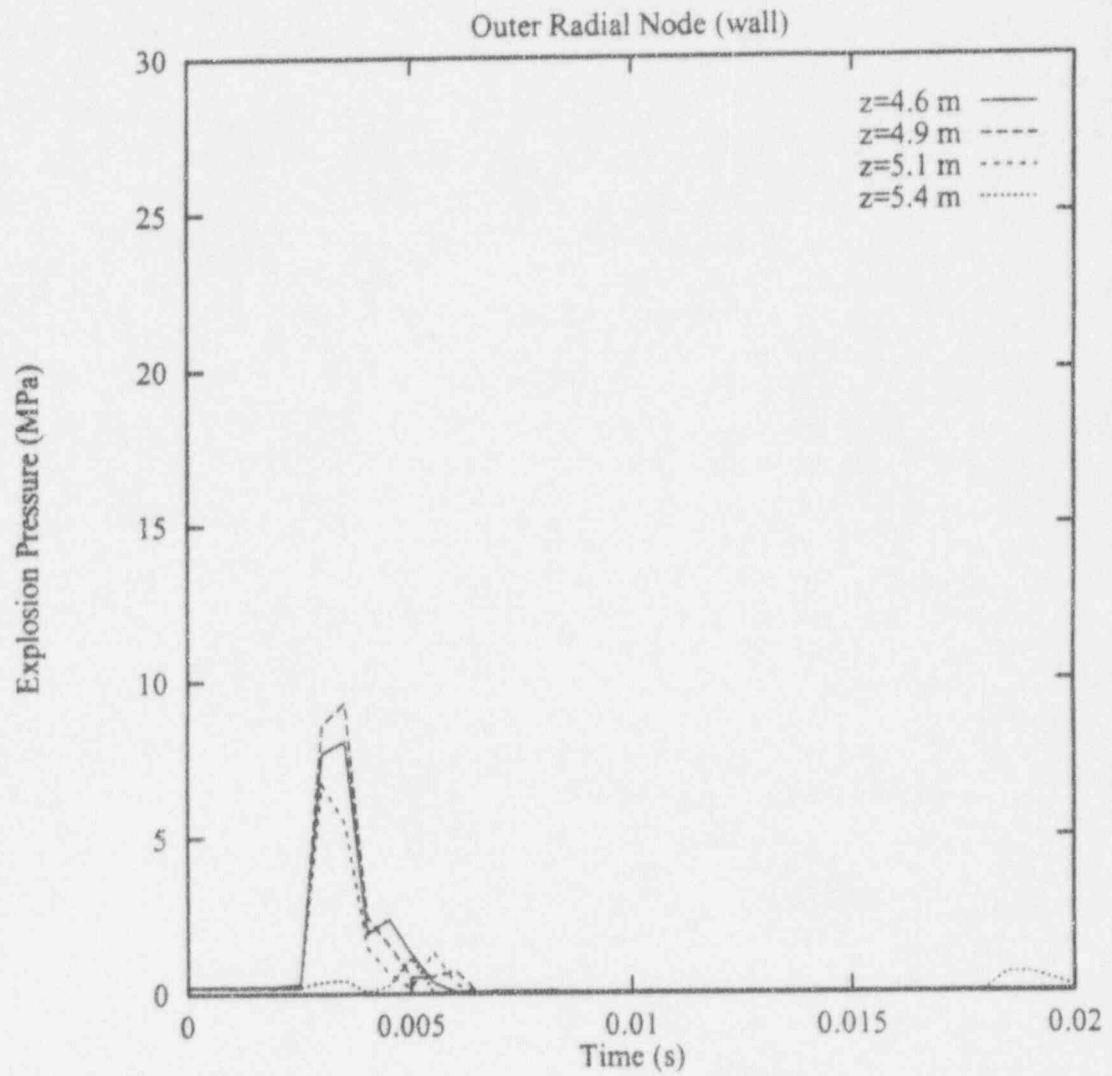


Figure 14 Predicted explosion pressure history at different axial locations in the outer radial node (wall) using IFCI computer code (scenario A, base case)

5.1.2

Sensitivity Calculations

5.1.2.1

Sensitivity to the Water Pool Depth of 3 m (S-1)

Even though the simulations with a pool depth of 3 m were categorized as sensitivity calculations, they are important in the assessment of the pressure impulse loads on the cavity wall below the corbel support region. Both TEXAS and IFCI calculations have been performed to examine the range of dynamic pressures that would be obtained. IFCI was used primarily to assess qualitatively the pressure wave decay with radial distance below the corbel support region.

The results of TEXAS calculation for the 3 m water pool depth are shown in Figures 15 and 16. In this case, the jet velocity at the water surface was approximately 67% higher than the base case calculation, and the jet diameter was approximately reduced by 25%. Figure 15 shows the void fraction in the water pool as a function of distance from the bottom of the pool. The maximum local void fraction was 30% higher than the base case. The increase in the void fraction in this case was due to higher particle fragmentation during the mixing calculation. The particle fragmentation depends on the relative velocity between the particle and the coolant. Even though the initial radius of the jet was lower than in the base case, the final fragmented particle area in contact with the water coolant was higher than the base case due to higher particle fragmentation induced by higher relative velocity between the particle and the coolant. As mentioned previously, an increase in the local void fraction tends to decrease the peak pressure during the propagation phase of the interaction. Figure 16 shows the explosion pressures as a function of distance from the bottom of the pool in the fuel-coolant mixture region. The peak pressure in this case was approximately 16 MPa and occurred at an axial distance of 2.1 m from the bottom of the pool, however, the maximum explosion pressures at axial distances of 2.4 m and 2.6 m were substantially lower. The reason for the peak pressure of 16 MPa at 2.1 m is the fact that the particle fragmentation was higher at this location. The total mass of the particles fragmented during the propagation phase of the interaction was approximately 2.1 kg which was lower than the base case. However, approximately 95% of the fragmented particles were at the axial location of 2.1 m.

In the IFCI model for this sensitivity calculation, the cavity was modelled as a cylindrical geometry with a radius of 3.5 m and a height of 6 m to determine the expected pressure loads on the cavity wall below the corbel support region. A total number of 24 axial nodes ($\Delta z = 0.25$ m), and 5 equally-spaced radial nodes ($\Delta r = 0.7$ m) were chosen for this calculation with 12 axial nodes in the water pool. The radial nodalization was extremely coarse, however, an attempt to double the number of radial nodes produced numerical errors during premixing. The same numerical difficulties have also been encountered during the FARO calculations in the IFCI operational assessment report [14] (these difficulties appeared to be related to the rate of vaporization and time step control as stated in Reference [14]). A number of strategies were tried as suggested in Reference [14]. These included reducing the convergence criteria on the

pressure iteration calculation from 10^{-4} used in the base calculations to 10^{-6} . This variation did not affect the final results, and the simulation would terminate as result of iteration failure and prediction of negative volume fractions in the computational domain. The compressibility of the coolant pool was varied by introducing between 0.1-1 % vapor in the coolant pool which was also unsuccessful. The maximum number of pressure iterations was doubled from the suggested value of 10 to 20 and again the same numerical difficulties were encountered. The maximum time step in the problem was kept at 10^{-5} s and not allowed to increase during the calculation, however, this sensitivity also produced the same numerical problems. Given these numerical difficulties, it was decided to proceed with the nominal calculations using only 5 radial nodes. Even though one could increase the number of radial nodes to greater than 5 nodes to determine the highest number of radial nodes for which the calculation would proceed, this exercise would not considerably change the results of the calculation since even 10 radial nodes was considered to be coarse.

The melt was poured into the inner radial cell at the top of the computational domain located 6 m above the cavity floor and it would take the melt approximately 2.7 seconds to reach the bottom of the pool (0.8 second to reach the top of the water pool from the bottom of reactor vessel), and the minimum particle diameter during the premixing calculation was found to be approximately 5 mm. Figure 17 shows the vapor void fraction and melt volume fraction. The vapor void fraction in the coolant pool is very small considering the relatively large radial nodalization.

The explosion was triggered by specifying a pressure threshold value of 0.2 MPa and a fragmented particle size of 0.1 mm in IFCI. The explosion pressures at various locations in the coolant pool are shown in Figures 18 and 19. In the TEXAS calculation, the melt would travel only 2 m in the coolant pool (during 1 second of premixing calculation) before the melt particles began to quench (the TEXAS results would only be shown for the upper 2 m of pool where the melt remained before the explosion was triggered).

Table 12 lists the comparison of the predicted pressure impulses at various axial locations using TEXAS and IFCI computer codes. In the IFCI calculation, the ratio of the maximum pressure impulse in the inner node (the local value) is approximately 2.5 time the corresponding value in the outer node (wall). The maximum pressure impulses calculated by IFCI and TEXAS are 25 kPa-s and 46 kPa-s which is considered to be indicative of similarity in predictive trends considering the large differences between the two codes.

Table 12 Comparison of the pressure impulse in scenario A (3 m pool)

Axial Distance, z (m)	Pressure Impulse (kPa-s)		
	TEXAS	IFCI	
		Inner Nodes	Wall Nodes
0.1	-	15	10
0.4	-	15	10
0.6	-	12	10
0.9	-	15	10
1.1	46	13	9
1.4	45	14	8
1.6	44	15	8
1.9	43	16	6
2.1	40	18	5
2.4	20	21	4
2.6	7	25	3
2.9	-	17	3

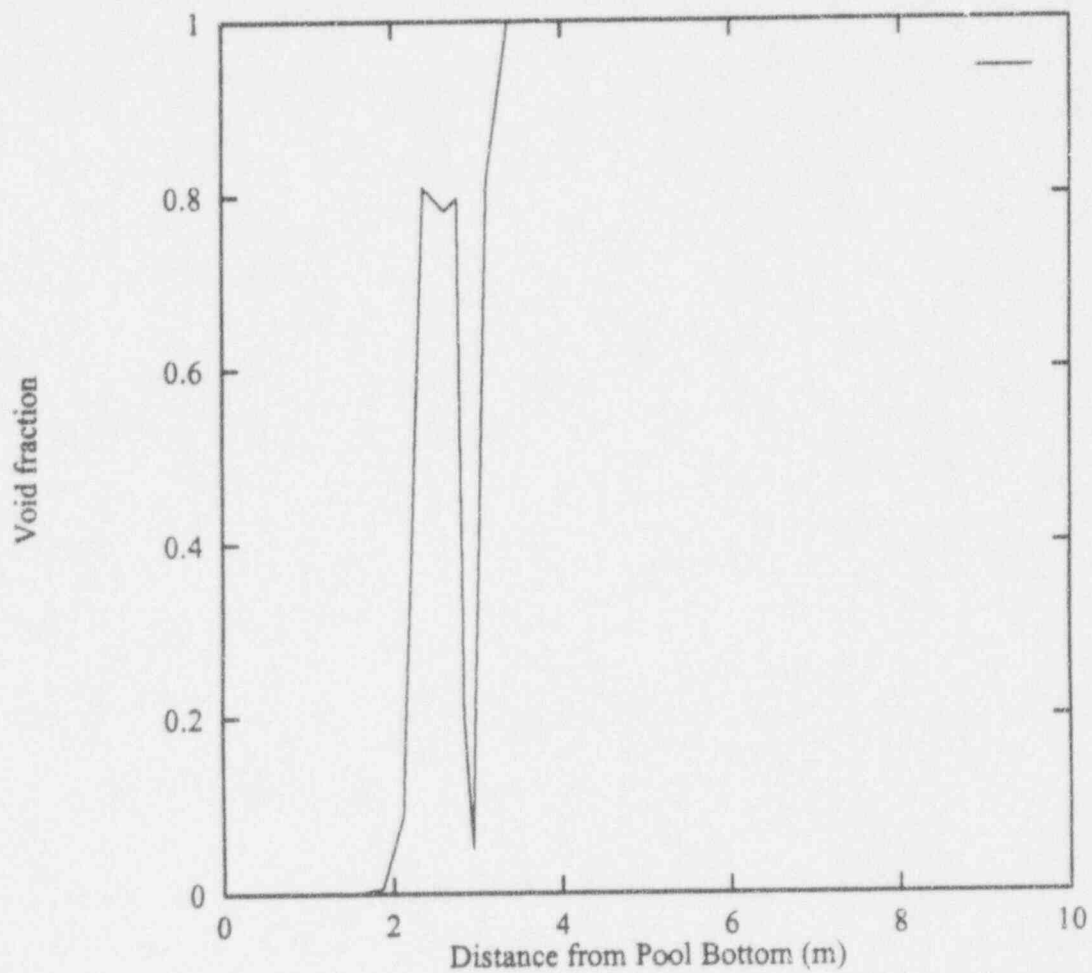


Figure 15 Predicted vapor void fraction at the end of premixing calculation (1 second) using TEXAS computer code (scenario A, 3 m pool depth)

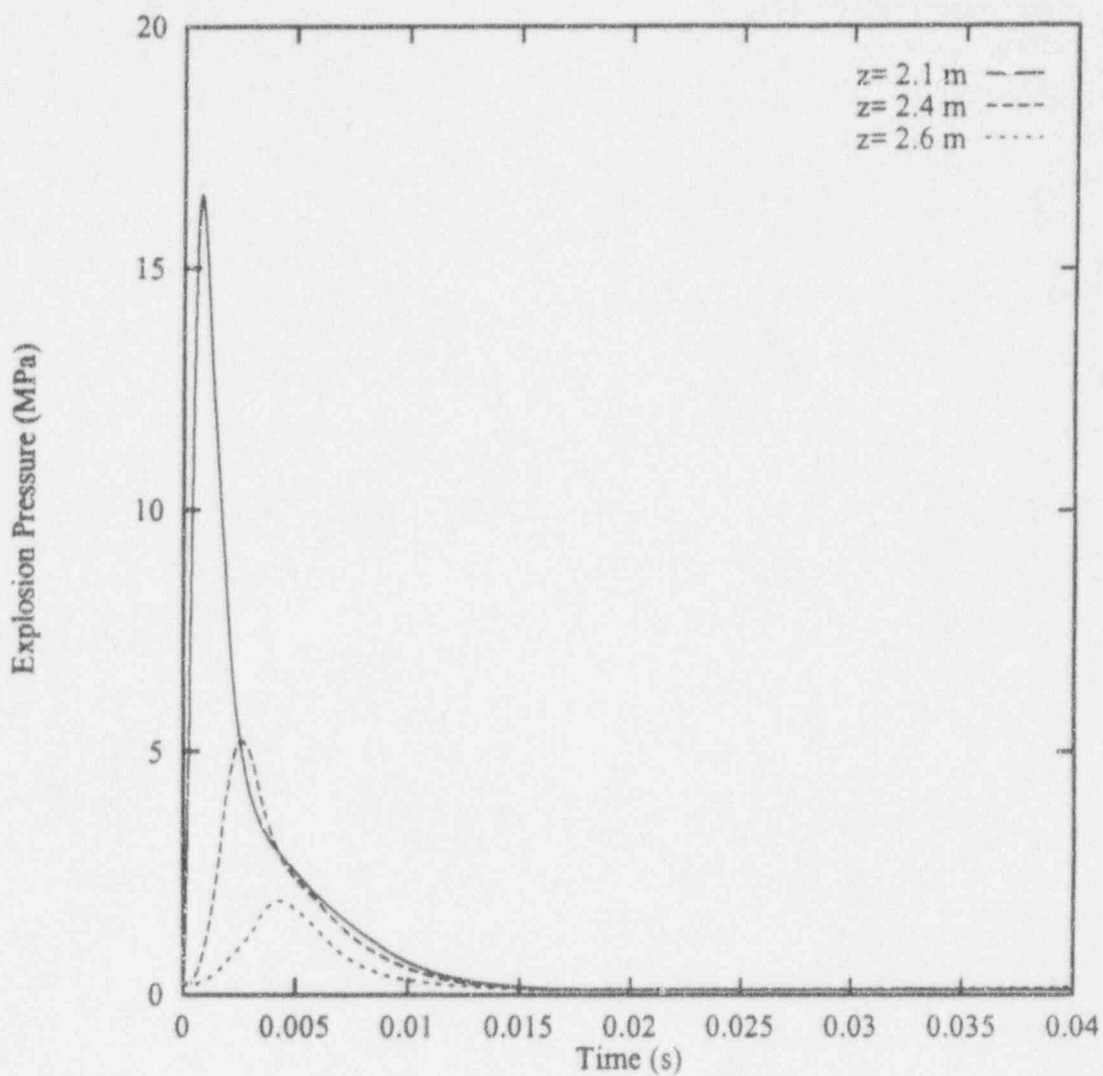


Figure 16 Predicted explosion pressure history at different axial locations using TEXAS computer code (scenario A, 3 m pool depth)

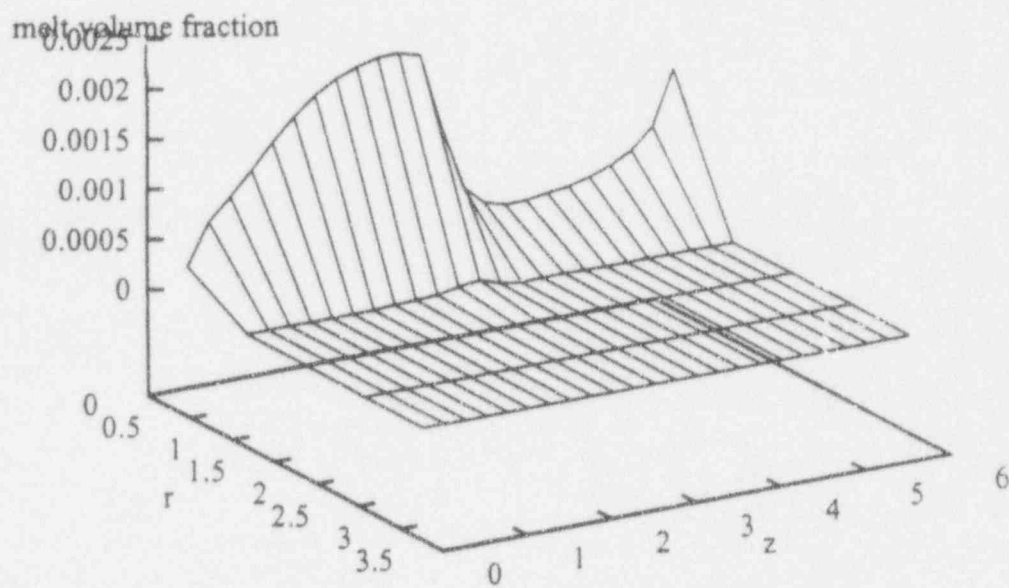
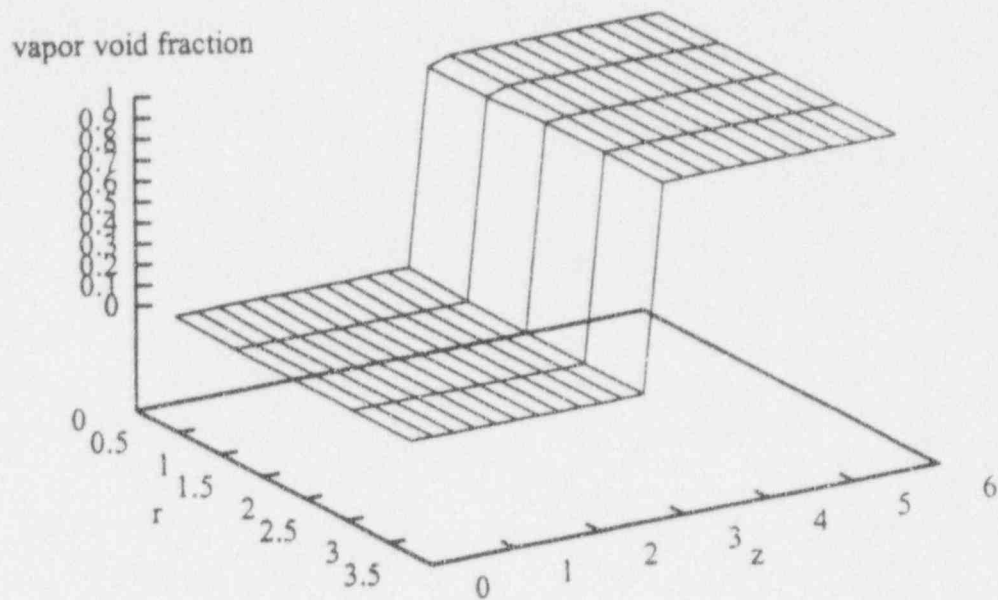


Figure 17 Predicted vapor void fraction and melt volume fraction at the end of the premixing calculation using IFCI computer code (scenario A, 3 m pool depth)

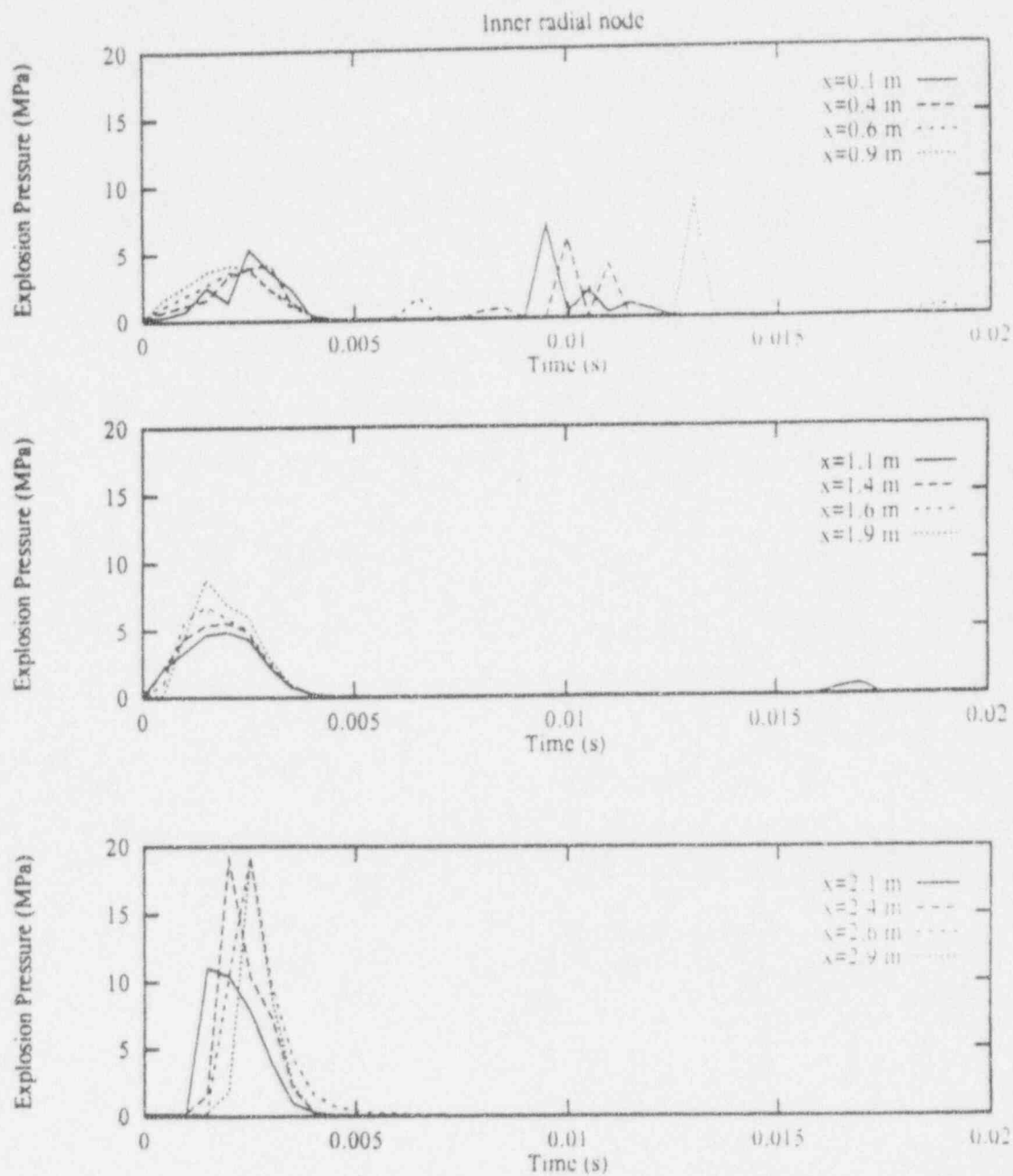


Figure 18 Predicted explosion pressure history at different axial locations in the inner radial node using IFCI computer code (scenario A, 3 m pool depth)

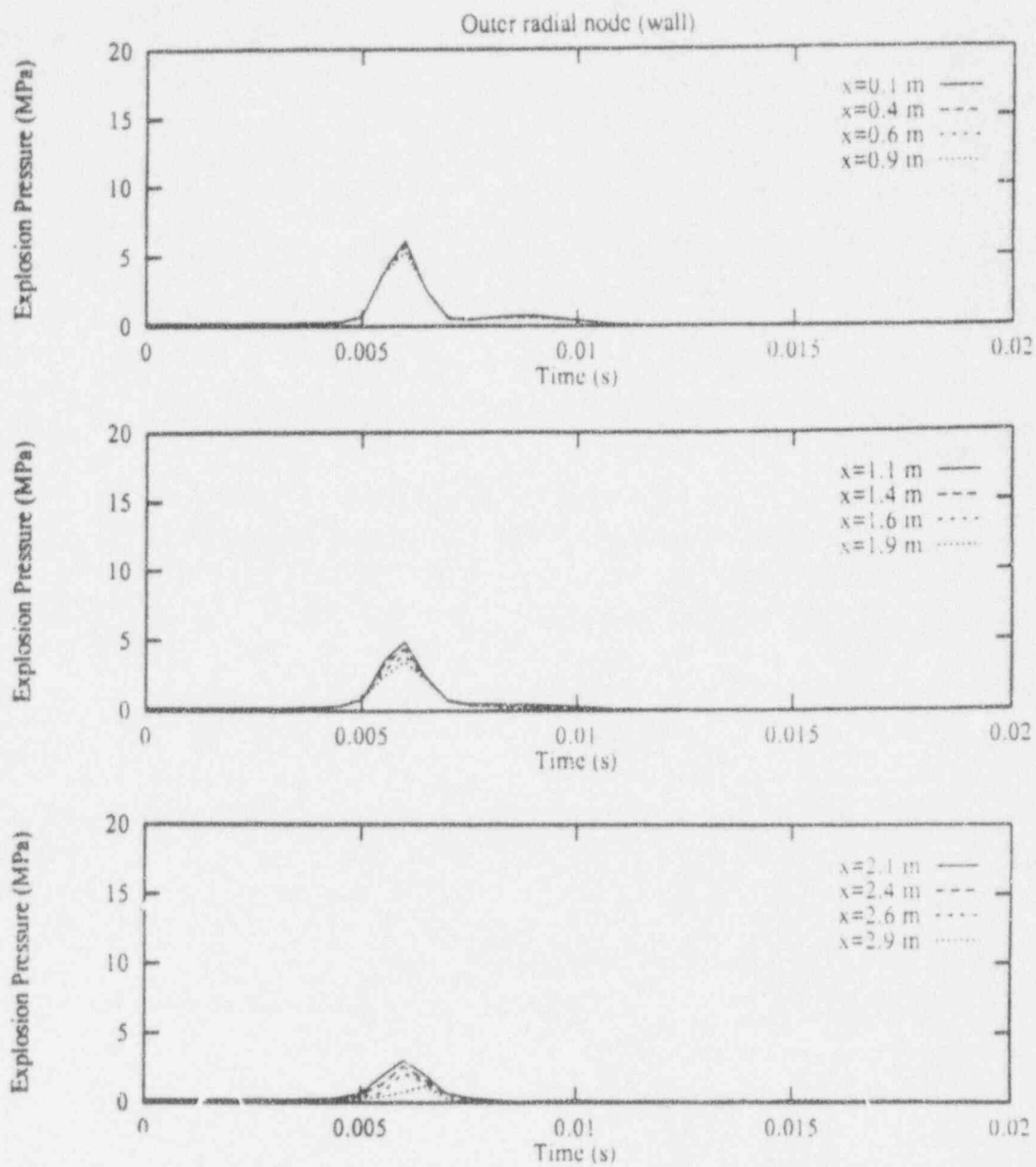


Figure 19 Predicted explosion pressure history at different axial locations in the outer radial node (wall) using IFCI computer code (scenario A, 3 m pool depth)

5.1.2.2 Sensitivity to the Water Pool Depth of 4.5 m (S-2)

The amount of water in the reactor cavity at the time of vessel breach can vary significantly for different accident sequences. To assess the sensitivity of the calculated pressure impulse to the cavity water pool depth, an additional sensitivity calculation (using only TEXAS computer code) corresponding to a water pool depth of 4.5 m was also performed for scenario A.

Figure 20 shows the distribution of the void fraction in the water pool. The maximum local void fraction in the water pool was somewhat lower than in the base case. The reduction in the void fraction tends to increase the mixture compressibility and the pressure rise during the propagation phase of the interaction. It should be noted that for a lower water depth of 4.5 m, the corium jet leaving the reactor vessel accelerated and had a higher velocity at the pool surface as compared to the base case. The jet diameter at the water surface was lower than the base case since the mass flow rate was assumed to be conserved. A combination of both these effects (i.e., smaller jet diameter and higher jet velocity) resulted in a relatively smaller maximum void fraction compared to the base case.

Figure 21 shows the explosion pressures at various axial locations in the water pool. The maximum explosion pressure was slightly higher than the base case which was believed to be mainly due to smaller void fraction. The total mass of fragmented particles during the propagation phase was 3.9 kg. A summary of the calculated pressure impulses are provided in Table 13.

Table 13 Predicted pressure impulse in scenario A using TEXAS computer code (3 m pool)

Axial Distance, z (m)	Pressure Impulse (kPa-s)
3.4	49
3.6	44
3.9	32
4.1	16

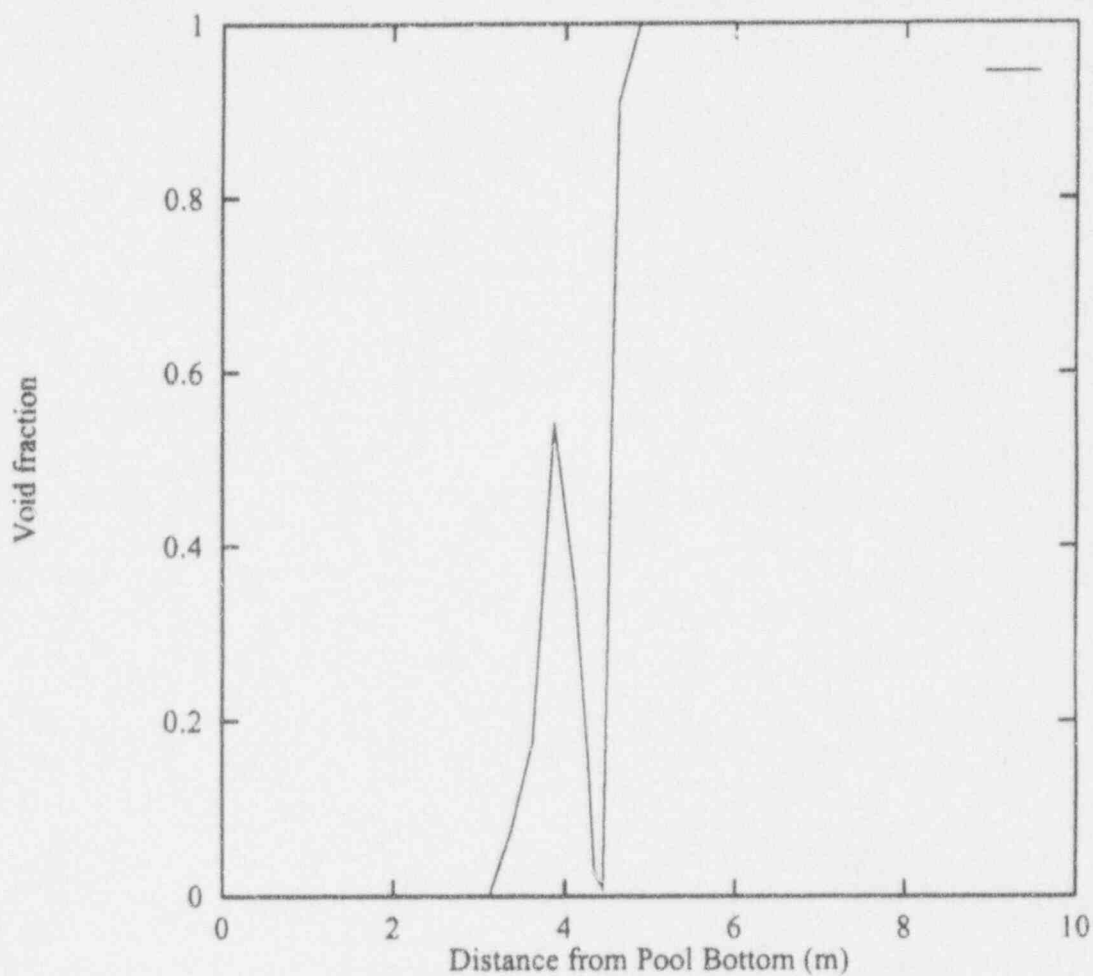


Figure 20 Predicted vapor void fraction at the end of premixing calculation (1 second) using TEXAS computer code (scenario A, 4.5 m pool depth)

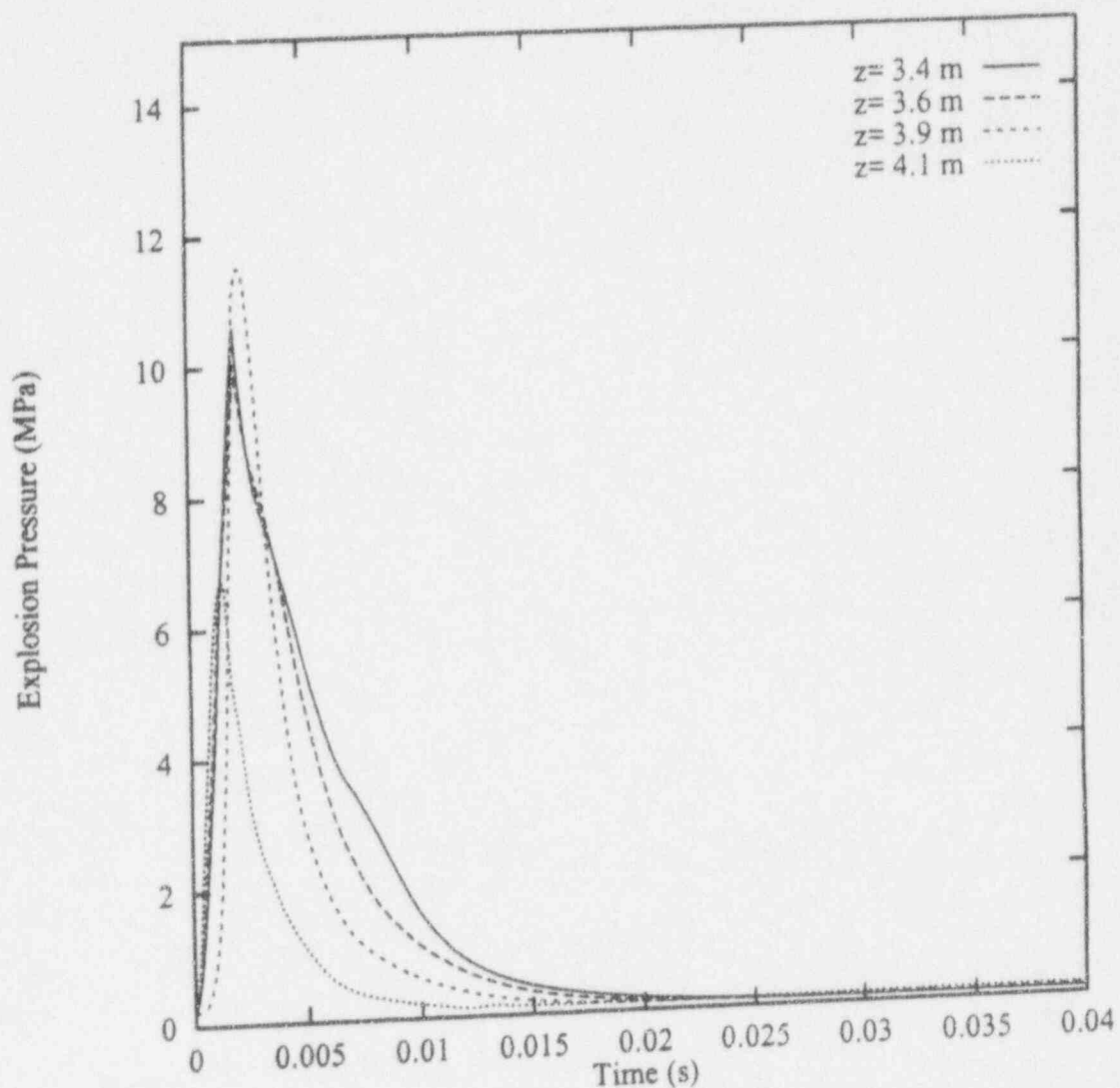


Figure 21 Predicted explosion pressure history at different axial locations using TEXAS computer code (scenario A, 4.5 m pool depth)

5.1.2.3 Sensitivity to Melt Superheat of 200 K (S-3)

Due to uncertainties regarding the melt superheat at the time of vessel breach and given the maximum melt superheat of 200 K from the results of SCDAP/RELAP5 calculation [19], it was decided to perform a sensitivity calculation with a higher melt superheat of 200 K. The melt superheat in this calculation was 200 K corresponding to the melt temperature of 3000 K. Figure 22 shows the distribution of the vapor void fraction in the coolant pool. The vapor void fraction shows the same qualitative, as well as quantitative behavior as the base case. There are no significant differences to be noted. At these high melt temperatures, a higher superheat of 200 K is not expected to significantly alter the rate of the heat transfer from the particles to the coolant. However, the explosion pressures could be higher since there are less quenched particles that can participate in the explosion. Figure 23 shows the results of the pressure impulse sensitivity to the melt superheat. The peak pressure of approximately 14 MPa occurred at an axial location of 4.4 m from the bottom of the pool. The peak pressure was higher than the base case calculation since more melt mass was available to thermally drive the explosion. The total particle fragmentation during the propagation phase was approximately 4.3 kg which was higher than the base case calculation. Table 14 provides a summary of the predicted pressure impulses using TEXAS computer code.

Table 14 Predicted pressure impulse in scenario A using TEXAS computer code (200 K melt superheat)

Axial Distance, z (m)	Pressure Impulse (kPa-s)
4.4	60
4.6	52
4.9	37
5.1	15

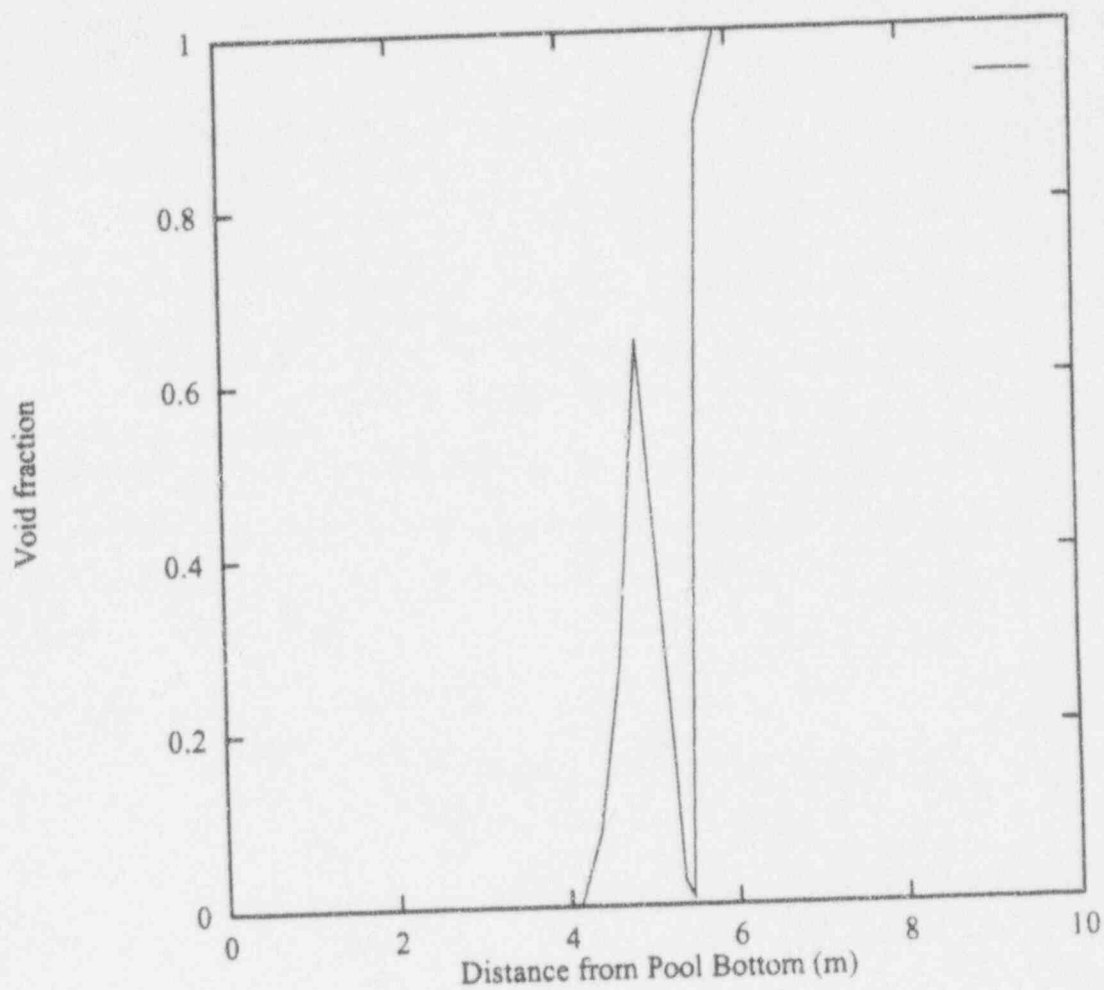


Figure 22 Predicted vapor void fraction at the end of premixing calculation (1 second) using TEXAS computer code (scenario A, melt superheat of 200 K)

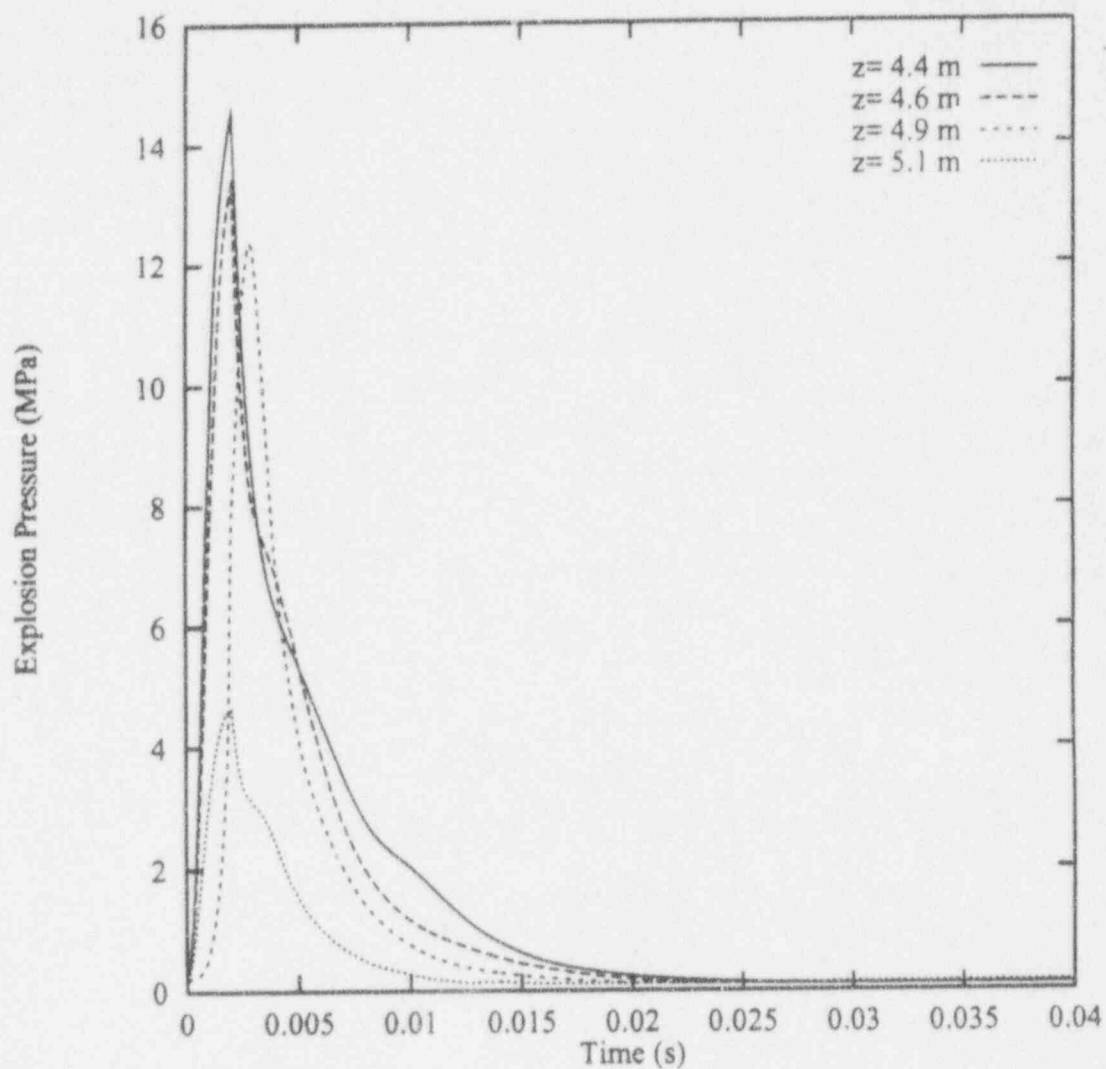


Figure 23 Predicted explosion pressure history at different axial locations using TEXAS computer code (scenario A, melt superheat of 200 K)

5.1.2.4 Sensitivity to the Number of Failed Penetrations (S-4)

In the calculations presented here, it was assumed that eight instrument tube penetrations in the lower head fail simultaneously. All other initial conditions were similar to those of the base case. For the case of a single penetration failure, it was possible to calculate the radial spreading of the jet in the water pool. As discussed previously, there are 61 penetrations staggered across reactor lower head. An estimate of the cross-sectional area was made by considering only the eight central penetrations. The cross-sectional area corresponding to these penetrations was approximately 1 m^2 . The cross-sectional area estimated for a single penetration was 0.2 m^2 , therefore, an estimate of the total cross-sectional area using eight jets was 1.6 m^2 . The calculations with a mesh cross-sectional area of 1.6 m^2 indicated smaller pressure impulses. Thus, it was decided to perform this sensitivity calculation using a mesh cross-sectional area of 1 m^2 . It should be noted that the penetrations may fail simultaneously at any location in the reactor lower head.

Figure 24 shows the local void fraction in the water pool as a function of distance from the bottom of the pool. In this case, the maximum local void fraction was approximately 0.5. Figure 25 shows the explosion pressures at various axial locations in the water pool. The maximum explosion pressure was approximately 30 MPa and occurred at an axial distance of 4.6 m measured from the bottom of the water pool. The differences in the peak explosion pressures at various axial locations were mainly due to the local void fraction and the fraction of particles that participated in the explosion. Table 15 gives a summary of the predicted pressures impulses. The total mass of fragmented fuel during the propagation phase of the interaction was approximately 45 kg.

Table 15 Predicted pressure impulse in scenario A using TEXAS computer code (simultaneous failure of eight penetrations)

Axial Distance, z (m)	Pressure Impulse (kPa-s)
4.4	160
4.6	149
4.9	135
5.1	119

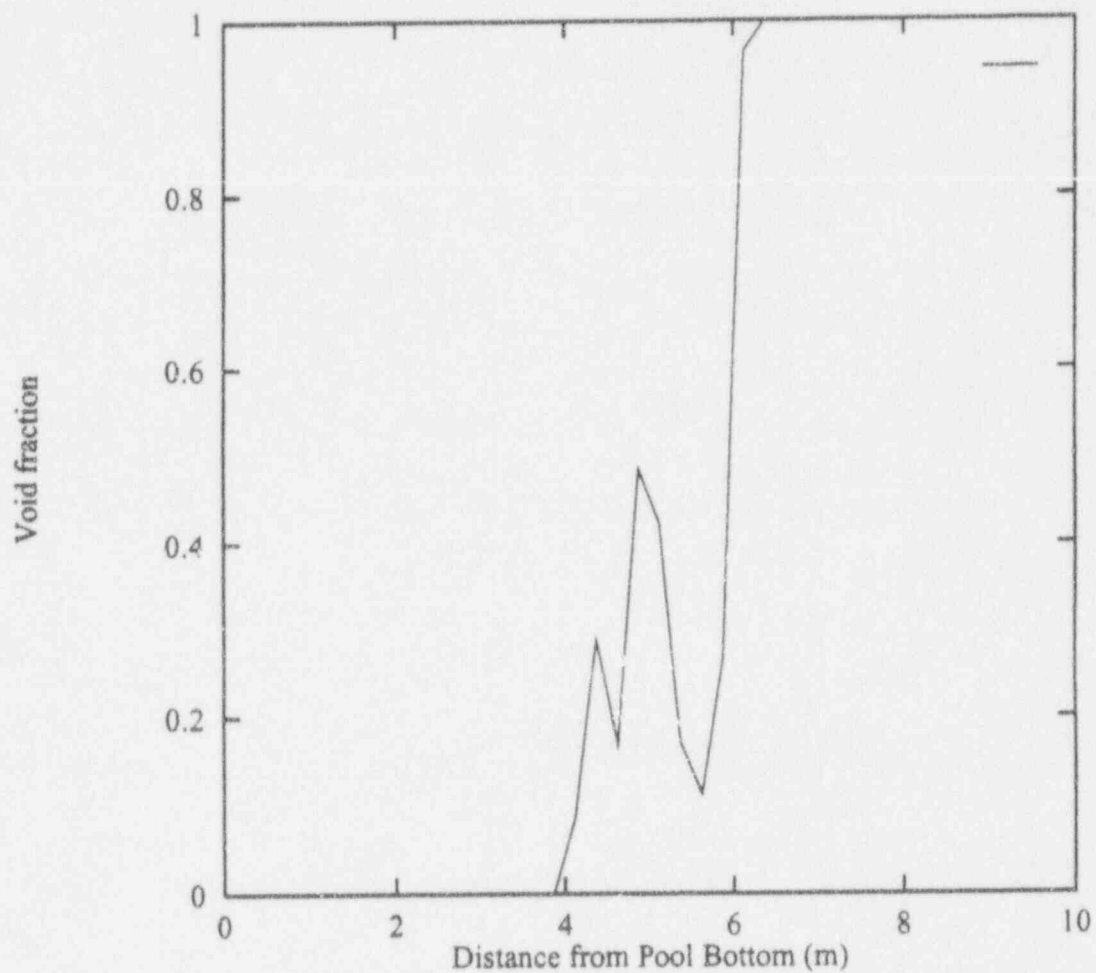


Figure 24 Predicted vapor void fraction at the end of premixing calculation (1 second) using TEXAS computer code (scenario A, simultaneous failure of eight penetrations)

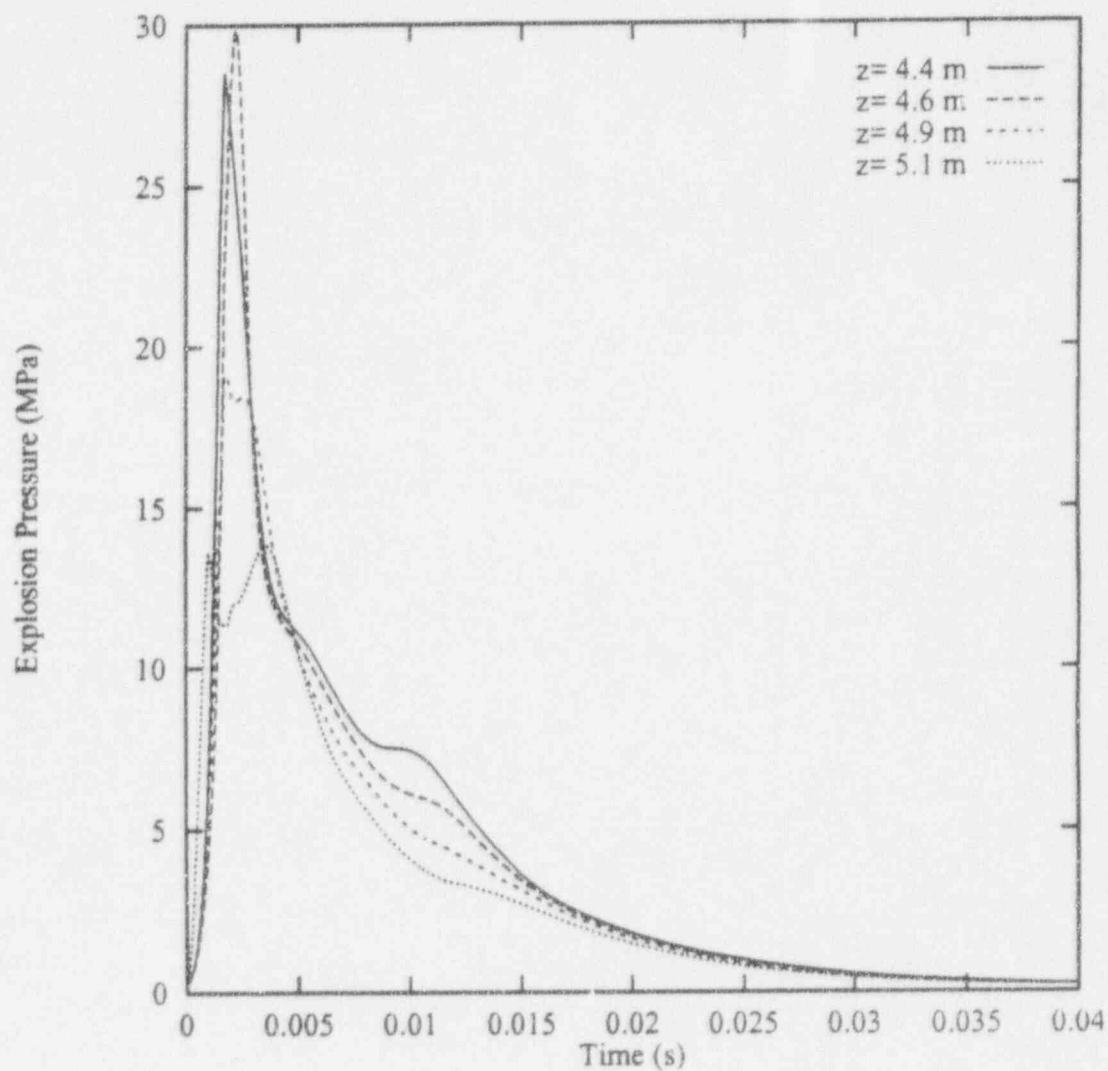


Figure 25 Predicted explosion pressure history at different axial locations using TEXAS computer code (scenario A, simultaneous failure of eight penetrations)

5.1.2.5 Sensitivity to Initial Melt Velocity (S-5)

In this sensitivity calculation, a higher corium discharge velocity of 8 m/s was assumed corresponding to a pressure difference of 0.2 MPa between the reactor pressure vessel and the containment atmosphere (at vessel breach). As the driving pressure difference (ΔP) and thereby fuel entrance velocity increase, the fuel jet will increase in its breakup, i.e. the jet will fragment more quickly into smaller sizes (and higher vapor void fractions).

Figure 26 shows the local vapor void fraction in the water pool. Since the initial jet velocity was higher than the base case, the fuel jet fragmented more readily in the water pool and the cross-sectional area of the fragmented particles was therefore higher. The higher particle surface area as compared to the base case resulted in higher heat transfer from the fuel surface to the coolant pool. The higher maximum void fraction for this sensitivity calculation as compared to the base case was a result of the higher heat transfer. In addition, since the velocity of the jet was higher, the mass flow rate was also higher (57 kg/s) than the base case (35 kg/s).

The explosion pressures are shown in Figure 27. The maximum explosion pressure was approximately 30 MPa which was considerably higher than the base case. The total fragmented mass of particles (that participate in the explosion) during the propagation phase of the interaction was approximately 6.6 kg. The higher explosion pressure in this sensitivity calculation was a result of the higher mass flow rate and the higher mass of melt that participated in the explosion process. Table 16 provides a summary of the predicted pressure impulses.

Table 16 Predicted pressure impulse in scenario A using TEXAS computer code (melt velocity of 8 m/s)

Axial Distance, z (m)	Pressure Impulse (kPa-s)
4.4	92
4.6	70
4.9	43
5.1	14

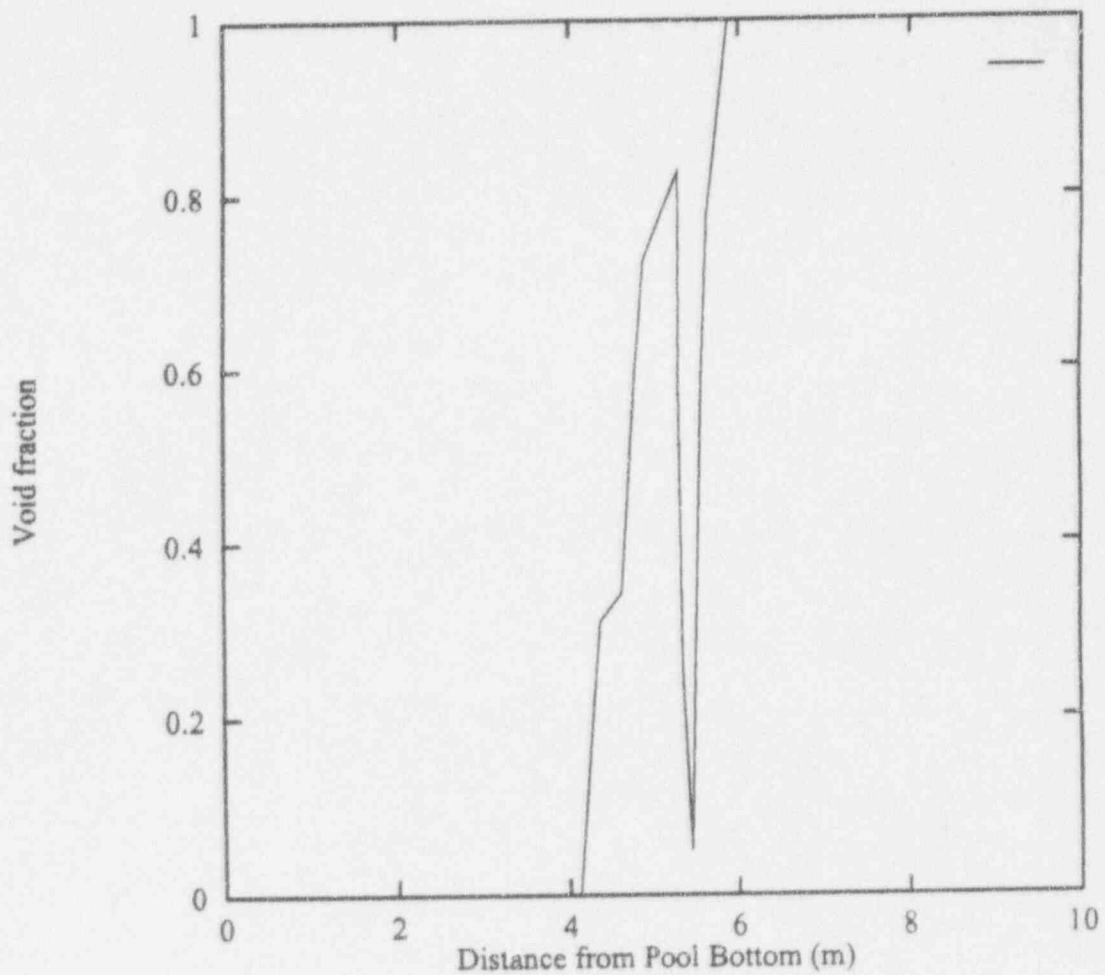


Figure 26 Predicted vapor void fraction at the end of premixing calculation (1 second) using TEXAS computer code (scenario A, initial melt velocity of 8 m/s)

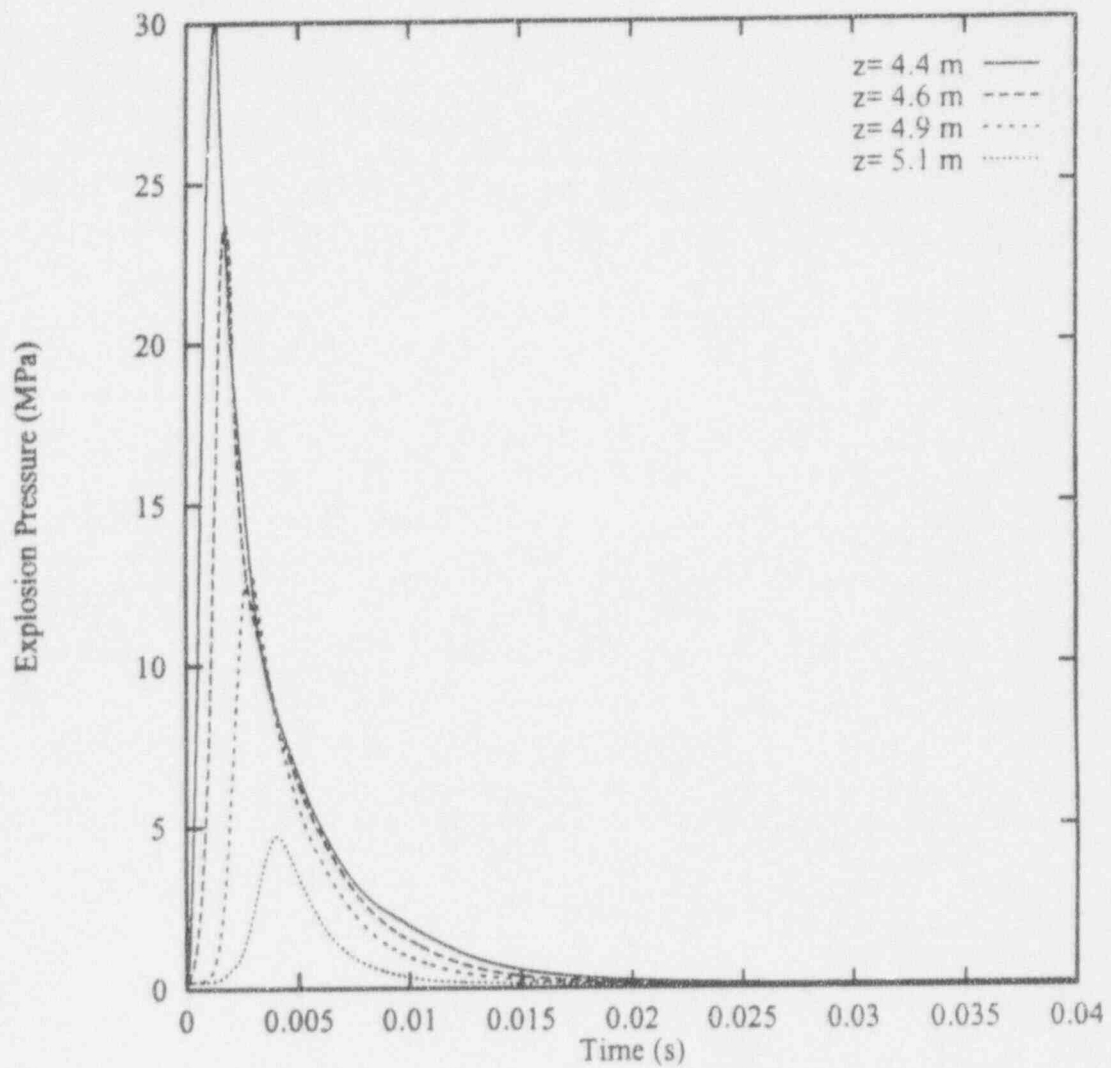


Figure 27 Predicted explosion pressure history at different axial locations using TEXAS computer code (scenario A, initial melt velocity of 8 m/s)

5.1.2.6 Sensitivity to the Saturated Water Pool (S-7)

The sensitivity of FCI energetics to the initial water pool temperature was examined in this subsection, assuming a saturated water pool. The temperature of water pool was 393 K corresponding to the saturation temperature of water at a pressure of 0.2 MPa.

The results of the TEXAS calculations for the saturated pool are presented in Figures 28 and 29. The maximum void fraction in the water pool was higher than the base case due to higher steam generation. The higher void fraction in the pool tends to decrease the maximum pressure and thus the local pressure impulse. Figure 29 shows the explosion pressures at various axial locations within the coolant pool. The maximum explosion pressure was approximately 6 MPa which was lower than the base case. The total mass of fragmented fuel was approximately 1.8 kg. The summary of the predicted pressure impulses at various axial locations are shown in Table 17.

Table 17 Predicted pressure impulse in scenario A using TEXAS computer code (saturated water pool)

Axial Distance, z (m)	Pressure Impulse (kPa-s)
4.4	31
4.6	20
4.9	12
5.1	3

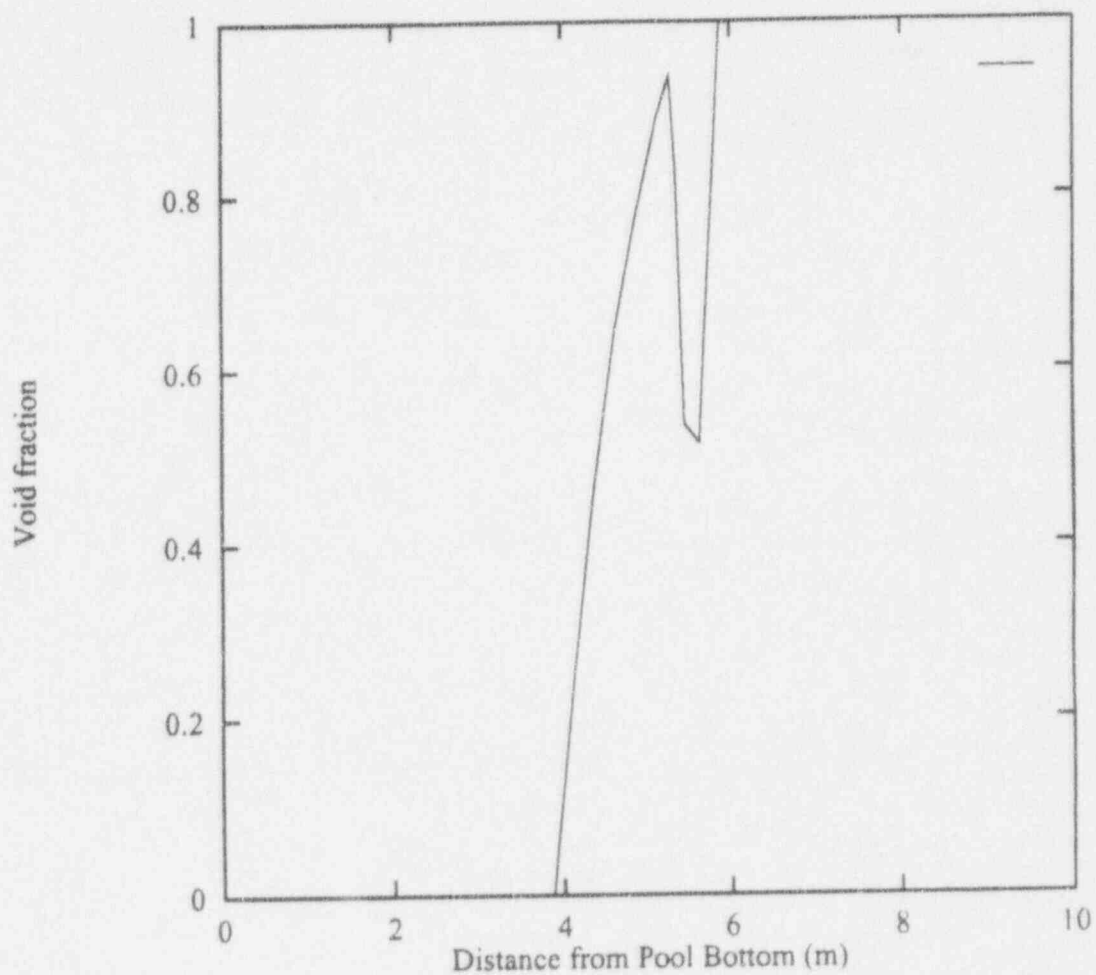


Figure 28 Predicted vapor void fraction at the end of premixing calculation (1 second) using TEXAS computer code (scenario A, saturated water pool)

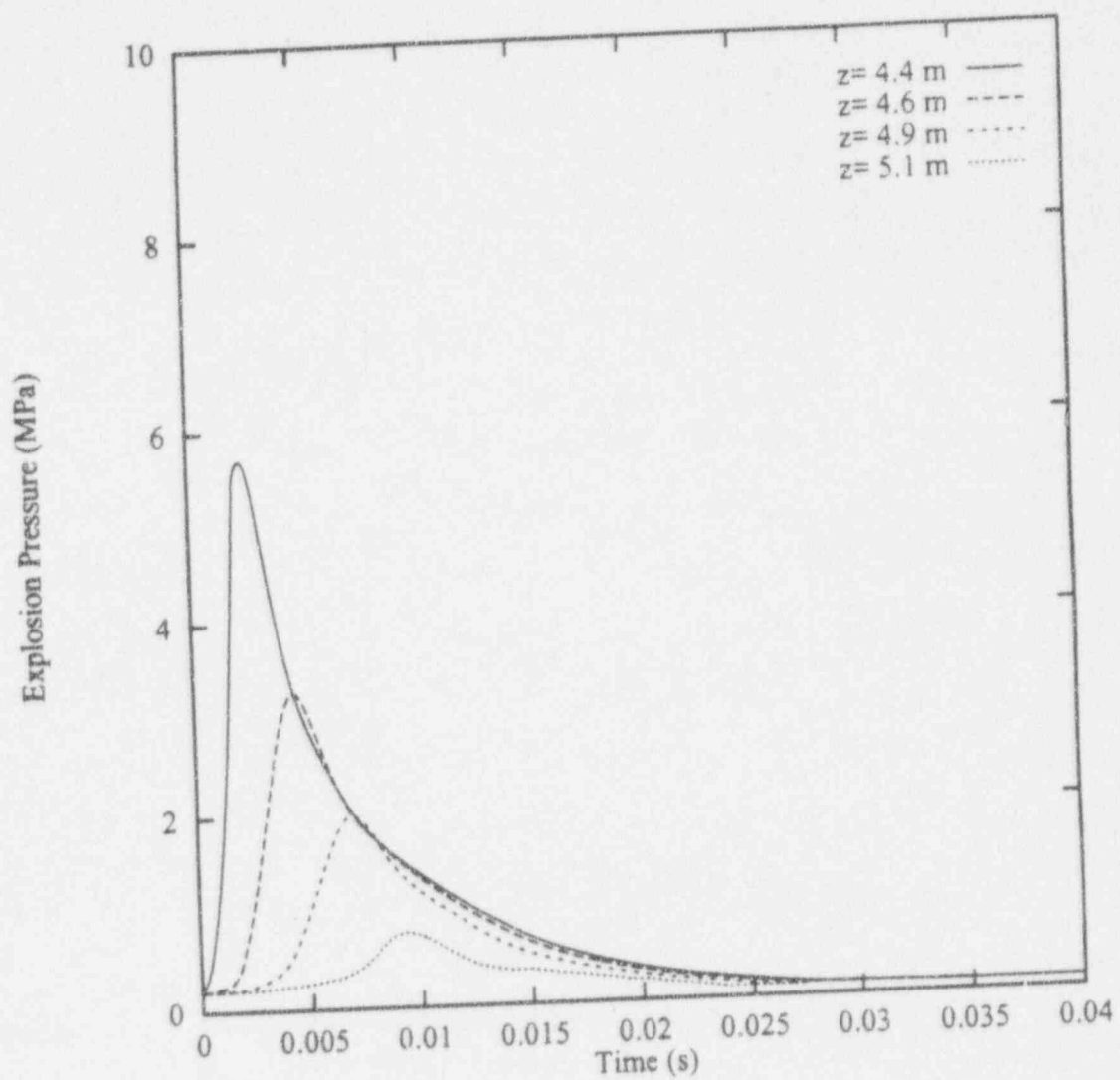


Figure 29 Predicted explosion pressure history at different axial locations using TEXAS computer code (scenario A, saturated water pool)

5.2 Scenario B

5.2.1 Base Case Calculations

An estimate of the mesh cross-sectional area in the TEXAS calculations was obtained from the results of IFCI premixing calculation. Therefore, the results of IFCI calculations will be discussed first. In the FCI input model, the cavity was modelled as a 2.5 m high cylindrical computational domain with 8 axial nodes (0.25 m) in the water pool to assess the FCI energetics in the corbel support region. The radial size of the computational domain was 1.5 m, and the radial nodalization employed 6 equally-spaced radial cells (0.25 m). The melt jet diameter was specified as 0.4 m, and the melt was poured in the inner radial node at the top of the computational domain, and a constant pressure outflow boundary condition was specified at the outer radial node at the top of the computational domain.

During the premixing calculation, it was estimated that it would take the melt approximately 0.4 seconds to travel down the corbel support region and the minimum particle diameter during the premixing phase was approximately 25 cm. Figure 30 shows the vapor void fraction and melt volume fraction. The vapor void fraction was somewhat higher than in scenario A due to larger melt volume fraction. The radial spreading of the melt jet would extend to the fourth radial cell location located 1 m from the center of the cavity (this radial distance will be used to estimate the mesh cross-sectional area in the TEXAS calculation).

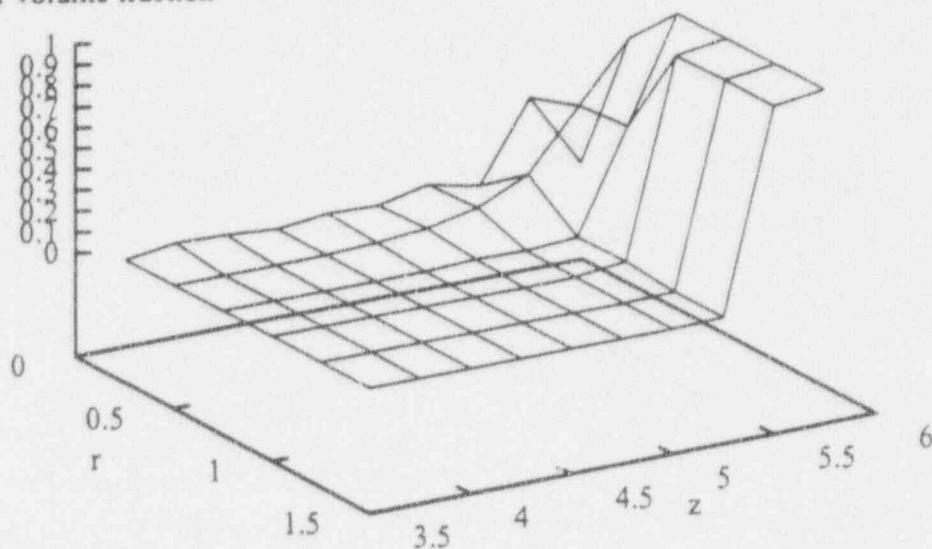
The explosion was triggered from this premixing initial condition by specification of the pressure threshold value of 0.22 MPa, and a fragmented particle diameter of 0.1 mm. This simulation resulted in numerical errors due iteration failure and the code would predict negative values of the volume fractions. The maximum number of pressure iterations was doubled (default value of 10) and the maximum time step in the problem was set to 10^{-6} s (from an original value of 10^{-5} s). The simulation would run for approximately 2 ms before the calculation was terminated due to numerical problems (during this time pressures of the order of 60-70 MPa were observed). This problem requires further investigation; however, in order to assess the propagation of the pressure wave and its radial decay, it was decided to run the same simulation with a larger particle fragment size of 1 mm. It should be noted here that we expect the pressures to be lower in this case, however, a qualitative assessment can still be made. Figures 31 and 32 show the explosion pressures at various locations in the coolant pool. The maximum explosion pressure in this scenario was approximately 28 MPa which is similar to scenario A. This pressure appears to be rather low considering the higher amount of melt that would be involved in the explosion in comparison to scenario A. The main reason for this is the larger fragmented particle size (a sensitivity calculation with this larger particle diameter was performed for scenario A, and it was observed that the maximum pressure was approximately 0.5 MPa). Table 18 shows the predicted pressure impulses at various locations in the coolant pool. No attempt will be made here to compare these values to the TEXAS calculation since

the maximum pressures and pressures impulses are expected to be much higher in the TEXAS calculation. As shown in the table, the maximum pressure impulse of 52 kPa-s occurred near the top of the pool in the first radial node. The maximum pressure impulse was approximately 34 kPa-s at the corbel wall indicating a reduction of a factor of 1.5 from the explosion zone.

Table 18 Predicted pressure impulse for the base case condition in scenario B using IFCI computer code (particle fragment size of 1 mm)

Axial location, z (m)	Pressure Impulse (kPa-s)					
	Radial location, r (m)					
	0.25	0.5	0.75	1.0	1.25	1.5
3.6	40	27	33	35	27	34
3.9	33	36	27	28	36	34
4.1	35	36	30	31	35	28
4.4	39	34	34	29	29	31
4.6	48	35	32	29	24	29
4.9	41	35	27	31	30	24
5.1	52	37	26	24	17	20
5.4	48	38	19	15	17	24

vapor volume fraction



melt volume fraction

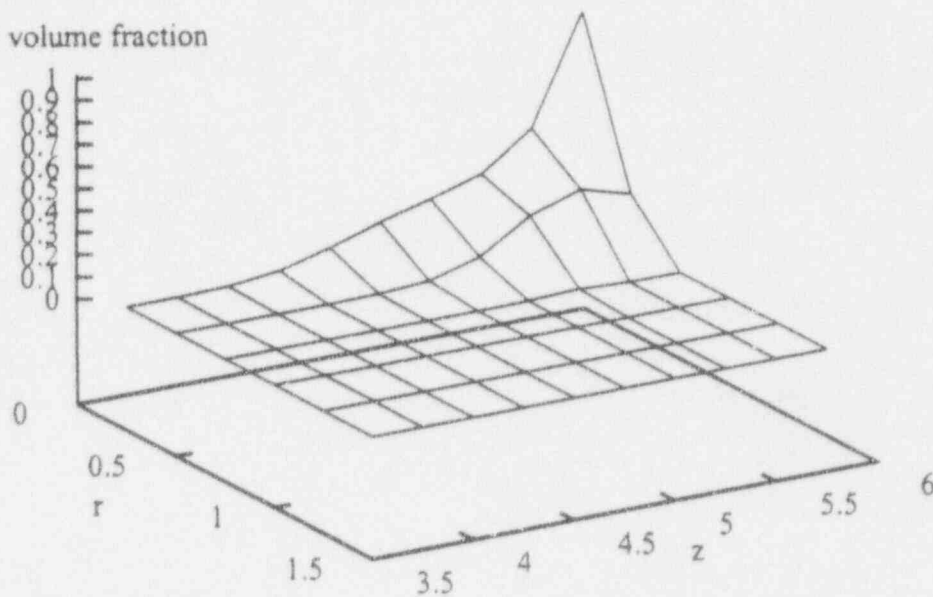


Figure 30 Predicted vapor void fraction and melt volume fraction at the end of the premixing calculation using IFCI computer code (scenario B, base case)

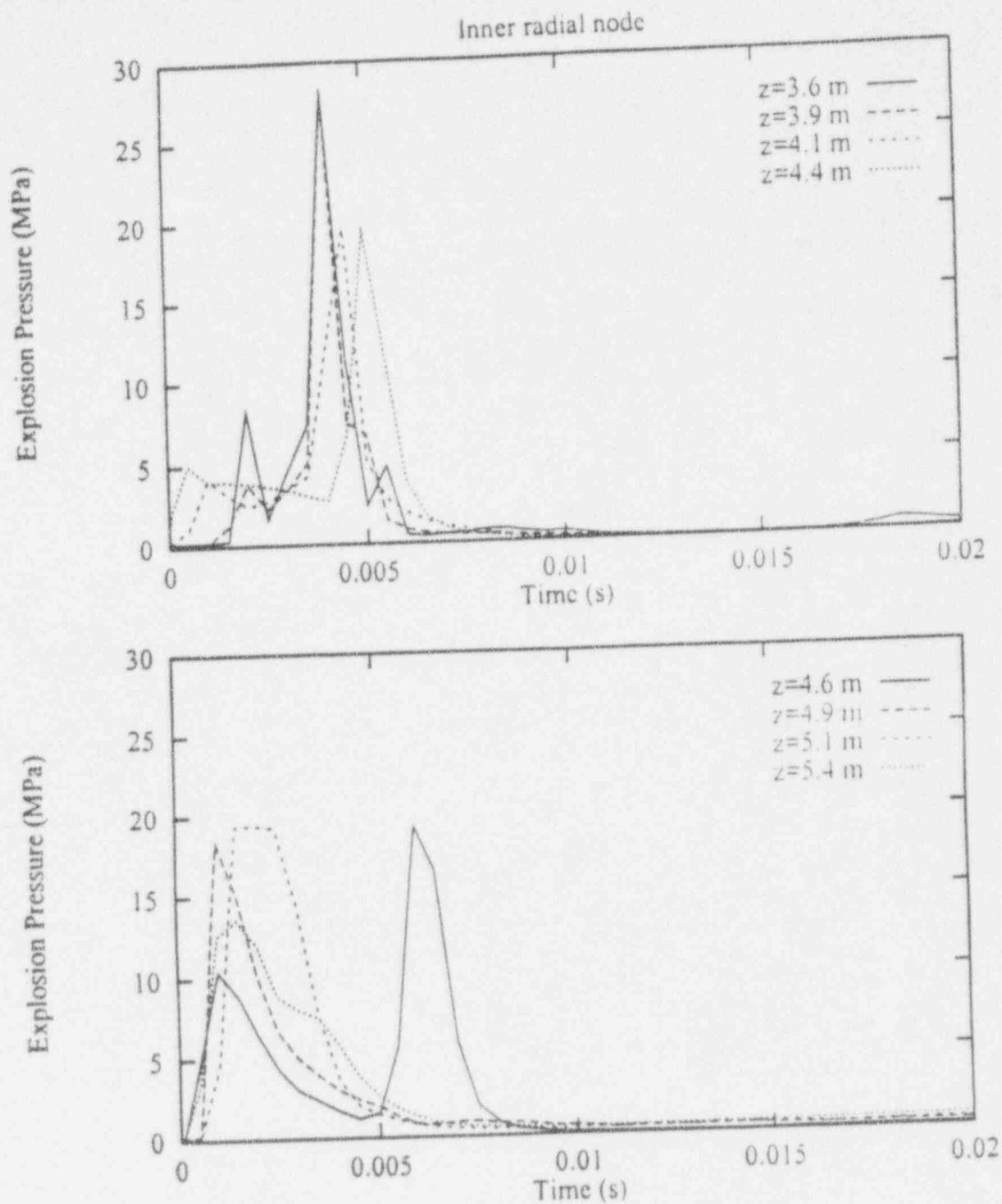


Figure 31 Predicted explosion pressure history at different axial locations in the inner radial node using IFCI computer code (scenario B, base case)

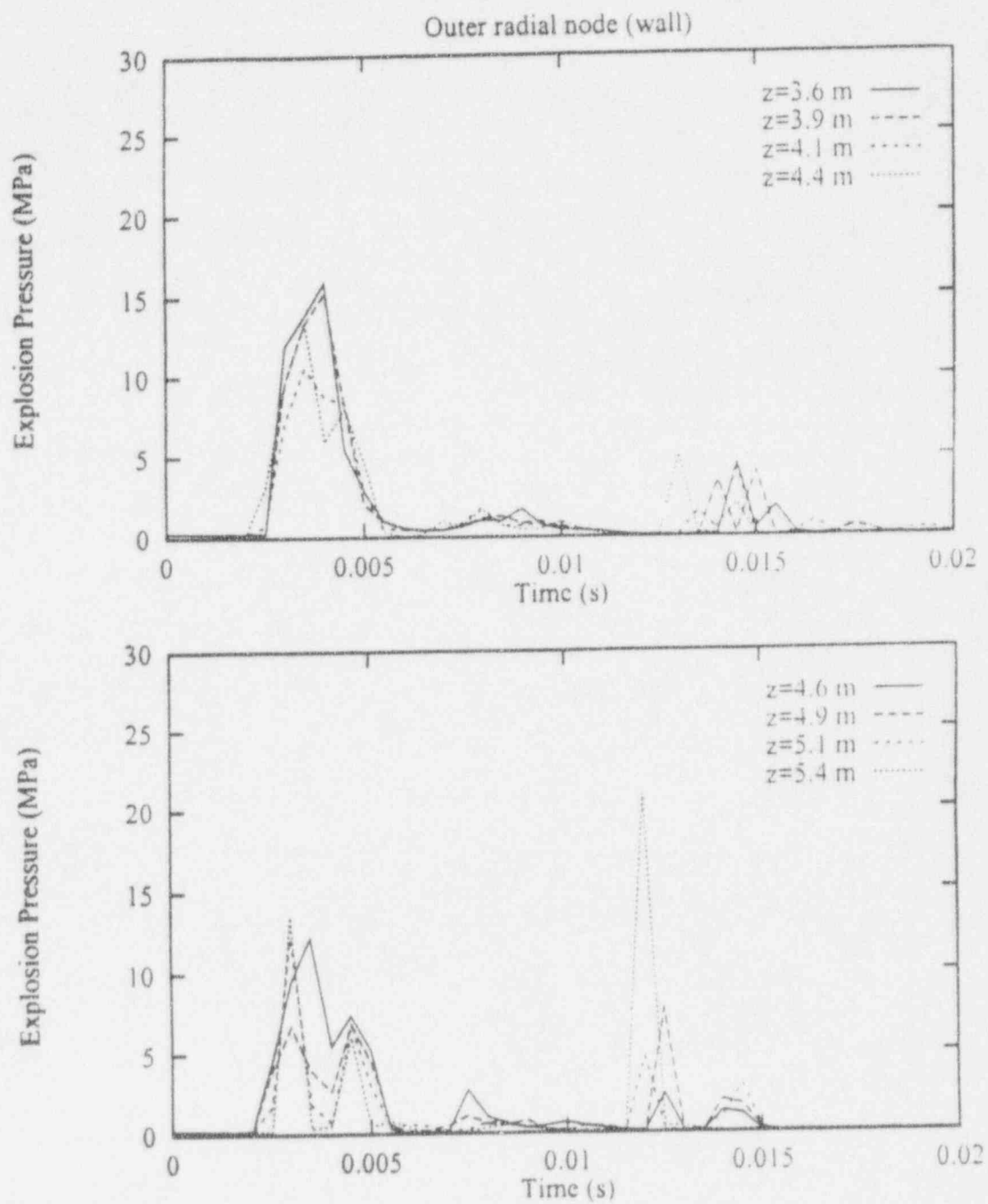


Figure 32 Predicted explosion pressure history at different axial locations in the outer radial node (wall) using IFCI computer code (scenario B, base case)

In the TEXAS model, the mesh cross-sectional area was chosen to be 3 m^2 which was estimated based on the radial spreading of the melt from the IFCI calculation. The axial nodalization in TEXAS was 0.5 m (this value was chosen since the diameter of the melt particles was 0.4 m). In the TEXAS calculation, the premixing was simulated for 1 second and during this time, the melt would reach the cavity floor. The minimum particle size resulting from particle breakup during the premixing calculation was approximately 4 mm ; however, the mass of particles in this diameter range was only 10% of the total mass and the majority of the particles were between 10 cm to 40 cm . Figure 33 shows the vapor void fraction as a function of distance from the bottom of the cavity. The maximum vapor void fraction in scenario A was approximately 0.6 and as Figure 33 indicates, the maximum vapor void fraction in scenario B was comparable to scenario A (note that the nodal cross-sectional area in one-dimensional TEXAS calculations were different in the two scenarios). During this premixing calculation, no significant quenching of the melt particles occurred as they travelled toward the bottom of the cavity (in scenario B, the diameter of the particles was larger and particle quenching was not anticipated). Figure 34 shows the explosion pressures in the corbel support region at various axial locations. The maximum explosion pressure is approximately 80 MPa . Table 19 gives a summary of the predicted pressure impulses.

Table 19 Predicted pressure impulse for the base case condition in scenario B using TEXAS computer code

Axial Distance, z (m)	Pressure Impulse (kPa-s)
3.75	512
4.25	443
4.75	368

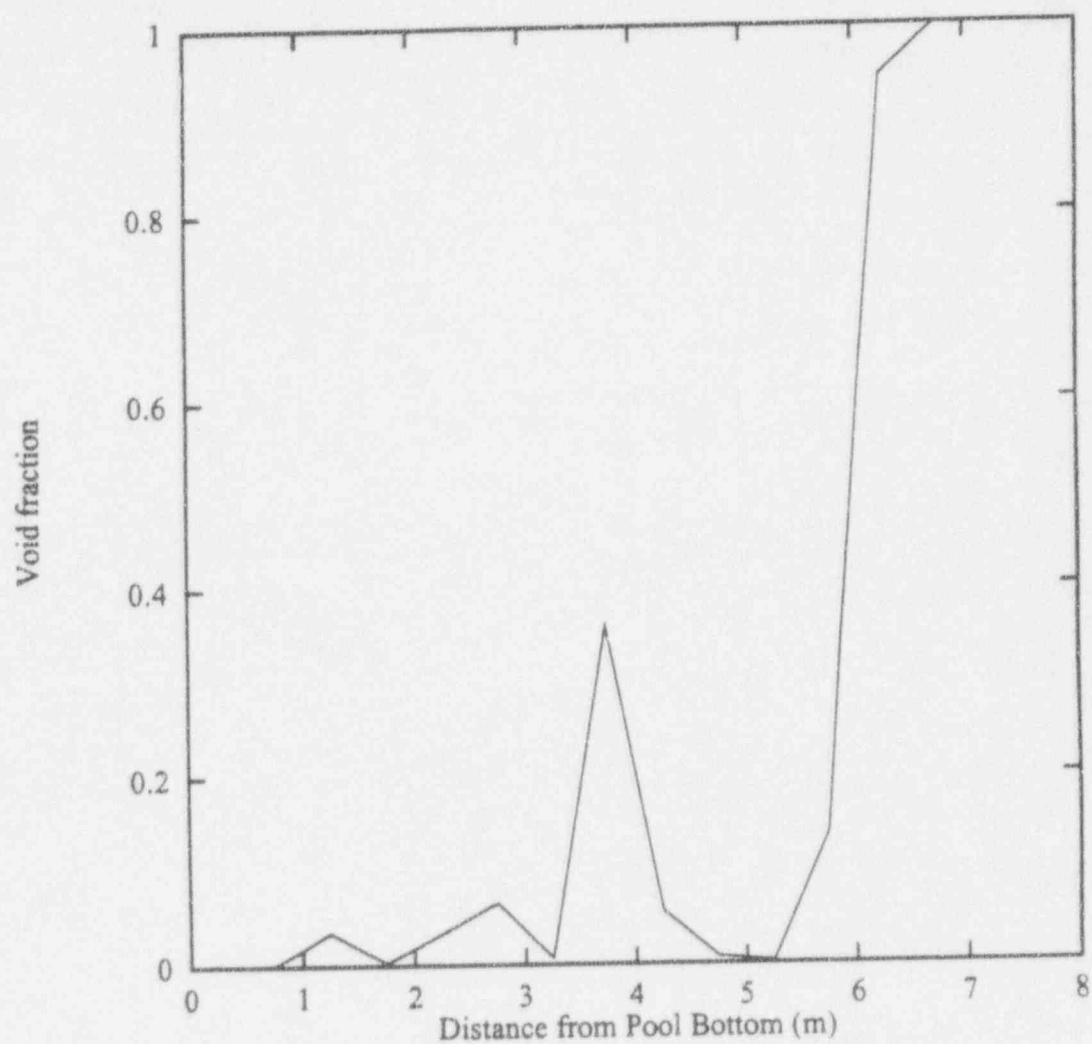


Figure 33 Predicted vapor void fraction at the end of the premixing calculation using TEXAS computer code (scenario B, base case)

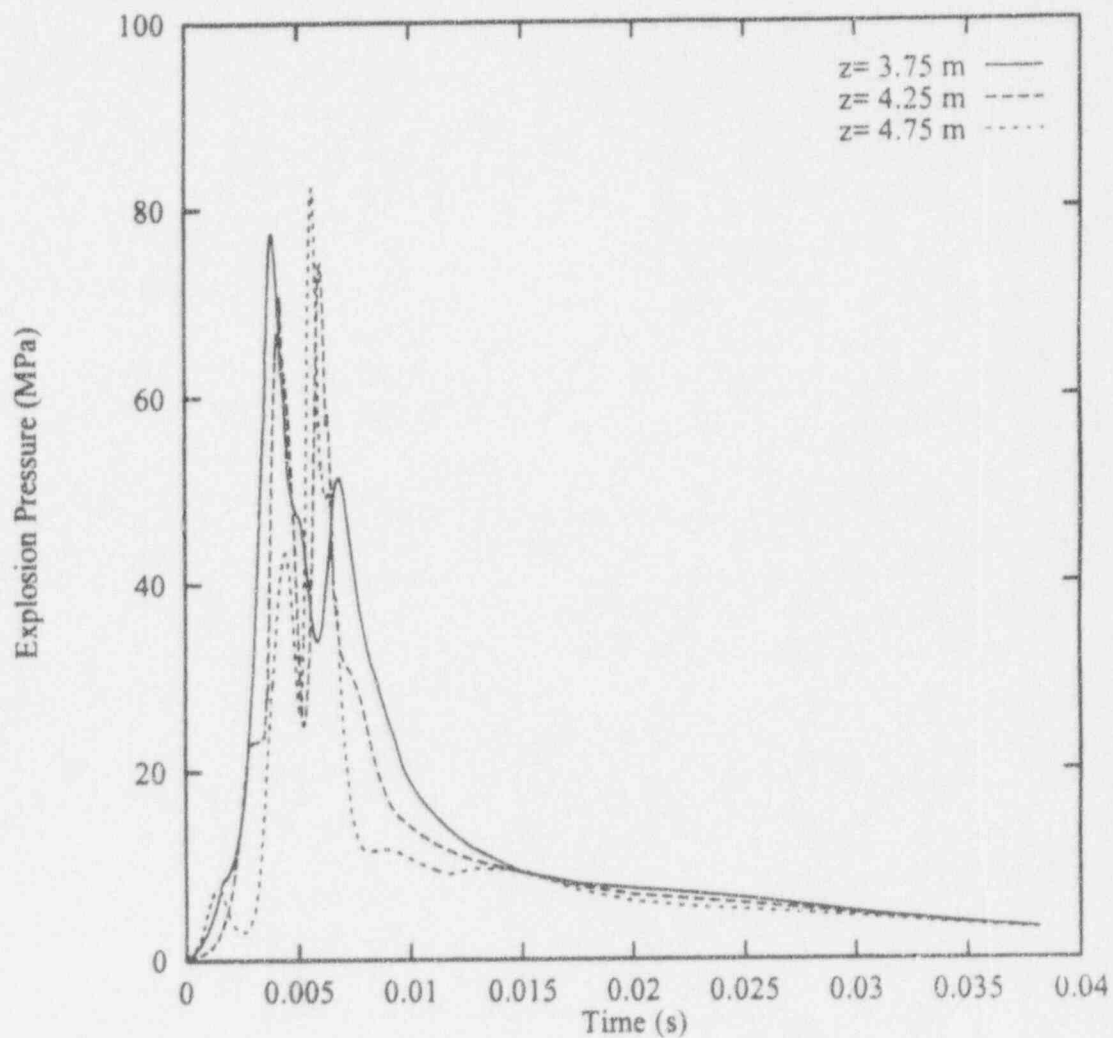


Figure 34 Predicted explosion pressure history at different axial locations using TEXAS computer code (scenario B, base case)

5.2.2 Sensitivity Calculations

A number of sensitivity calculations for scenario B have been performed. These include the 3 m deep water pool (S-1), a higher initial melt velocity of 15 m/s (S-6) and a saturated water pool (S-7). These last two sensitivity calculations were chosen based on the observation that for scenario A, the pressure impulses showed a higher sensitivity to these initial conditions. IFCI and TEXAS computer codes were used for sensitivity case S-1 while only TEXAS computer code was used for sensitivity cases S-6 and S-7. The higher initial melt velocity of 15 m/s corresponds to pressure difference of 1.2 MPa between the primary system and the containment. The TEXAS nodalization and all other initial conditions for these sensitivity calculations were exactly the same as the base case conditions.

5.2.2.1 Sensitivity to Water Pool Depth of 3 m (S-1)

The nodalization in the IFCI model for scenario B was similar to scenario A, except the melt particle diameter was changed from 0.03 m (single instrument tube failure) to 0.4 m (rupture). It took the melt approximately 1.6 s to reach the bottom of the water pool from the time pouring began in the inner radial node at the top of the computational domain. An outflow boundary condition has been specified in the last radial node at the top of the computational domain for all the IFCI calculations presented here. During this time the minimum particle diameter was found to be approximately 0.25 m at the bottom of the coolant pool. Figure 35 shows the vapor void fraction and melt volume fraction in the coolant pool. The radial spreading of the melt indicated that the melt remained primarily in the first and second radial nodes (i.e., the radial spreading of the melt extended 1.4 m away from the cavity center). The same explosion parameters as the base case were also used here (the fragmented particle diameter was chosen to be 1 mm; using a smaller fragmented particle diameter resulted in the same numerical difficulties as discussed for the base case). Using this fragmented particle diameter for the explosion and propagation phase of the interaction also indicated smaller pressure impulses as compared to TEXAS calculations which will be shown later. The explosion pressures (with a fragmented particle size of 1 mm) are shown in Figures 36 and 37. Table 20 lists the predicted pressure impulses at various nodal positions. The maximum pressure is 57 kPa-s in the inner radial node, and the maximum pressure impulse is 20 kPa-s at the cavity wall (outer radial node), therefore, a reduction of a factor of 2.9 was observed. Again, it should be mentioned that ideally one would prefer a finer nodalization in the two-dimensional calculations to ensure numerical accuracy. Finer nodalization is also expected to affect the results of the premixing calculations (smaller radial spreading of the melt).

Table 20 Predicted pressure impulse for the 3 m pool sensitivity calculation using IFCI computer code (scenario B; particle fragment size of 1 mm)

Axial location, z (m)	Radial location, r (m)				
	0.7	1.4	2.1	2.8	3.5
0.1	42	32	26	22	20
0.4	42	32	26	22	20
0.6	43	32	26	21	20
0.9	43	32	26	21	19
1.1	45	32	25	20	18
1.4	43	32	25	19	17
1.6	52	32	24	18	17
1.9	57	31	22	16	16
2.1	57	29	21	15	14
2.4	47	26	17	13	12
2.6	45	22	17	10	10
2.9	29	15	16	6	6

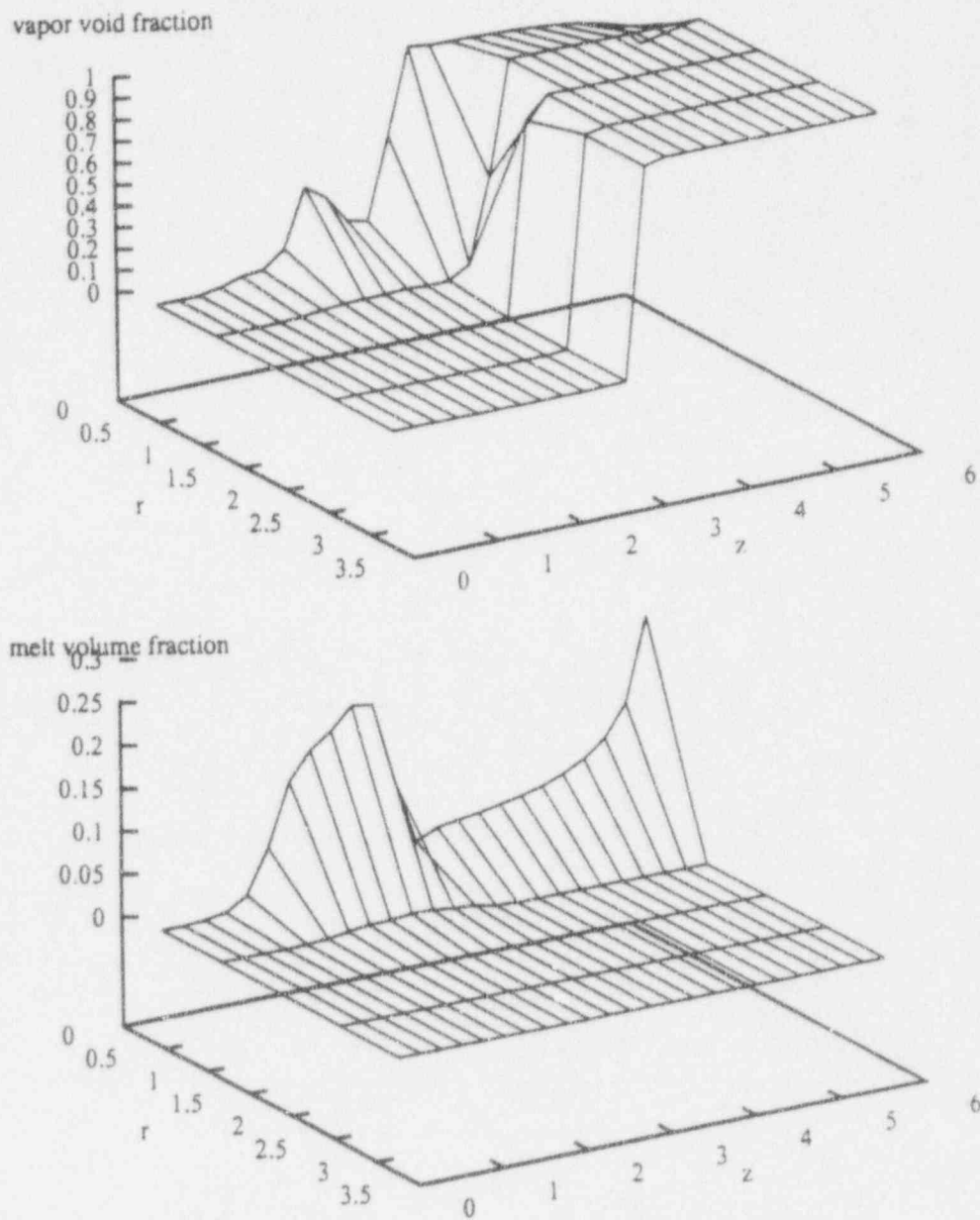


Figure 35 Predicted vapor void fraction and melt volume fraction at the end of the premixing calculation using IFCI computer code (scenario B, 3 m pool depth)

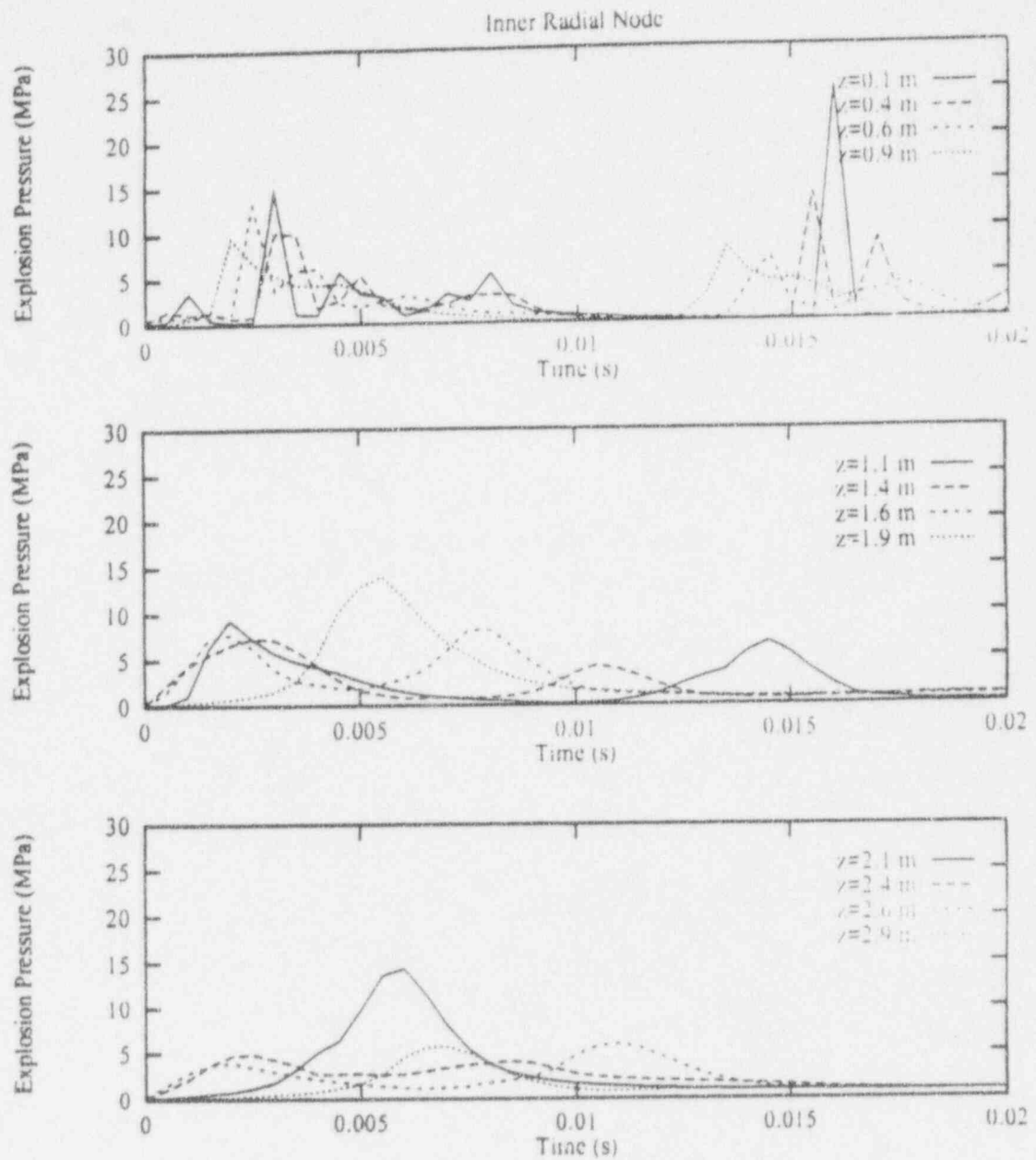


Figure 36 Predicted explosion pressure history at different axial locations in the inner radial node using IFCI computer code (scenario B, 3 m pool depth)

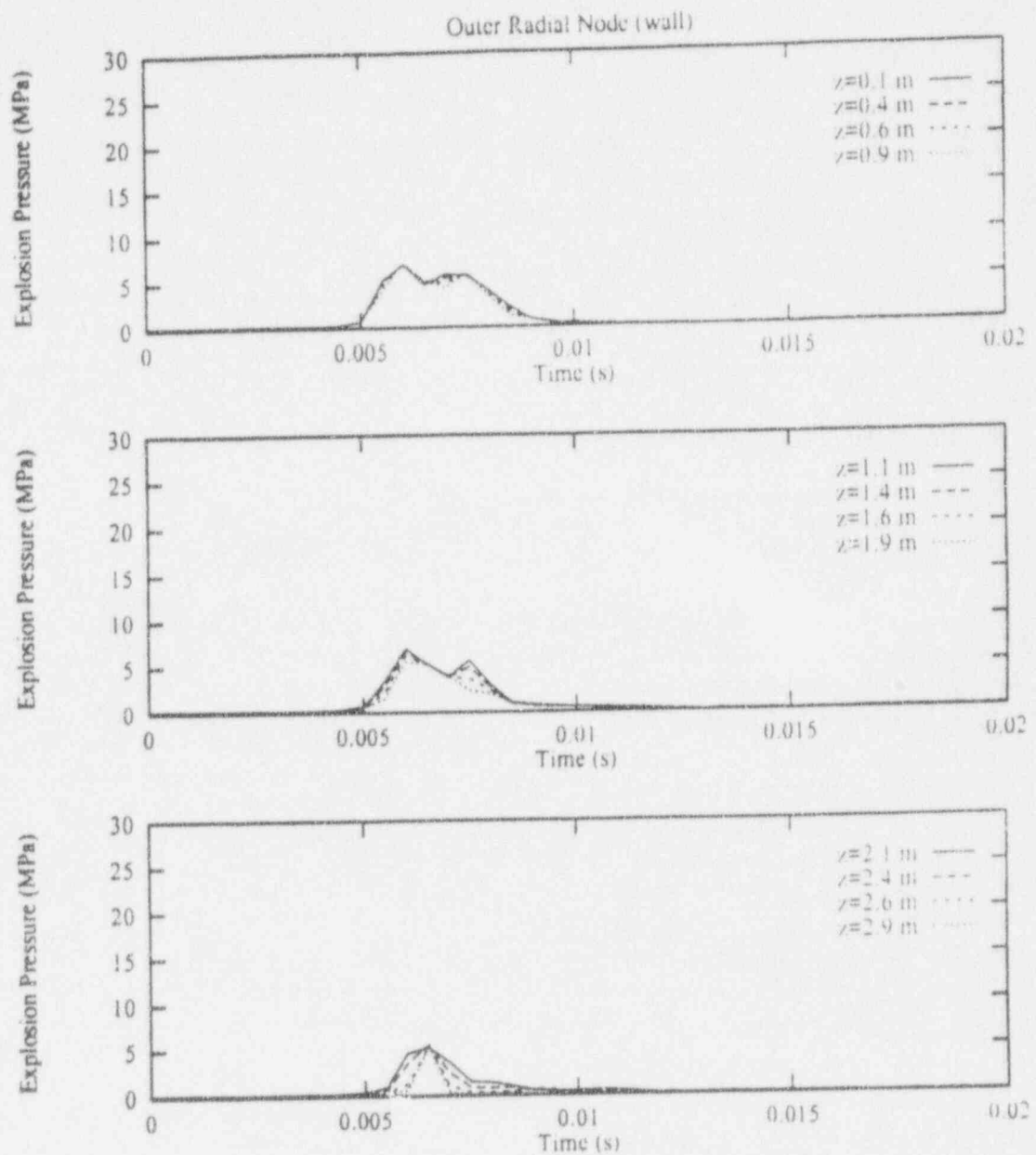


Figure 37 Predicted explosion pressure history at different axial locations in the outer radial node (wall) using IFCI computer code (scenario B, 3 m pool depth)

The TEXAS nodalization for this sensitivity case was similar to the base case condition in scenario B, except the coolant pool was changed to 3 m (6 axial nodes in water). The results of the simulation are presented in Figures 38 and 39. The maximum vapor void fraction was somewhat lower than the base case which was believed to be a result of smaller melt mass in the 3 m pool as compared to the 5.5 m pool. It was expected that the lower vapor void fraction (assuming all other conditions being similar) would support higher explosion pressure, and the maximum explosion pressure in this case (~ 95 MPa) was somewhat higher than the base case. Table 21 provides a summary of the predicted pressure impulses.

Table 21 Predicted pressure impulse for the 3 m Pool sensitivity calculation using TEXAS computer code (scenario B)

Axial Distance, z (m)	Pressure Impulse (kPa-s)
1.25	490
1.75	440
2.75	390

5.2.2.2 Sensitivity to the Initial Melt Velocity and Saturated Water Pool (S-6 and S-7)

Figures 40 through 43 show the local vapor void fraction and the explosion pressures for these two sensitivity calculations. The vapor void fraction for higher initial melt velocity of 15 m/s is higher than the base case calculation due to increased particle breakup and smaller size of the particles during the premixing phase. The minimum particle diameter at the end of the premixing phase was approximately 2 mm compared to 4 mm for the base case, and a larger number of particles broke up into smaller size particles as compared to the base case. This particle breakup would increase the melt-coolant interfacial area and enhance the rate of heat transfer from the particles to the coolant. The maximum explosion pressure in this case was approximately 140 MPa as compared to 80 MPa for the base case condition.

The vapor void fraction for an initially saturated water pool is shown in Figure 42. The maximum vapor void fraction is considerably higher due to higher steam generation rate for the saturated pool as compared to the subcooled pool for the base case. The higher vapor void fraction would also limit the maximum explosion pressures as evidenced in Figure 43. The explosion pressures in this sensitivity calculation are considerably lower than the base case which would also indicate lower pressure impulses. Table 22 provides a summary of the predicted pressure impulses for these sensitivity cases.

Table 22 Predicted pressure impulse for sensitivity cases S-6 (melt velocity) and S-7 (saturated water pool) using TEXAS computer code (scenario B)

Axial Distance, z (m)	Pressure Impulse (kPa-s)	
	S-6	S-7
3.75	1715	84
4.25	1620	70
4.75	1470	56

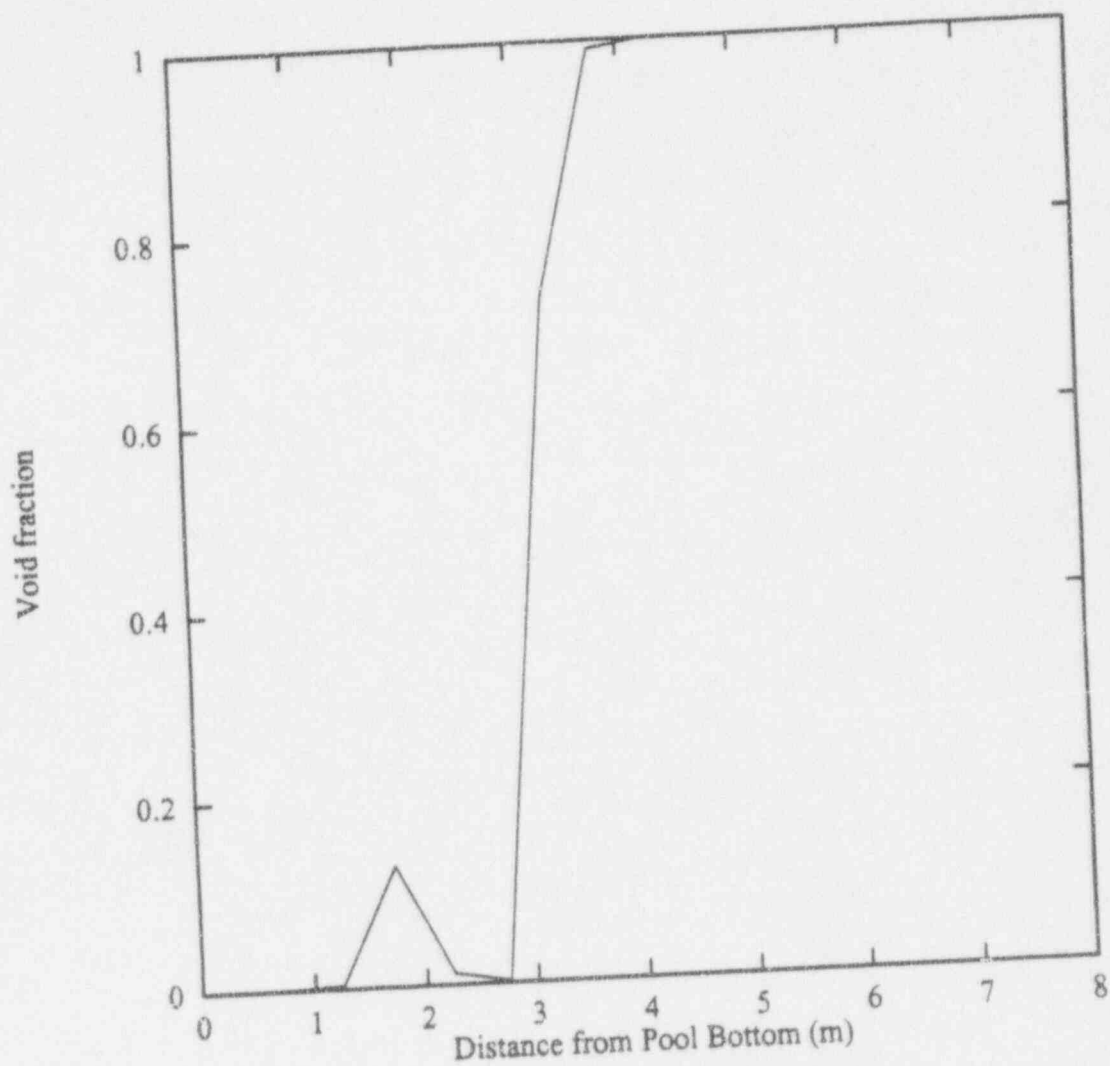


Figure 38 Predicted vapor void fraction for scenario B using TEXAS computer code (3 m pool depth)

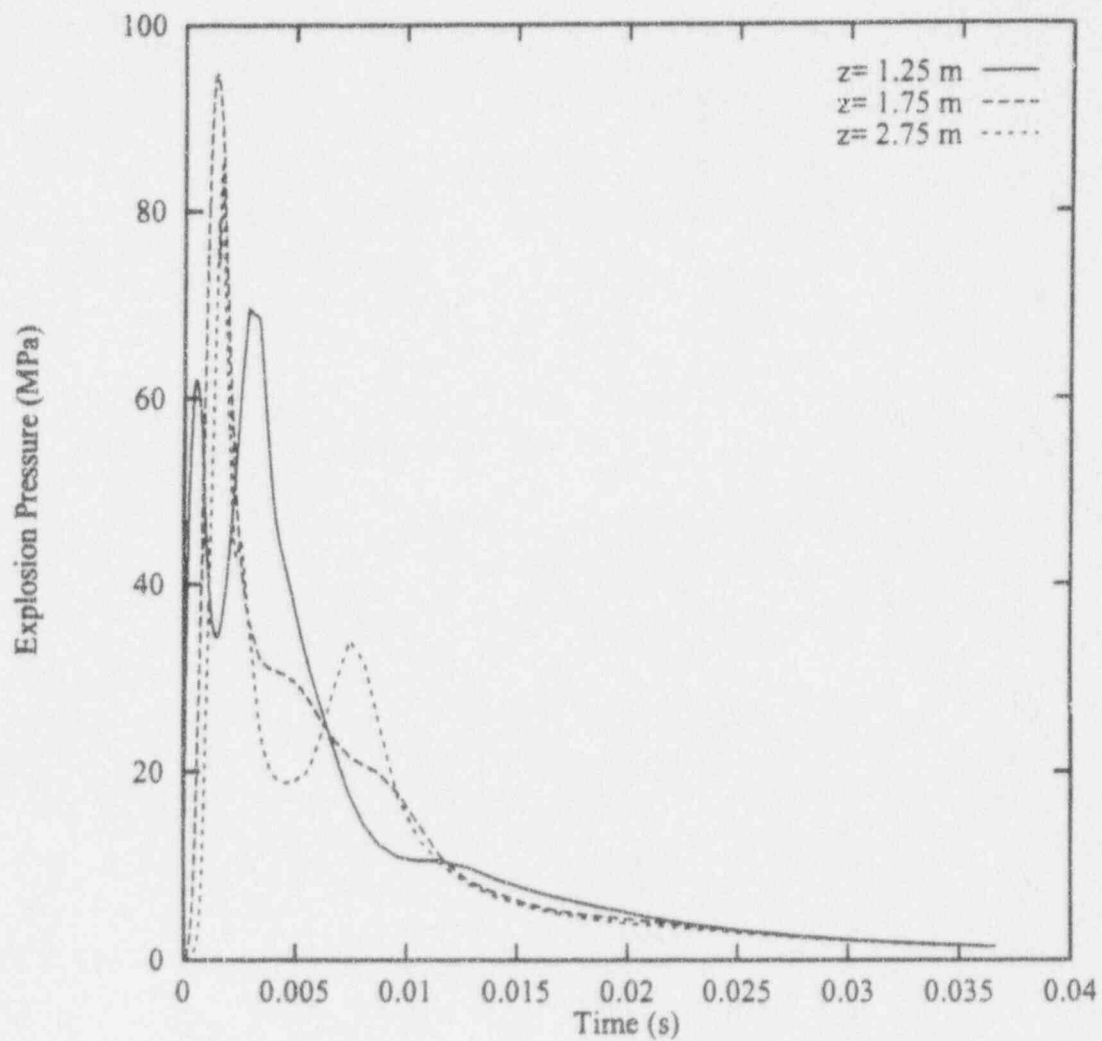


Figure 39 Predicted explosion pressure history at different axial locations using TEXAS computer code (scenario B, 3 m pool depth)

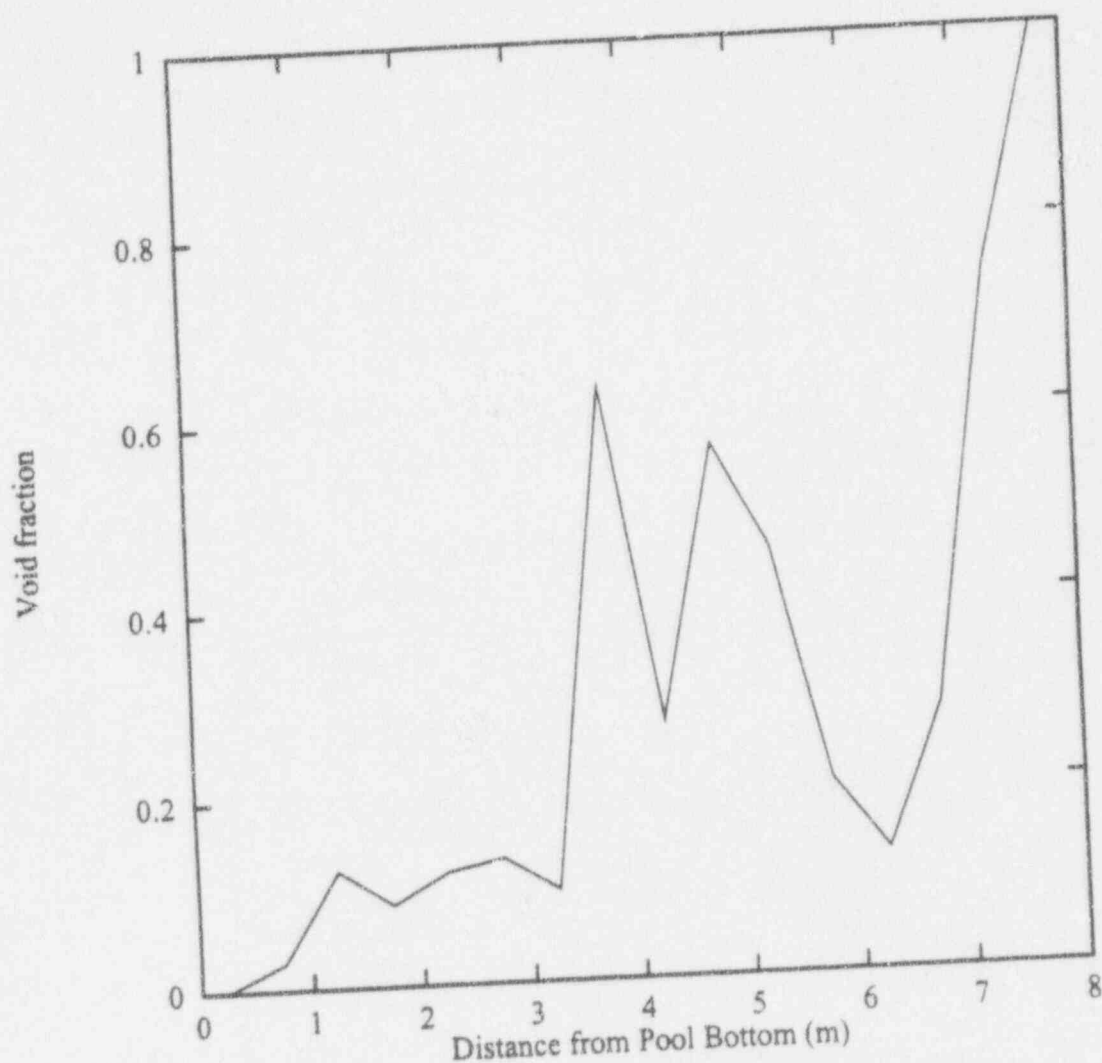


Figure 40 Predicted vapor void fraction for scenario B using TEXAS computer code (initial melt velocity of 15 m/s)

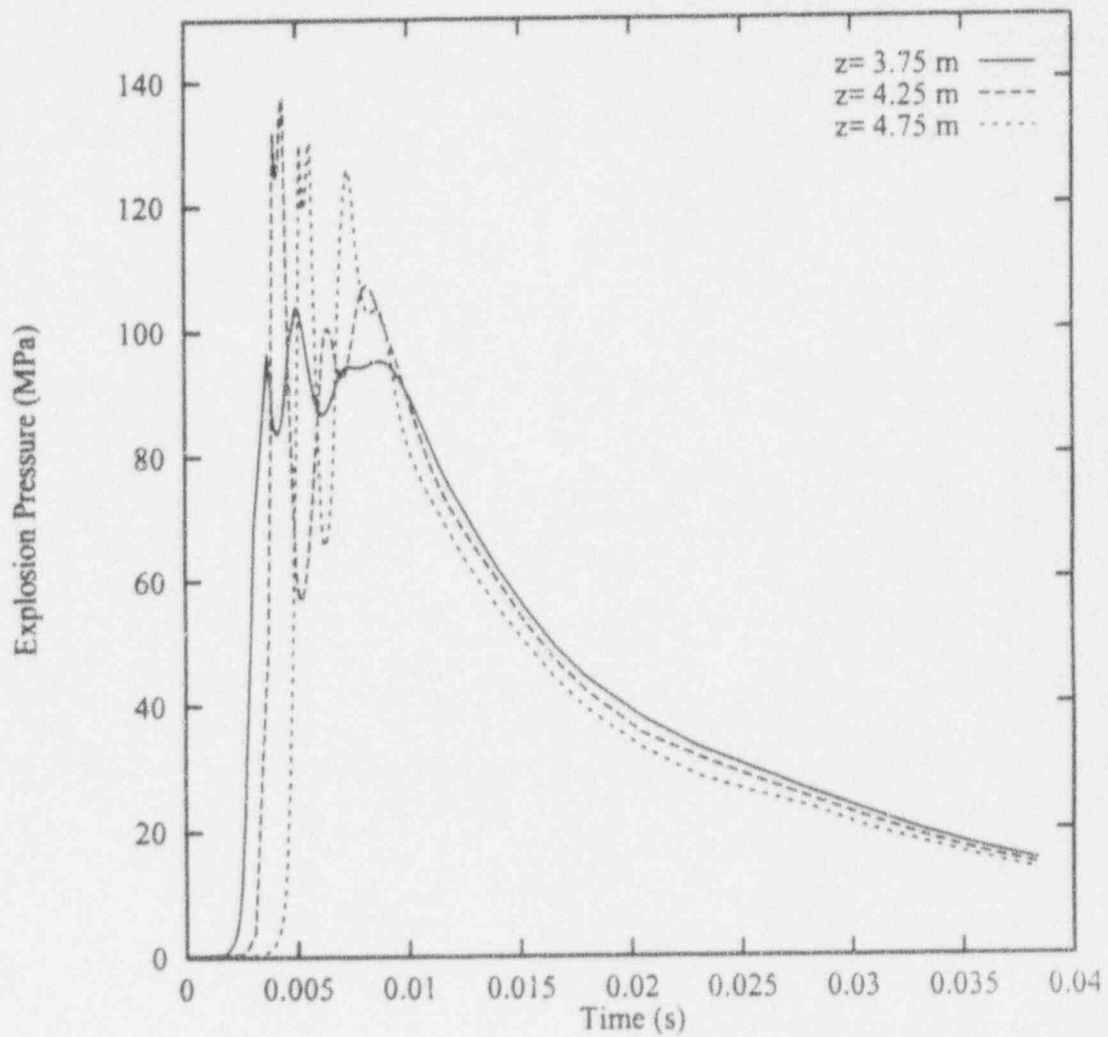


Figure 41 Predicted explosion pressure history at different axial locations using TEXAS computer code (scenario B, initial melt velocity of 15 m/s)

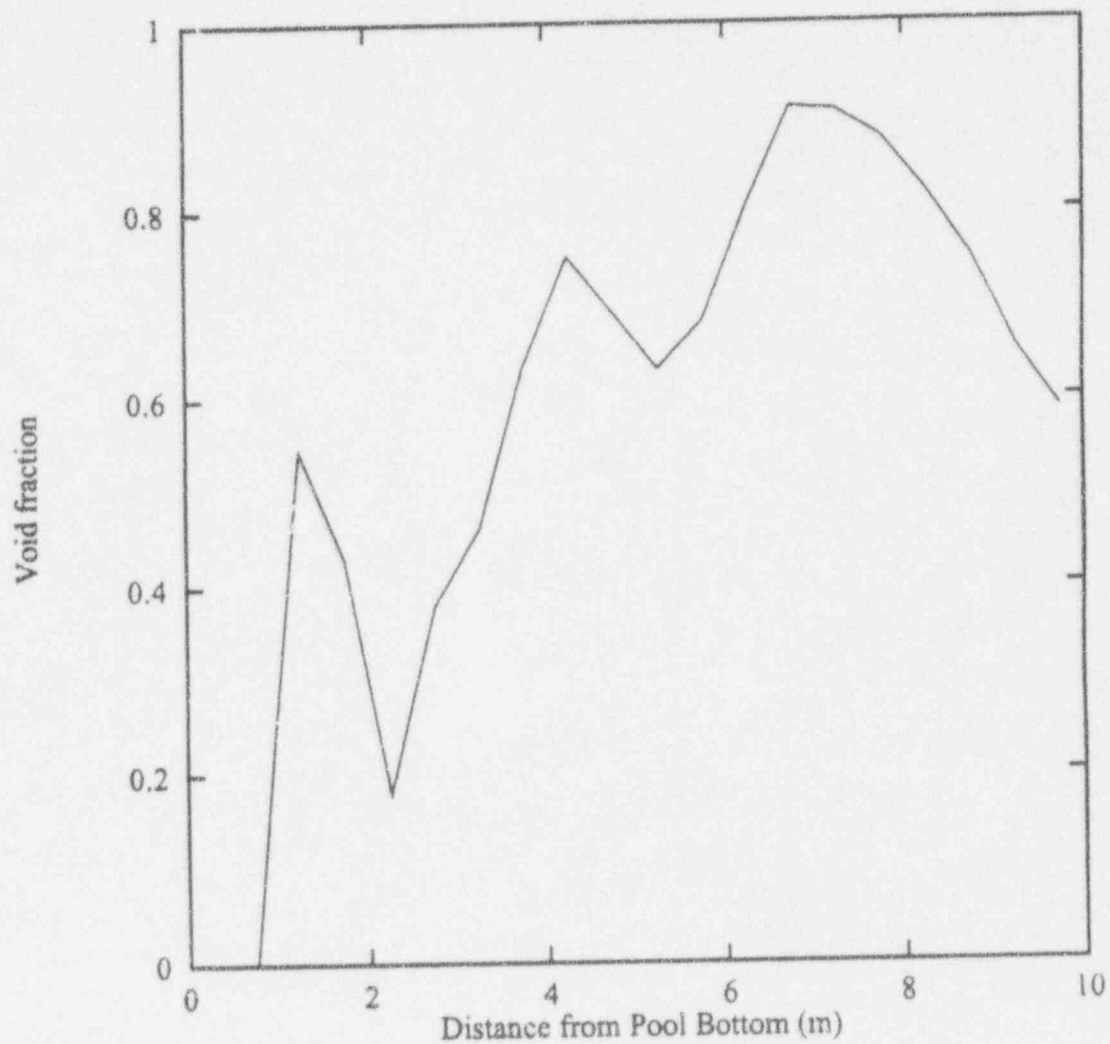


Figure 42 Predicted vapor void fraction for scenario B using TEXAS computer code (saturated water pool)

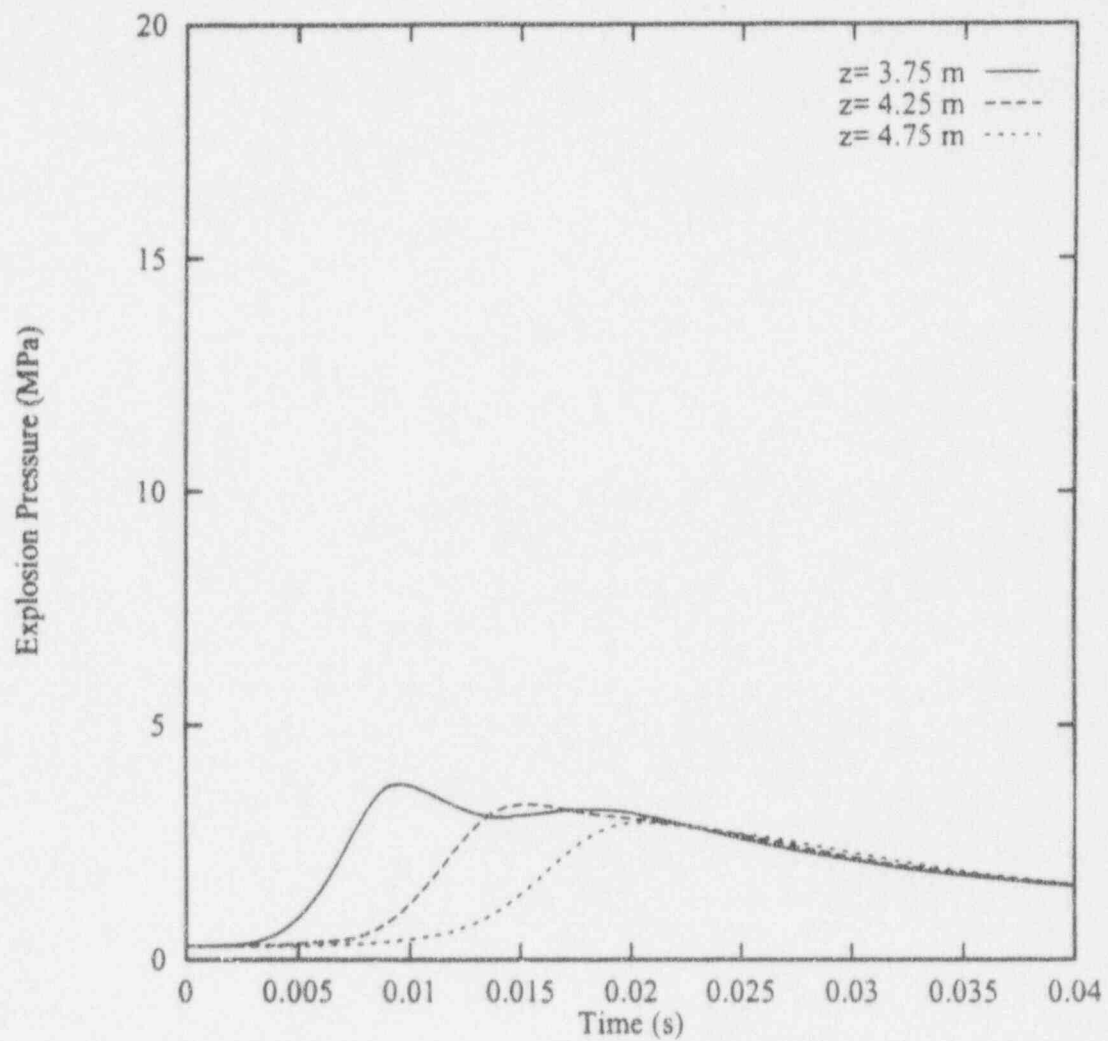


Figure 43 Predicted explosion pressure history at different axial locations using TEXAS computer code (scenario B, saturated water pool)

6. SUMMARY AND CONCLUDING REMARKS

6.1 Summary and Insights

An assessment of the consequences of an ex-vessel energetic fuel-coolant interaction in the reactor cavity of CE System 80+ containment has been made. In this study two mechanistic computer codes (TEXAS and IFCI) have been used to predict the dynamic pressures and the resulting pressure impulses during postulated severe accidents involving failure of the reactor lower head and subsequent pouring of the melt into the flooded cavity. In the IFCI calculations, the melt was poured into the inner radial node corresponding to a failure near the center of the lower head.

A perspective on the predictive capability of the TEXAS computer code was provided and the effect of the variations in the modelling parameters and their impacts on the prediction of explosion pressures have been investigated by a limited comparison to the KROTOS experimental data. The most important modeling parameters during the propagation phase of the interaction in the TEXAS computer code were the proportionality constant and the fragmentation time in the empirical fragmentation model. For the CE System 80+ calculations, the fragmentation model parameters in TEXAS were selected based on the comparison with a limited number of KROTOS experiments.

The KROTOS-26 simulation using IFCI computer code was not successful. A number of numerical difficulties with the IFCI computer code were observed during the course of this investigation. An important shortcoming in the IFCI computer code was the radial nodalization, i.e., increasing the number of the radial nodes always produced numerical errors. Another difficulty with IFCI involved using a small fragmented particle size (0.1 mm) for the scenario B calculations, which would result in iteration failure and prediction of unphysical results (negative volume fractions). The finer radial nodalization becomes a necessity both in premixing and explosion propagation phases of the interaction. The nodalization directly affects the radial spreading of the melt, the propagation of pressure wave, and the accuracy of the computations. Therefore, a limited number of IFCI calculations with relatively coarse radial nodalization were performed to assess, qualitatively, the radial propagation of explosion and the resulting impulse loads on the cavity boundaries.

Prediction of the ex-vessel fuel-coolant interaction energetics for CE System 80+ required specification of the relevant initial conditions. The most important initial conditions for the present analysis were the melt mass, composition, and temperature in the lower head prior to vessel breach, the mode, size and the location of the vessel breach, the height of the water pool in the cavity, and the conditions in the primary system and the containment. The initial conditions proposed were based on the recent results of SCDAP/RELAP5 calculations for station blackout scenarios in Surry scaled to CE System 80+ configuration. A comparison between

thermal hydraulic features of Surry and CE System 80+ was also provided. Two scenarios corresponding to a single penetration failure (scenario A) and a rupture (scenario B) were proposed given the uncertainties in the mode of lower head failure; and a number of sensitivity calculations have been performed to envelope the range of expected dynamic pressures and pressure impulses. The results of these calculations indicated that the pressure impulses could vary between 30 and 1700 kPa-s depending on the initial and boundary conditions.

The predicted pressure impulses in the TEXAS and IFCI simulations for scenario A were comparable. There were, however, major discrepancies for scenario B as TEXAS predicted much higher pressure impulses compared to IFCI. The major reason for these discrepancies was believed to be the choice of fragmented particle size in the IFCI simulations for scenario B. Therefore, the maximum pressures and the predicted pressure impulses in scenario B using IFCI were expected to be substantially higher if the simulations with a fragmented particle size of 0.1 mm had been successful. The maximum impulse loads for scenario B using a fragmented particle diameter of 1 mm (57 kPa-s) were comparable to scenario A (39 kPa-s) which did not appear to be reasonable. Table 23 presents a summary of the comparison of maximum pressure impulses between the two codes for scenario A.

Table 23 Maximum predicted pressure impulses: comparison of codes

Simulation of Scenario A	Pressure Impulse (kPa-s)		
	TEXAS	IFCI	
		Inner Node	Wall Node
Base Case	42	39	15
3 m pool	46	25	10

Due to numerical difficulties with the IFCI computer code (lack of sufficiently fine radial nodalization and experimental validation of the explosion model), it was not possible to determine conclusively the pressure wave decay at the cavity boundaries. However, IFCI provided a quantitative estimate of the radial decay of the pressure away from the explosion zone. In all of the IFCI calculations presented in this report, the melt was assumed to pour into the inner node (corresponding to a failure at the center of the RPV lower head), and the cylindrical computational geometries included the corbel supports region (radial distance of 1.5 m from the center of the cavity), and the cavity wall below the corbel supports region (radial distance of 3.7 m from the center of the cavity). For scenario A involving a single instrument tube penetration at the center of the cavity, the results of the base case and 3 m pool sensitivity calculations with IFCI indicated that the pressure impulses at the cavity boundaries were reduced

by approximately a factor of 2.5 from the interaction zone. For scenario B with a relatively large local rupture size at the center of the cavity, the results of the base case and 3 m pool sensitivity calculations with IFCI indicated that the pressure impulses at the cavity boundaries were reduced by approximately factors of 1.5 and 3 from the interaction zone, respectively.

The impulse loads at the wall are expected to be reduced as the pressure wave expands radially within the subcooled water. This is especially true for the case of failure near the central region of the lower head such that the explosion is expected to occur in the center of the cavity and the pressure wave would decay radially within the water pool. However, if the failure occurs away from the center of the lower head (e.g., a single instrument tube penetration near the corbel supports), then a decay of pressure wave is not expected at the corbel supports and the pressure and the dynamic loads on the corbel supports would be similar to the pressure impulses in the explosion zone. However, the cavity wall is approximately 3.7 m from the center of the cavity, and if an explosion would occur near the corbel supports, the pressure impulses on the cavity wall would be reduced as the pressure wave traverses this distance, however, at the present time we do not take any credit for the radial decay on the corbel supports or the cavity wall should a failure occur near the cavity boundaries.

A simple analysis based on irrotational flow theory for the motion of an initial spherical cavity produced by an underwater explosion is provided in Batchelor [24], McCormack and Crane [25], and Cole [26]. The analytical pressure distribution indicates that the pressure at any radial distance away from the explosion zone decreases as $1/r$. Strictly speaking, this $1/r$ behavior is true for a point source explosion in an infinite medium. The effects of confinement (the cavity wall is a finite distance from the center of the explosion) and proximity of the explosion zone to the free surface could impact the $1/r$ scaling. Theofanous et al. [3] used PM-ALPHA/ESPROSE calculations to provide some insights into the propagation phase of an ex-vessel steam explosion in a reactor cavity. These calculations were not meant to provide any specific scenario but were used mainly for illustration purposes. The pour radius was 0.3 m and the melt volume fraction at the inlet was 0.05. The radius of the reactor cavity was assumed to be 3 m, and two pool depths of 1 m and 3 m were chosen. The results of these calculations indicated that the explosion would occur at the center of the cavity and decay radially towards the cavity wall. The maximum pressure in the explosion zone was approximately 25 MPa while the maximum pressures at the cavity wall were approximately 2 MPa, thus relatively low pressures at the wall were observed as compared to the explosion zone. These results further indicated that peak pressures in the explosion zone and the cavity wall would decay approximately as the ratio of the corresponding radii (0.3/3). Even though these two specific simulations indicated that under certain conditions the $1/r$ scaling may apply, there is no evidence that this would be universally true. A recent calculation by Corradini [27] using the CTH computer code indicated that a ten-fold reduction in the peak explosion pressure at a distance of 1.5 m from the explosion zone was predicted. This calculation was consistent with cases involving an instrument tube penetration failure.

A number of sensitivity calculations involving the initial and boundary conditions have been performed for scenarios A and B using the TEXAS computer code. The maximum predicted impulse loads for these sensitivity calculations including the base cases are shown in Table 24. As far as estimating the loads on the cavity boundaries (both the corbel supports and the cavity wall), a reduction of a factor of 2.5 for all cases involving a single instrument tube penetration (based on the IFCI calculations for scenario A) is assumed, while for large pours, a factor of 1.5 reduction has been credited (based on the IFCI calculations for scenario B). The most severe cases occurred for scenario B where the predicted pressure impulses were significantly higher than in scenario A. The estimated loads on the cavity boundaries are based on the assumption that the failure would occur at the center of the cavity, however, for failures near the corbel supports, the explosion zone impulses should be used to determine the impulse loads.

Table 24 Summary of the maximum impulse loads at the cavity boundaries for the CE System 80+ using TEXAS

Scenario A	Pressure Impulse (kPa-s)	
	Explosion Zone	Cavity Boundaries
Base case	42	17
S-1 (3 m pool)	46	18
S-2 (4.5 m pool)	49	20
S-3 (200 K melt superheat)	60	24
S-4 (failure of 8 penetrations)	160	107
S-5 (initial melt discharge velocity = 8 m/s)	92	37
S-7 (saturated pool)	31	12
Scenario B		
Base case	512	341
S-1 (3 m pool)	490	327
S-6 (initial melt discharge velocity = 15 m/s)	1716	1144
S-7 (saturated pool)	84	56

The structural analyses reported in Reference [17] assert that the corbel supports can withstand a pressure impulse of at least 32 kPa-s (corresponding to zero percentile of the failure probability distribution), while the structural strength of the cavity wall is assessed by CE to be much lower (see Figure 4). The cavity wall can withstand an impulse load of at least 5 kPa-s (corresponding to zero percentile of the failure probability distribution); however, the median capacity reported in Reference [17] for the cavity wall is approximately 22.6 kPa-s.

Based on the range of impulse loads estimated for scenario A involving a single instrument tube penetration failure near the center of the lower head, the failure likelihood of the corbel supports is low, however, higher likelihoods are expected for the cavity wall. If an instrument tube penetration fails near the corbel supports, the loads on the cavity boundaries are expected to be higher (corresponding to the values for the explosion zone), and the likelihood of the corbel supports failure as well as the cavity wall become relatively high. For scenario A involving failure of multiple instrument penetrations, the failure likelihood of both the cavity wall and the corbel supports are expected to be high (see Figure 44).

For scenario B (see Figure 45), the high impulsive loads on the corbel supports and cavity wall indicate a high likelihood of failure for all cases considered. Scenario B was considered based on the uncertainties regarding the mode and size of the lower head failure, and given these uncertainties, conditions in scenario B cannot be ruled out at the present time.

However, to obtain an estimate of the probability of failure for the corbel supports and the cavity wall, the impulsive load uncertainties must also be considered. The present analyses did not attempt to provide probabilistic distributions for the FCI-induced loads. Furthermore, it should also be noted that the failure of the cavity does not automatically lead to containment failure. Reference [17] assigns a conditional probability of 0.05 for containment failure given cavity failure.

It is important to note that the underlying phenomena associated with the steam explosion issue are still not well understood and the current hypotheses remain technically controversial. Therefore, the present study is not intended to provide the NRC with a definitive quantitative estimate of the ex-vessel steam explosion energetics for the CE System 80+ containment, rather, it is directed at providing a calculational method and/or framework for exploring the possible range of impulsive loads based on our current understanding of these complex phenomena.

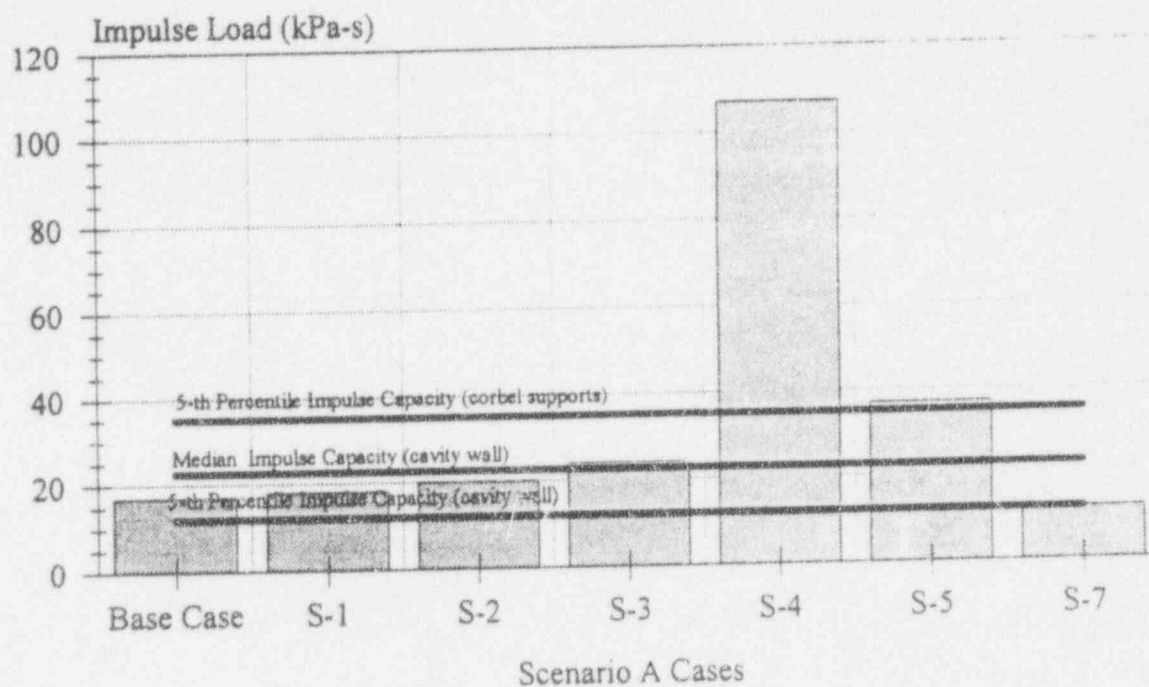


Figure 44 Comparison of the TEXAS estimated impulsive loads on the cavity boundaries with the CE System 80+ containment capacity for scenario A

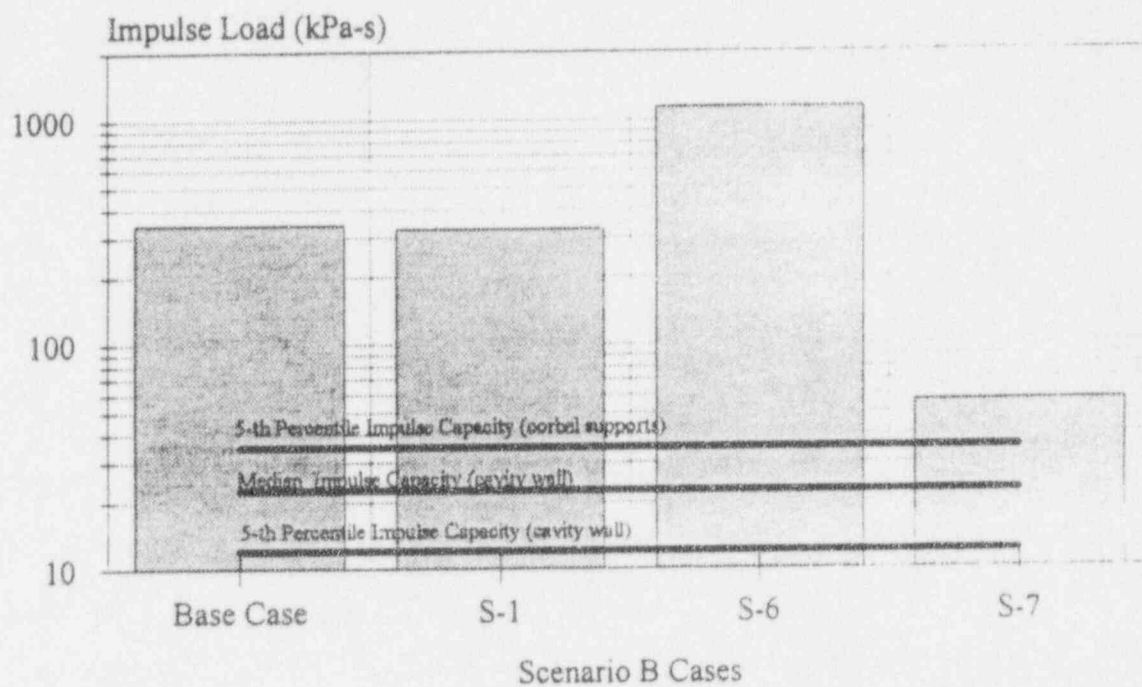


Figure 45 Comparison of the TEXAS estimated impulsive loads on the cavity boundaries with the CE System 80+ containment capacity for scenario B

7. REFERENCES

1. M. D. Oh and M. L. Corradini, "A Propagation/Expansion Model for Large Scale Vapor Explosions," *Nucl. Sci. Eng.*, **96**, 225-240 (1987).
2. C. C. Chu, "One-Dimensional Transient Fluid Model for Fuel-Coolant-Interactions," Ph.D. Dissertation, Department of Nuclear Engineering and Engineering Physics, University of Wisconsin at Madison (1986).
3. T. G. Theofanous, et al., "Steam Explosions: Fundamentals and Energetic Behavior," NUREG/CR-5960 (1994).
4. F. J. Davis and M. F. Young, "Integrated Fuel-Coolant Interaction (IFCI) Code: User's Manual," Draft Copy, (1993).
5. H. Hohmann, et al., "KROTOS 26 to KROTOS 30: Experimental Data Collection," Commission of the European Communities, Joint Research Center, Technical Note No. I.92.115.
6. M. Burger, et al., "Analysis of Thermal Detonation Experiments by Means of a Transient Multiphase Detonation Code," Proceedings of the International Meeting on Nuclear Reactor Thermal Hydraulics, Karlsruhe, (October 1989).
7. T. G. Theofanous, Summary of the CSNI Specialist's Meeting on Fuel-Coolant Interaction, University of California, Santa Barbara, (August 1993).
8. M. Pilch, "Acceleration Induced Fragmentation of Liquid Drops," Ph.D. Dissertation, University of Virginia (1981).
9. M. L. Corradini, et al., "Vapor Explosions in Light Water Reactors: A Review of Theory and Modelling," *Progress in Nuclear Energy*, **22** (1), 1-117 (1988).
10. Joint Research Center, "FARO LWR Programme: Scoping Test Data Report," Technical Note No. I.92.135, Institute of Safety Technology, Ispra, Italy (1992).
11. Joint Research Center, "FARO LWR Programme: Quenching Test-2 Data Report," Technical Note No. I.93.154, Edited by D. Magallon, Institute of Safety Technology, Ispra, Italy (1993).

12. M. D. Allen, et al., "Experiments to Investigate the Effects of Fuel/Coolant Interactions on Direct Containment Heating, The IET-8A and IET-8B Experiments," SAND92-2849, Sandia National Laboratories, Albuquerque, NM (1993).
13. J. Tang, "Modeling of the Complete Process of One-Dimensional Vapor Explosions," Ph.D. Dissertation, Department of Nuclear Engineering and Engineering Physics, University of Wisconsin at Madison (1993).
14. F. J. Davis, "IFCI 6.0 Operational Assessment Letter Report," Sandia National Laboratories (October 1993).
15. M. Snodderly, U. S. Nuclear Regulatory Commission, *Private Communication*, (January 1994).
16. DCH Working Group, "Integrated Report on DCH Issue Resolution for PWRs," NUREG/CR-6109, Draft for Peer Review (August 1993).
17. "System 80+ Severe Accident Phenomenology and Containment Performance," Combustion Engineering, Inc. Report (1993).
18. Additional information on containment design for the CE System 80+ provided by NRC to Energy Research, Inc (March 1993).
19. D. L. Knudson and C. A. Dobbe, "Assessment of the Potential for High Pressure Melt Ejection Resulting from a Surry Station Blackout Transient," NUREG/CR-5949 (May 1993).
20. P. D. Bayless, "Analyses of Natural Circulation During a Surry Station Blackout Using SCDAP/RELAP5," (input deck), NUREG/CR-5214 (1988).
21. "An Integrated Structure and Scaling Methodology for Severe Accident Technical Issue Resolution," NUREG/CR-5809 (1991).
22. M. M. Pilch, H. Yan, and T. G. Theofanous, "The Probability of Containment Failure by Direct Containment Heating in Zion," NUREG/CR-6075 (June 1993)
23. J. L. Rempe, et al., "Light Water Reactor Lower Head Failure Analysis," NUREG/CR-5642, EGG-2618, Draft (March 1993).
24. G. K. Batchelor, *An Introduction to Fluid Dynamics*, Cambridge University Press (1980).

25. P. D. McCormack and L. Crane, *Physical Fluid Dynamics*, Academic Press (1973).
26. R. H. Cole, *Underwater Explosions*, Princeton University Press (1948).
27. M. L. Corradini, University of Wisconsin, *Private Communication*, (March 1994).
28. E. P. Hicks and D. C. Menzies, "Theoretical Studies on the Fast Reactor Maximum Accidents," Argonne National Laboratory Report ANL-7120, pp. 654-670 (1965).

APPENDIX

THERMODYNAMIC ANALYSIS OF STEAM EXPLOSIONS

In the thermodynamic analysis of steam explosions, the equilibrium pressure, the work potential and the mass of steam are predicted in a two step process. In the first step, the melt and coolant achieve thermodynamic equilibrium in an adiabatic, constant volume process. During the second step, the work potential of the interaction is determined based on the assumption that the melt and coolant expand isentropically to a final prescribed state.

To determine the equilibrium temperature, the change in the internal energy for each component of the mixture (fuel and coolant) can be expressed as:

$$\begin{aligned}\Delta U_c &= m_c c_{v,c} (T_e - T_{c,1}) \\ \Delta U_f &= m_f c_{v,f} (T_e - T_{f,1})\end{aligned}\tag{A.1}$$

where ΔU is the change in the internal energy, m is the mass, C_v is the specific heat at constant volume, and T is the temperature. The subscripts c , f , e , 1 refer to coolant, fuel, equilibrium condition, and initial state, respectively. It has been assumed in the formulation of Equation (A.1) that there is no heat or work transfer to the surroundings, the changes in potential and kinetic energies are negligible, and the changes in heat capacities with temperature are also negligible. The equilibrium temperature is obtained by equating the changes in the internal energies of the fuel and coolant:

$$T_e = \frac{T_{c,1} + (m_f c_{v,f} / m_c c_{v,c}) T_{f,1}}{1 + (m_f c_{v,f} / m_c c_{v,c})}\tag{A.2}$$

In the second step, the fuel-coolant mixture is assumed to expand isentropically to the final state [28]. The final state is either a specified volume or pressure. In reactor cavities with large volumes of water, the final state is specified by the pressure. Since the coolant and fuel are prescribed to remain in thermal equilibrium, the entropy of the coolant increases and the entropy of the fuel decreases. During the expansion process, the coolant passes into the two-phase region and the final state of the coolant may be superheated vapor. The fuel, however, remains in a subcooled state during this process. In this analysis, the control mass includes the fuel-coolant mixture. From the first law of thermodynamics, the net work is computed by considering the change in the internal energy of the mixture,

$$W_{net} = -m_m \Delta u_m = -(m_c \Delta u_c + m_f \Delta u_f) \quad (A.3)$$

$$= -[m_c(u_{c,2} - u_{c,e}) + m_f(u_{f,2} - u_{f,e})]$$

where the subscripts m and 2 refer to the mixture and final state of the mixture, respectively.

The internal energy is defined as:

$$u = c_v T + x u_{fg} = c_v T + x(h_{fg} - p v_{fg}) \quad (A.4)$$

where x is the quality. Equation (A.3) can now be written as:

$$W_{net} = m_c [c_v(T_e - T_2) + x_e(h_{fg} - p v_{fg})_e - x_2(h_{fg} - p v_{fg})_2]_c \quad (A.5)$$

$$+ m_f [c_v(T_e - T_2) + x_e(h_{fg} - p v_{fg})_e - x_2(h_{fg} - p v_{fg})_2]_f$$

The efficiency of the process (conversion ratio) can be defined as the ratio of the net work to the thermal energy of the fuel, and using this definition, the net work becomes:

$$W_{net} = CR m_f c_{v,f} (T_{f,1} - T_{c,1}) \quad (A.6)$$

where CR is the conversion ratio.

For the isentropic expansion of the mixture, the change in the entropy of the mixture is zero, therefore,

$$T_m ds_m = dh_m - v_m dp_m = 0 \quad (A.7)$$

The mixture enthalpy and specific volume can be written as:

$$h_m = \frac{(m_c c_{p,c} + m_f c_{p,f})T + m_c x h_{fg,c}}{(m_c + m_f)} \quad (A.8)$$

$$v_m = \frac{x m_c v_g}{(m_c + m_f)} = \frac{x R_c T}{p} \frac{m_c}{(m_c + m_f)} \quad (A.9)$$

where R_c is the coolant gas constant and the subscript g refers to the coolant vapor. In writing Equation (A.9), it has been assumed that the specific volumes of the fuel melt and liquid coolant are negligible in comparison to the coolant vapor, and the perfect gas law applies to the coolant vapor.

Differentiating Equation (A.8) yields:

$$dh_m = \frac{(m_c c_{p,c} + m_f c_{p,f})dT + m_c h_{fg,c} dx}{(m_c + m_f)} \quad (A.10)$$

The change in the pressure can be calculated using the Clausius-Clapeyron equation and assuming that the equilibrium state is close to the saturation line and the expansion occurs in the two-phase region, therefore,

$$dp_m \cong \left. \frac{\partial p}{\partial T} \right|_{sat} dT = \frac{h_{fg,c}}{T v_{fg,c}} dT \cong \frac{p h_{fg,c}}{R_c} \frac{dT}{T^2} \quad (A.11)$$

Substituting Equations (A.9), (A.10), and (A.11) into Equation (A.7) yields,

$$(m_c c_{p,c} + m_f c_{p,f}) \frac{dT}{T} + m_c h_{fg,c} d\left(\frac{x}{T}\right) = 0 \quad (A.12)$$

and integration of this equation between the equilibrium state and the final state gives,

$$x_2 = T_2 \left[\frac{x_e}{T_e} + \left[\frac{m_c c_{p,c} + m_f c_{p,f}}{m_c h_{fg,c}} \right] \ln \frac{T_e}{T_2} \right] \quad (A.13)$$

Once the final quality is obtained, the final mixture temperature can also be determined. If the final quality is less than 1, the final coolant state is in the two-phase region. If x_e is greater than 1, the final coolant state is superheated. Under this condition, Equations (A.9) and (A.10) can be rewritten as:

$$v_m = \frac{R_c T}{p} \frac{m_c}{(m_c + m_f)} \quad (A.14)$$

$$dh_m = \frac{(m_c c_{p,c} + m_f c_{p,f})dT}{(m_c + m_f)} \quad (A.15)$$

Substitution of Equations (A.14) and (A.15) into Equation (A.7) yields:

$$\frac{(m_c c_{p,c} + m_f c_{p,f})}{m_c R_c} \frac{dT}{T} = \frac{dp}{p} \quad (A.16)$$

Integration of the Equation (A.16) between the equilibrium and final states gives:

$$T_2 = T_e \left(\frac{p_2}{p_e} \right)^{\frac{m_e R_e}{m_e c_{p,e} + m_f c_{p,f}}} \quad (\text{A.17})$$

where p_2 is the cavity pressure, and the equilibrium pressure p_e is obtained from:

$$\begin{aligned} p_e &= \rho_e R_e T_e \\ \rho_e &= \rho_{c,1} \end{aligned} \quad (\text{A.18})$$

assuming ideal gas behavior, and constant volume heating of the gas.

Therefore, given the mass of fuel and coolant participating in the explosion together with the fuel and coolant initial conditions, the thermodynamics analysis yields the upper bound values for the pressure and work potential during the expansion.

DISTRIBUTION LIST

Dr. A. Behbahani (6 copies)
U. S. Nuclear Regulatory Commission
Office of Nuclear Regulatory Research
5650 Nicholson Lane
Rockville, Maryland 20852

Professor M. L. Corradini (1 copy)
Department of Nuclear Engineering and Engineering Physics
University of Wisconsin
Madison, WI 53706

Professor S. I. Abdel-Khalik (1 copy)
3579 Midvale Cove
Tucker, GA 30084

Energy Research, Inc. (4 copies)

ATTACHMENT 1

Comments by Professors Abdel-Khalik and Corradini on the Draft ERI/NRC 94-201 Report

S. I. ABDEL-KHALIK
Consultant
3579 Midvale Cove, Tucker, Georgia 30084

February 21, 1994

Dr. M. Khatib-Rahbar, President
Energy Research, Inc.
P.O. Box 2034
Rockville, Maryland 20847

Subject: Review of draft document entitled: "Analysis of Ex-Vessel Steam Explosion Energetics for the Combustion Engineering System 80+", ERI/NRC 94-201

Dear Dr. Khatib-Rahbar:

Per your request, an independent technical review of the above-referenced document has been conducted. The purpose of the review, as stated in your letter of February 9, 1994, was to "...evaluate:

1. *The adequacy and the basis for the selected initial and boundary conditions, and other parameters and variables of importance for ex-vessel FCI calculations, and their applicability to CE system 80+ design, to ensure that this information is representative of typical accident conditions in the CE system 80+.*
2. *The approach for analysis, and the calculated results on which the conclusions are based, are technically consistent and portray the uncertainties associated with the issue."*

In conducting the evaluation, I have also examined your earlier report entitled: "An Assessment of Ex-Vessel Fuel Coolant Interactions Energetics for the Combustion Engineering System 80+ Advanced Pressurizer Water Reactor", ERI/NRC 93-206 (August 1993).

Based on the review, several major deficiencies in the modeling approach have been identified; such deficiencies bring into question the validity of the analyses, results, and conclusions presented in the report. Details of those deficiencies, along with other errors and ambiguities found in the report are outlined below.

I. Major Deficiencies in Modeling Approach

1. Two computer codes, TEXAS and IFCI, have been used to estimate the dynamic pressures and the resulting impulsive loads on the containment cavity walls resulting from the interaction of core debris material relocating into the pre-existing reactor cavity water following core melt accidents. TEXAS is a one-dimensional code, whereas IFCI is two-dimensional. On page 35, the report states that: *"...The IFCI computer code is used here mainly to assess the radial spreading of the melt in the pool in order to determine the mesh cross-sectional area in the one-dimensional TEXAS calculations,..."*

The report also states on page 15 that: *"IFCI also shows strong sensitivity to the nodalization of the computational domain. Increasing the radial resolution seems to be a major problem, i.e. numerical errors and unphysical results were observed for finer radial nodalization."* Similar statements regarding the problems encountered with the radial resolution of the computational domain for IFCI were made at several other locations within the report. **This means that IFCI is being used to do the very thing which it is currently incapable of doing!!** Given the fact that the problem at hand is clearly multi-dimensional, the validity of the one-dimensional TEXAS calculations is questionable especially since no attempts were made to examine the sensitivity of such calculations to the size of the mesh cross sectional area.

2. A comparison of TEXAS simulations with KROTOS-26 experiment was presented; a similar comparison with the KROTOS-21 experiment was presented in reference [13] of the report (ERI/NRC 93-206, August 1993). By assigning values of 0.001 and 2 ms to the empirical parameters C_k and τ_k in the TEXAS fragmentation model, the predicted maximum explosion pressures were matched with the experimental values. Aside from the details of such comparisons (more on that later), **the fact remains that while the code predictions for peak pressures can be forced to match the experimental data, the code does not adequately predict the corresponding impulse values (integral of the pressure-time history curves)** as can be seen from Figure 3, page 14 of the report. Given the fact that the impulsive loads, rather than peak pressures, are used as the main criteria for assessing the survivability of the corbel supports and cavity walls, it is not clear how such comparisons with experimental data can provide any confidence in the code's ability to model the problem at hand.
3. All the sensitivity calculations presented in the report, as well as those in the earlier report (ERI/NRC 93-206, August 1993), assume that the instrument tube failure (scenario A) or vessel rupture (scenario B) will take place at the center of the cavity. The impulse load on the corbel supports and cavity walls are then determined using $1/r$ scaling. Aside from the validity of such scaling (more on that later), the fact remains that for 1.17 m corium height

in the 5.4 m diameter vessel (page 33 of the report), **all instrument tube connections at the bottom of the vessel will be submerged** (see Figure 8). It is not clear why the instrument tube at the center of the vessel would be more likely to fail than any other instrument tube. Failure of an "outer" instrument tube may be equally likely. In that case, for the same set of parameters, a somewhat weaker explosion may result because of the lower initial melt velocity. However, the radial proximity of the failed tube to the corbel supports and cavity walls may produce significantly higher impulse loadings than a similar failure near the vessel center. Therefore, it appears that an extremely important variable, namely the radial location of the failure, has not been taken into account. Consideration of such a variable may alter the conclusions presented in the report regarding the potential impact of single instrument tube failures on the survivability of the corbel supports and cavity walls.

II. OTHER ERRORS AND AMBIGUITIES

1. Page ii of the report states that: "... For the CE System 80⁺ plant calculations, the model parameters are considered to be conservative". The validity of this assertion is questionable. **There is no fundamental theoretical basis for the TEXAS fragmentation model.** Given the empirical nature for the model, the report correctly states (page 11) that: "...The experimentally determined values of the proportionality constant and fragmentation time obtained from the one-dimensional experiments does not automatically assure that these values would be universal (i.e. the effects of scale up to reactor conditions and multi-dimensionality effects cannot be addressed within the one dimensional experimental framework." This means that these parameters may be case specific, inasmuch as we simply do not know how these empirical constants will depend on the various problem variables. In other words, showing that a C_F value of 0.0015 produces higher peak pressures in KROTOS 21 and KROTOS 26 does not necessarily mean that it will produce conservative predictions for other experiments or for the real problem at hand.
2. Page ii of the report states that "...The most important initial conditions for the present analysis are the melt mass, composition, and temperature in the lower head prior to vessel breach, the size of the vessel breach, the height of the water...". As stated in Part I.3 above, the radial location of the vessel breach may be considerably more important than some of the other parameters listed in the report.
3. Page ii of the report states that: "...Given the structural fragility estimates provided by CE are acceptable, the probability of ex-vessel steam explosion-induced containment failure for CE are acceptable, the probability of ex-vessel steam explosion-induced containment failure for CE System 80⁺ is expected to be relatively small for all

conditions examined for scenario A (failure of instrument tube penetration except cases involving failure of multiple instrument tube penetrations...". Clearly, this may not be the case depending on the radial location of the failure.

4. Page iii of the report states that "[the report] is directed at providing a calculational method and/or framework for exploring the possible range of impulsive loads based on our current understanding of these complex phenomena." Given the fundamental concerns raised in Section I above, clearly the calculational methods and framework presented in the report are inadequate and do not represent the current state of the art.
5. Equation (2) page 6 of the report describes the fragmentation model used in TEXAS. There is no fundamental theoretical basis for this equation; it should always be referred to as an empiricism.
6. Page 6 of the report states that for the TEXAS simulations "... In addition, the water pool conditions and initial vapor void fraction are also required." What were the initial void fractions used in the calculations?
7. Page 9 of the report states that: "...additional work is required to increase the level of confidence in the predictive capabilities of the IFCI computer code. On the other hand, the TEXAS model has produced relatively good agreement with the one-dimensional experimental data." Given the concerns raised above, it is clear that the predictive capabilities of the TEXAS code are equally questionable.
8. Page 9 of the report states that: "The maximum explosion pressures measured was approximately 25 MPa which caused significant damage to the upper water container and the level meter." Examination of Figure 3, page 14 of the report reveals that the signals for the K1, K2, and K3 transducers were clearly "saturated", i.e. the actual peak pressures may have been significantly higher than 25 MPa.
9. Page 11 of the report states that: "...Using these parameters, we were able to match the maximum explosion pressures determined experimentally...". See comment II.8 above.
10. Page 11 of the report states that: "...With a higher proportionality constant of $C_{fr} = 0.0015$ the maximum explosion pressure of 50 MPa occurs at K5 pressure transducer which is approximately twice the value measured experimentally...". See comment #II.8 above.
11. Page 12 of the report states that: "...a conservative value of 0.0015 would be chosen for the proportionality constant...". See comment #II.1 above.

12. Figure 3, page 14 of the report. See comments #I.2 and II.8 above.
13. Page 15 of the report states that "...the detonation model in IFCI is purely parametric." The detonation model in TEXAS is also parametric. (See comment #II.5 above).
14. Page 15 of the report states that "...In the present simulation, the explosion process was initiated by assigning a pressure threshold value of 0.05 MPa and a fragmented debris size of 0.1 mm." Where did the 0.05 MPa value come from? Why were different values used in various calculations (see pages 37, 43, and 52 of the report where values of 0.22, 0.22, and 0.2 MPa are reported)?
15. Page 15 of the report states that "...IFCI also shows strong sensitivity to nodalization...". See comment #I.1 above.
16. Figure 5, page 16 of the report. See comment #II.8 above.
17. Page 23 of the report states that: "...The delineation of the initial and boundary conditions involves the specifications of ...". Failure location should be added to the items which need to be examined (see comment #I.3 above).
18. Page 23 of the report states "...In the present analysis, the containment pressure at the time of vessel breach is assumed to be 0.2 MPa." Why was this value selected instead of a bounding value? (0.1 - 0.28 MPa)
19. Page 24 of the report states that: "... the potential for ex-vessel failure before lower head failure is expected to be at least as high as in Surry...". How and why does the lower L/D in the CE System 80* hot leg impact the potential for ex-vessel failure?
20. Page 25 of the report states: "...Given the expected high failure probabilities in the hot leg/surge line for CE System 80* (based on the comparison with Surry), in the present analysis the primary system is assumed to be depressurized at the time of vessel breach, ...". While this may be true, the discussion presented in the report does not clearly support this assertion.
21. Page 30 of the report states: "...the difference in the melt discharge velocity is approximately 15% and this variation is not expected to impact the melt discharge time and the particle break up in the coolant pool." Significantly larger variations in melt discharge velocity would be obtained if the radial location of the failed instrument tube is taken into consideration (see comment #I.3 above).

22. Page 31 of the report states that: "...However, to account for uncertainties in the rupture size, a hole size of 0.4 m has been assumed in the present study." Why was this done instead of following the recommendation of Pilch et al (reference 22 of the report)?
23. Page 31 of the report states: "...Scenario A represents an instrument tube penetration failure (0.3 m) while...". Should read 0.03 m instead of 0.3 m.
24. Page 35 of the report states: "...The IFCI computer code is used here mainly to assess the radial spreading...". See comment #I.1 above.
25. Page 36 of the report states: "...the axial mesh size was selected to be 0.25 m with a cross-sectional area of 0.2 m²." How sensitive are the results to the selected value of cross-sectional area? (See comment I.1, II.24 above).
26. Page 36 of the report states: "...The value of proportionality constant was considered conservative." See comments I.2, II.1 above.
27. Page 36 of the report states: "...The decay of the pressure wave (and thus the pressure impulse) were estimated to be directly proportional to the inverse of the radial distance from the center of the explosion...". While this may be true for spherical geometries, it is not necessarily the case here. Note also that for failures involving instrument tubes away from the vessel center line, the radial attenuation factor will be inappropriate. In addition, for such cases, a one-dimensional code will certainly be inadequate.
28. Page 37 of the report states: "...The explosion was triggered from this pre-mixing condition by specifying a pressure trigger threshold value of 0.22 MPa and ...". Where did the 0.22 MPa value come from? (See comment #II.14 above.)
29. Page 38 of the report states: "...Using the explosion zone radius, the predicted pressure impulse at the wall should have decayed by a factor of 3 (1.5/0.5) assuming a 1/r radial decay from the explosion zone. This value is close to the predicted value of 2.6 from the calculation." This discussion is clearly nonsensical in view of the difficulties encountered with the radial noding scheme for IFCI. If a finer radial mesh was possible the predicted radial penetration may have been much smaller than 0.5 m especially since very little melt has actually spread into the second radial zone (see Figure 9, page 40 of the report).
30. Page 43 of the report states: "...Given the radial spreading of the melt (radius of 1 m), and the radial distance to the carbide wall (1.5 m), it would be expected...". This discussion is clearly inappropriate given the coarse nature of the radial nodalization (see comment #II.29 above).

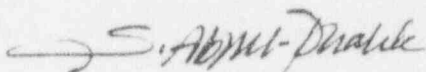
31. Figures 12, 13, and 14, pages 45, 46, and 47 of the report and all related discussion are not very enlightening. We know that the parameters used in the calculations were inappropriate.
32. Page 48 of the report states that: *"...In the TEXAS model, the mesh cross-sectional area was chosen to be $3m^2$ which was estimated based on the radial spreading of the melt from the IFCI calculation."* Given the coarse nature of the IFCI mesh, how appropriate is this cross-sectional area, and how sensitive are the results to the selected cross-sectional area?
33. Page 48 of the report states that: *"...In the TEXAS calculation, the premixing was simulated for 1 second and during this time, the melt would reach the cavity floor."* Why is 1 second still appropriate for this scenario, and how much would the results change if a shorter premixing time were used?
34. Page 48 of the report states that: *"...The maximum explosion pressure in the IFCI calculation with a fragmented particle size of 0.1 mm was observed to be close to TEXAS prediction (~70 MPa) before the calculation was terminated."* This statement is meaningless since the pressure value at the time the calculation was terminated may be significantly different than the predicted peak pressure had the entire transient been successfully modeled.
35. Page 52 of the report states that: *"...The explosion was triggered by specifying a pressure threshold value of 0.2 MPa..."*. Where did this value come from? (See comment #II.14 above).
36. Page 62 of the report states that: *"...Recall that the results of IFCI calculations with a fragmented particle diameter of 0.1 mm predicted a maximum pressure of approximately 90 MPa before the simulation was terminated."* There is no significance to the value of the pressure at the time the calculation was terminated. See comment #II.34 above.

III. CONCLUDING REMARKS

The above discussion identifies several major deficiencies and numerous errors and ambiguities in the modeling approach. Such deficiencies bring into question the validity of the analysis, results, and conclusions presented in the report.

I appreciate the opportunity to work with you. Please do not hesitate to call me if you have any questions.

Sincerely,

A handwritten signature in dark ink, appearing to read "S. I. Abdel-Khalik". The signature is fluid and cursive, with a long horizontal stroke extending to the left.

S. I. Abdel-Khalik

SLAK/bc

P.S. The reports will be returned to you after you have had an opportunity to review and discuss the comments presented above; please let me know if you want them returned sooner.



Department of Nuclear Engineering and Engineering Physics
University of Wisconsin

153 Engineering Research Building
1500 Johnson Drive
Madison, WI 53706-1687
Phone (608) 263-1646
Fax: (608) 262-6707

Dr. Mohsen Khatib-Rahbar
Energy Research, Inc.
P.O. Box 2034
Rockville, MD 20847

February 23, 1994

Dear Mohsen,

I have reviewed the draft report you sent me (ERI/NRC-94-201). Of course, I am familiar with ERI's work on ex-vessel FCI energetics and the CE System 80+ issue in particular. In general I think the report provides a good discussion of the CE 80+ design, the initial and boundary conditions used in the analysis, a description of the FCI models and a consistent discussion of the results. I do have specific comments on particular areas where the report can be strengthened in its analysis or discussion of the results. Let me detail each below.

[1] The analysis of KROTOS-26 with TEXAS and IFCI is encouraging. However, the initial conditions of the test were somewhat more complex than your staff interpreted and I wanted just to clarify a couple of points. First, the actual pouring time of the jet until the gas trigger is initiated is not precisely known, because of a malfunction of the crucible opening device. In the analysis a delay/mixing time of 1.5 seconds was assumed and I think the actual value is closer to 0.35 to 0.5 seconds. This will affect the mixing process and the associated explosion propagation. I have sent Dr. Esmaili Tang's thesis and the K-26 TEXAS-III input we have used to help in his analysis.

[2] The initial conditions and boundary conditions used in the analysis generally seem reasonable. However, I am unclear why the assumed pour size from a creep rupture was 0.4 meter. Surely, it is a bounding value, but it is not clear why it can expand to this large value within a few seconds from a creep rupture breach. Since the whole mixing process would occur in a few seconds, it seems the actual pour stream size ought to be near that of the initial failure size. The ERI report gives a good argument why this might be near 0.2 meter because of the spacing between the lower head penetrations. Thus, 0.2 meter seems more defensible to me and does not detract from the bounding nature of the calculation.

[3] For the dynamic water phase pressure propagation behavior, we have now gotten CTH to function for this problem and I would suggest ERI (and NRC) consider using it to compare to the hand-calculations used in the ERI report. The $1/r$ dependence used to reduce the pressure magnitude at the structural wall is an estimate for a point source of pressure in an infinite medium; thus it is an estimate that should be checked. An upper bound empirical estimate would be a line source of pressure in a cylindrical geometry where the pressure would decay as $\ln(\text{Router/Rinner})$. Both of these additional estimates should be considered especially when the impulse approaches the structural capability of the wall.

I will gladly answer any questions you may have about these points or other aspects of the report.

Sincerely,

A handwritten signature in cursive script, appearing to read 'Mike' or 'Michael'.

Michael Corradini

ATTACHMENT 2

Responses to Comments by Dr. Abdel-Khalik

I. Major Deficiencies in Modeling Approach

Comment I.1

Two computer codes, TEXAS and IFCI, have been used to estimate the dynamic pressures and the resulting impulsive loads on the containment cavity walls resulting from the interaction of core debris material relocating into the pre-existing reactor cavity water following core melt accidents. TEXAS is a one-dimensional code, whereas IFCI is two-dimensional. On page 35, the [draft] report states that, "...*The IFCI computer code is used here mainly to assess the radial spreading of the melt in the pool in order to determine the mesh cross-sectional area in the one-dimensional TEXAS calculations...*".

The [draft] report also states on page 15 that: "*IFCI also shows strong sensitivity to the nodalization of the computational domain. Increasing the radial resolution seems to be a major problem, i.e. numerical errors and unphysical results were observed for finer radial nodalization.*" Similar statements regarding the problems encountered with the radial resolution of the computational domain for IFCI were made at several other locations within the [draft] report. **This means that IFCI is being used to do the very thing which it is currently incapable of doing!** Given the fact that the problem at hand is clearly multi-dimensional, the validity of the one-dimensional TEXAS calculations is questionable especially since no attempts were made to examine the sensitivity of such calculations to the size of the mesh cross-sectional area.

Response I.1

In general, it should be recognized that given the current state-of-the-art, it is difficult to expect anything more than a prediction of the trends of explosive fuel-coolant interactions following severe accidents. Therefore, the present study was not intended to provide NRC with a definitive quantitative estimate of the ex-vessel steam explosion energetics for the CE System 80+ containment, rather, it was directed at providing a calculational method and/or framework for exploring the possible range of impulsive loads based on the current understanding of these complex phenomena.

IFCI computer code had been used to estimate the radial spreading of the melt jet corresponding to a single instrument tube penetration and the results were presented in the ERI/NRC 93-206 report. In that simulation, the computational domain was simulated as a cylindrical geometry with a height of 3 m and a radius of 0.5 m, and a fine nodalization was employed in the central inner nodes where the melt mostly resided (see Figures 3 and 4 in ERI/NRC 93-206). Even

though the radius of the computational domain was smaller than the distance to the corbel supports (1.5 m) and the cavity wall (3.7 m), this simulation was found to be adequate due to the much smaller size of the melt jet diameter (0.03 m) with respect to the computational domain diameter (1 m) in the simulation, i.e., increasing the radius of the computational domain would not strongly impact the radial spreading of the melt. For the case of larger melt jet diameter (0.4 m), the radial mesh radius was 0.25 m (6 uniform radial nodes) which was comparable to the radius of melt. Therefore, the IFCI calculations were found to be adequate as far as *estimating* the radial spreading of the melt and the mesh cross-sectional area for the TEXAS calculations were concerned.

Comment I.2

A comparison of TEXAS simulations with KROTOS-26 experiment was presented; a similar comparison with the KROTOS-21 experiment was presented in reference [13] of the report (ERI/NRC 93-206, August 1993). By assigning values of 0.001 and 2 ms to the empirical parameters C_{fr} and τ_{fr} in the TEXAS fragmentation model, the predicted maximum explosion pressures were matched with the experimental values. Aside from the details of such comparisons (more on that later) **the fact remains that while the code predictions for peak pressures can be forced to match the experimental data, the code does not adequately predict the corresponding impulse values (integral of the pressure-time history curve) as can be seen from Figure 3, page 14 of the [draft] report.** Given the fact that the impulsive loads, rather than peak pressures, are used as the main criteria for assessing the survivability of the corbel supports and cavity walls, it is not clear how such comparisons with experimental data can provide any confidence in the code's ability to model the problem at hand.

Response I.2

In the KROTOS-26 the melt delivery was incomplete. The analysis by Tang¹ indicated that the melt remained in the upper portion of the pool before the explosion was triggered and the premixing time was approximately 0.65 seconds. The values of C_{fr} and τ_{fr} were chosen to be 0.002 and 0.5 ms and the pressure pulse duration showed good agreement with the experimental data. In the KROTOS-26 simulation in the [draft] report, the premixing time was 1.5 seconds and during this time the melt penetrated all the way down towards the bottom of the pool. Therefore, our initial conditions at the end of premixing calculations (before the onset of explosion) were different from those of Tang. The section on the comparison the KROTOS experiments in the final report was expanded to include a discussion of the Tang's results and the rationale for the choice of the model parameters.

¹ J. Tang, "Modeling of the Complete Process of One-Dimensional Vapor Explosions," Ph.D. Dissertation, University of Wisconsin (1993).

Comment I.3

All the sensitivity calculations presented in the [draft] report, as well as those in the earlier report (ERI/NRC 93-206, August 1993), assume that the instrument tube failure (scenario A) or vessel rupture (scenario B) will take place at the center of the cavity. The impulse load on the corbel supports and cavity walls are then determined using $1/r$ scaling. Aside from the validity of such scaling (more on that later), the fact remains that for 1.17 m corium height in the 5.4 m diameter vessel (page 33 of the [draft] report), **all instrument tube connections at the bottom of the vessel will be submerged (see Figure 8 in the [draft] report)**. It is not clear why the instrument tube at the center of the vessel would be more likely to fail than any other instrument tube. Failure of an "outer" instrument tube may be equally likely. In that case, for the same set of parameters, a somewhat weaker explosions may result because of the lower initial melt velocity. However, the radial proximity of the failed tube to the corbel supports and cavity walls may produce significantly higher impulse loadings than a similar failure near the vessel center. Therefore, it appears that an extremely important variable, namely the radial location of the failure, has not been taken into account. Consideration of such a variable may alter the conclusions presented in the [draft] report regarding the potential impact of single instrument tube failures on the survivability of the corbel supports and cavity walls.

Response I.3

We have included a discussion related to the failure location of the penetration tube in the final report. If the outer instrument tubes fail (see Figure 8 in the [draft] report or Figure 6 in the final report), the loads on the corbel supports would be similar to the local impulse values, i.e., we would not expect any radial decay of the pressure and clearly some of the corbel supports in the vicinity of the instrument tube penetrations may experience higher loads.

II. Other Errors and Ambiguities

Comment II.1

Page ii of the [draft] report states that, "...For the CE System 80+ plant calculations, the model parameters are considered to be conservative". **There is no fundamental theoretical basis for the TEXAS fragmentation model.** Given the empirical nature for the model, the [draft] report correctly states (page 11) that, "...The experimentally determined values of the proportionality constant and fragmentation time obtained from the one-dimensional experiments does not automatically assure that these values would be universal (i.e. the effects of scale up to reactor conditions and multi-dimensionality effects cannot be addressed within the one-dimensional experimental framework)". This means that these parameters may be case specific, inasmuch as we simply do not know how these empirical constants will depend on the various problem variables. In other words, showing that a C_{fr} value of 0.0015 produces higher peak pressures

in KROTOS 21 and KROTOS 26 does not necessarily mean that it will produce conservative predictions for other experiments or for the real problem at hand.

Response II.1

The references to the model parameters as being conservative have been removed from the final report. However, it should be noted that the limited comparison of the code predictions of the recent experiments reveals that the fragmentation constants are not expected to underpredict the dynamic loads.

Comment II.2

Page ii of the [draft] report states that, "...The most important initial conditions for the present analysis are the melt mass, composition, and temperature in the lower head prior to vessel breach, the size of the vessel breach, the height of the water...". As stated in Part I.3 above, the radial location of the vessel breach may be considerably more important than some of the other parameters listed in the [draft] report.

Response II.2

See response I.3

Comment II.3

Page ii of the [draft] report states that, "...Given the structural fragility estimates provided by CE are acceptable, the probability of ex-vessel steam explosion-induced containment failure for CE are acceptable, the probability of ex-vessel steam explosion-induced containment failure for CE System 80+ is expected to be relatively small for all conditions examined for scenario A (failure of instrument tube penetration except cases involving failure of multiple instrument tube penetrations...". Clearly, this may not be the case depending on the radial location of the failure.

Response II.3

The discussions in section 6.1 of the final report have been changed to reflect this comment.

Comment II.4

Page iii of the [draft] report states the "[the report] is directed at providing a calculation method and/or framework for exploring the possible range of impulsive loads based on our current understanding of these complex phenomena". Given the fundamental concerns raised in Section

I above, clearly the calculational methods and framework presented in the [draft] report are inadequate and do not represent the current state of the art.

Response II.4

The reviewer did not explain his assertion that these codes do not characterize the current state-of-the-art. There are currently three computer code packages in the United States for steam explosion calculations; namely, IFCI, TEXAS, and PM-ALPHA/ESPROSE. Clearly, there are uncertainties associated with IFCI and TEXAS modeling of fragmentation kinetics, numerical difficulties (in the case of IFCI) and absence of multidimensional effects (i.e., TEXAS), which have been clearly discussed in the report. PM-ALPHA/ESPROSE also suffers from the same general shortcomings, i.e., parametric nature of the explosion model. An attempt to use PM-ALPHA/ESPROSE for the present assessment by Dr. H. Amarasooriya was unsuccessful (due to numerical and other difficulties).

Comment II.5

Equation (2) page 6 of the [draft] report describes the fragmentation model used in TEXAS. There is no fundamental theoretical basis for this equation; it should always be referred to as an empiricism.

Response II.5

We have not made any claim in the report as to fundamental theoretical basis for this equation. The explosion model in TEXAS is empirical (as stated in the report) just like any other fragmentation model in any other code presently available.

Comment II.6

Page 6 of the [draft] report states that for the TEXAS simulations, "*...In addition, the water pool conditions and initial vapor void fraction are also required*". What were the initial void fractions used in the calculations?

Response II.6

The initial vapor void fraction in the water pool was specified as 0 (only water), while in the vapor space above the pool, the vapor void fraction was specified as 1 (only vapor present).

Comment II.7

Page 9 of the [draft] report states that, "*...additional work is required to increase the level of confidence in the predictive capabilities of the IFCI computer code. On the other hand, the*

TEXAS model has produced relatively good agreement with the one-dimensional experimental data". Given the concerns raised above, it is clear that the predictive capabilities of the TEXAS code are equally questionable.

Response II.7

Based on the current comparison with the KROTOS experiments (see also response I.2 regarding Tang's analysis), we can conclude at this point that good agreement with the limited number of experiments have been achieved for TEXAS by the proper choice of the empirical constants in the TEXAS fragmentation model (see also response I.2). Validation studies of explosion model in the IFCI computer code are not yet available (at least to our knowledge).

Comment II.8

Page 9 of the [draft] report states that, "...*The maximum explosion pressures measured was approximately 25 MPa which caused significant damage to the upper water container and the level meter*". Examination of Figure 3, page 14 of the [draft] report reveals that the signals for the K1, K2 and K3 transducers were clearly "saturated", i.e. the actual peak pressures may have been significantly higher than 25 MPa.

Response II.8

This is recognized. An expanded discussion has been provided in the final report which should alleviate the reviewer's concern.

Comment II.9

Page 11 of the [draft] report states that, "...*Using these parameters, we were able to match the maximum explosion pressures determined experimentally...*". See comment II.8 above.

Response II.9

This statement has been modified in the final report. See also responses I.2 and II.8.

Comment II.10

Page 11 of the [draft] report states that, "...*With a higher proportionality constant of $C_{fr} = 0.0015$ the maximum explosion pressure of 50 MPa occurs at K5 pressure transducer which is approximately twice the value measured experimentally...*". See comment II.8 above.

Response II.10

The discussion on the KROTOS experiment has been expanded in the final report. See also responses I.2 and II.8.

Comment II.11

Page 12 of the [draft] report states that, "...a conservative value of 0.0015 would be chosen for the proportionality constant...". See comment II.1 above.

Response II.11

Any references to these values being conservative has been removed from the final report. See also responses I.2 and II.1.

Comment II.12

Figure 3, page 14 of the [draft] report. See comments I.2 and II.8 above.

Response II.12

See responses I.2 and II.8.

Comment II.13

Page 15 of the [draft] report states that, "...the detonation model in IFCI is purely parametric". The detonation model in TEXAS is also parametric. (See comment II.5 above).

Response II.13

See response II.5.

Comment II.14

Page 15 of the [draft] report states that, "...In the present simulation, the explosion process was initiated by assigning a pressure threshold value of 0.05 MPa and a fragmented debris size of 0.1 mm". Where did the 0.05 MPa value come from? Why were different values used in various calculations (see pages 37, 43 and 52 of the [draft] report where values of 0.22, 0.22 and 0.2 MPa are reported)?

Response II.14

The pressure threshold value in the current version of IFCI serves no purpose except to initiate the explosion. As mentioned in the report, if the pressure in a computational cells exceeds this value, the explosion is initiated by fragmenting the fuel drops to prescribed fine fragment sizes. These values are therefore arbitrary.

Comment II.15

Page 15 of the [draft] report states that, "...IFCI also shows strong sensitivity to nodalization...". See comment I.1 above.

Response II.15

We have mentioned this fact in the report. See also response I.1.

Comment II.16

Figure 5, page 16 of the [draft] report. See comment II.8 above.

Response II.16

The comparison of the IFCI simulation with the KROTOS-26 experimental data was removed from the final report due to difficulties in establishing the correct premixing conditions.

Comment II.17

Page 23 of the [draft] report states that, "...The delineation of the initial and boundary conditions involves the specifications of...". Failure location should be added to the items which need to be examined (see comment I.3 above).

Response II.17

We agree. See response I.3.

Comment II.18

Page 23 of the [draft] report states, "...In the present analysis, the containment pressure at the time of vessel breach is assumed to be 0.2 MPa". Why was this value selected instead of a bounding value (0.1 - 0.28 MPa)?

Response II.18

We do not expect the results to be very sensitive to this particular initial condition, therefore we chose an average value.

Comment II.19

Page 24 of the [draft] report states that, "...the potential for ex-vessel failure before lower-head failure is expected to be at least as high as in Surry...". How and why does the lower L/D in the CE System 80+ hot leg impact the potential for ex-vessel failure?

Response II.19

The higher the L/D value, the more difficult it is to expect establishment of counter-current natural circulation in the hot leg piping. Therefore, the smaller L/D of the CE System 80+ hot leg piping should facilitate the establishment of counter-current natural circulation that could potentially lead to temperature-induced creep rupture of the RCS pressure boundary, and eventual RCS depressurization prior to reactor lower head failure.

Comment II.20

Page 25 of the [draft] report states, "...Given the expected high failure probabilities in the hotleg/surge line for CE System 80+ (based on the comparison with Surry), in the present analysis the primary system is assumed to be depressurized at the time of vessel breach,...". While this may be true, the discussion presented in the [draft] report does not clearly support this assertion.

Response II.20

Specific comments would have been more useful. It should be noted that a comprehensive review of the state-of-the-art related to phenomena responsible for RCS depressurization is provided in the report. In addition, design-dependent differences and their impact on the progression of accidents were also documented. In the absence of any plant specific calculations, this is the most appropriate approach. In addition, we have performed sensitivity calculations with TEXAS using a higher primary system pressure (i.e., higher initial melt velocity) to assess the potential impact of the system pressure on steam explosion energetics.

Comment II.21

Page 30 of the [draft] report states, "...the difference in the melt discharge velocity is approximately 15% and this variation is not expected to impact the melt discharge time and the particle break up in the coolant pool". Significantly larger variations in melt discharge velocity

would be obtained if the radial location of the failed instrument tube is taken into consideration (see comment I.3 above).

Response II.21

It was estimated that the outer instrument tube penetrations are approximately 0.45 m above the central instrument tube penetration, and considering the melt would also accelerate by covering this distance, we would not expect larger variations in the melt discharge velocity.

Comment II.22

Page 31 of the [draft] report states that, "...However, to account for uncertainties in the rupture size, a hole size of 0.4 m has been assumed in the present study". Why was this done instead of following the recommendation of Pilch, et al. (reference 22 of the [draft] report)?

Response II.22

We have chosen to select this value given the lack of consensus regarding the size of the lower head failure. If a hot spot forms in the vicinity of the instrument tube penetrations where the distance between the penetrations is greater than 0.2 m (this is the minimum spacing), then the size of the rupture would scale with the size of hot spot (see Figure 8 in the [draft] report or Figure 6 in the final report). This value further bounds the resulting explosion pressures and removes the need for additional sensitivity studies. It should be noted that a failure size of 0.2 m would not alter the final conclusions. In fact, the failure of eight instrument tube penetrations leads to high enough impulsive loads that the likelihood of the failure becomes relatively high.

Comment II.23

Page 31 of the [draft] report states, "...Scenario A represents an instrument tube penetration failure (0.3 m) while...". Should read 0.03 m instead of 0.3 m.

Response II.23

We have corrected this typographical error.

Comment II.24

Page 35 of the [draft] report states, "...The IFCI computer code is used here mainly to assess the radial spreading...". See comment I.1 above.

Response II.24

See response I.1.

Comment II.25

Page 36 of the [draft] report states, "...the axial mesh size was selected to be 0.25 m with a cross-sectional area of 0.2 m²." How sensitive are the results to the selected value of cross-sectional area? (See comment I.1, II.24 above.)

Response II.25

The mesh cross-sectional area has some effects on the predicted explosion pressure and vapor void fractions. The two-dimensional IFCI computer code with finer nodalization near the melt jet (instrument tube penetration failure) was used to estimate the interaction zone which would alleviate the need to perform parametric area calculations. See also response I.1.

Comment II.26

Page 36 of the [draft] report states, "...The value of proportionally constant was considered conservative". See comments I.2, II.1 above.

Response II.26

See response II.1.

Comment II.27

Page 36 of the [draft] report states, "...The decay of the pressure wave (and thus the pressure impulse) were estimated to be directly proportional to the inverse of the radial distance from the center of the explosion...". While this may be true for spherical geometries, it is not necessarily the case here. Note also that for failures involving instrument tubes away from the vessel center line, the radial attenuation factor will be inappropriate. In addition, for such cases, a one-dimensional code will certainly be inadequate.

Response II.27

We agree. Strictly speaking, this 1/r behavior is true for a point source explosion in an infinite medium. The effects of confinement (the cavity wall is a finite distance from the center of the explosion) and proximity of the explosion zone to the free surface could impact the 1/r scaling. We have also included an expanded discussion on the recent results of Theofanous et al. [3] and Corradini (using the CTH computer code) where about ten-fold reduction in the peak explosion

pressures were observed at the wall in these limited calculations (see the final report). See also response I.3.

Comment II.28

Page 37 of the [draft] report states, "...*The explosion was triggered from this pre-mixing condition by specifying a pressure trigger threshold value of 0.22 MPa and ...*". Where did the 0.22 MPa value come from? (See comment II.14 above.)

Response II.28

See response II.14.

Comment II.29

Page 38 of the [draft] report states, "...*Using the explosion zone radius, the predicted pressure impulse at the wall should have decayed by a factor of 3 (1.5/0.5) assuming a 1/r radial decay from the explosion zone. This value is close to the predicted value of 2.6 from the calculation.*" This discussion is clearly nonsensical in view of the difficulties encountered with the radial nodding scheme for IFCI. If a finer radial mesh was possible the predicted radial penetration may have been much smaller than 0.5 m especially since very little melt has actually spread into the second radial zone (see Figure 9, page 40 of the [draft] report).

Response II.29

See response II.27.

Comment II.30

Page 43 of the [draft] report states, "...*Given the radial spreading of the melt (radius of 1 m), and the radial distance to the corbel wall (1.5 m), it would be expected...*". This discussion is clearly inappropriate given the coarse nature of the radial nodalization (see comment II.29 above).

Response II.30

See response II.27.

Comment II.31

Figures 12, 13 and 14, pages 45, 46 and 47 of the [draft] report and all related discussion are not very enlightening. We know that the parameters used in the calculations were inappropriate.

Response II.31

These figures are included in the report only to show the qualitative behavior of the explosion model in the IFCI code.

Comment II.32

Page 48 of the [draft] report states that, "...In the TEXAS model, the mesh cross-sectional area was chosen to be 3 m^2 which was estimated based on the radial spreading of the melt from the IFCI calculation". Given the coarse nature of the IFCI mesh, how appropriate is this cross-sectional area, and how sensitive are the results to the selected cross-sectional area?

Response II.32

See response I.1 and II.25.

Comment II.33

Page 48 of the [draft] report states that, "...In the TEXAS calculation, the premixing was simulated for 1 second and during this time, the melt would reach the cavity floor". Why is 1 second still appropriate for this scenario, and how much would the results change if a shorter premixing time were used?

Response II.33

This is the case of a large pour with a larger melt jet diameter (0.4 m) compared to the instrument tube penetration size (0.03 m). Therefore, as far as particle quenching is concerned, we do not anticipate much solidification of the particles. Reducing the premixing time may have some influence on the predicted void fraction and the resulting fragmentation during the propagation phase. However, the present results for this case clearly show that impulse loads are quite high.

Comment II.34

Page 48 of the [draft] report states that, "...The maximum explosion pressure in the IFCI calculation with a fragmented particle size of 0.1 mm was observed to be close to TEXAS prediction ($\sim 70 \text{ MPa}$) before the calculation was terminated". This statement is meaningless since the pressure value at the time the calculation was terminated may be significantly different than the predicted peak pressure has the entire transient been successfully modeled.

Response II.34

We agree that this statement is meaningless; it was not meant to provide the reader with any definitive numerical value for the explosion pressure. The purpose of this statement was for comparison purposes only, i.e., obviously the smaller fragment size particles produce much higher explosion pressures. We have removed this statement to avoid any unnecessary confusion on the part of the reader.

Comment II.35

Page 52 of the [draft] report states that, "...*The explosion was triggered by specifying a pressure threshold value of 0.2 MPa...*". Where did this value come from? (See comment II.14 above.)

Response II.35

See response II.14.

Comment II.36

Page 62 of the [draft] report states that, "...*Recall that the results of IFCI calculations with a fragmented particle diameter of 0.1 mm predicted a maximum pressure of approximately 90 MPa before the simulation was terminated*". There is no significance to the value of the pressure at the time the calculation was terminated. See comment II.34 above.

Response II.36

See response II.34

III. CONCLUDING REMARKS

Comment III.1

The above discussion identifies several major deficiencies and numerous errors and ambiguities in the modelling approach. Such deficiencies bring into question the validity of the analysis, results, and conclusions presented in the [draft] report.

Response III.1

We disagree with the reviewer's conclusions. Most of the so-called "deficiencies" that were alluded to, reflect lack of understanding of the fragmentation kinetics (during the propagation phase of the interaction). However, we agree with the reviewer that the IFCI multidimensional calculations were of limited use because of the numerical difficulties in some of the calculations.

Letter from M. Khatib-Rahbar to A. Behbahani
March 9, 1994

Page 27

Most of the calculations which encountered numerical difficulties are now deleted from the final report. The conclusion section in the final report has also been expanded to reflect the reviewer concerns.

ATTACHMENT 3

Responses to Comments by Dr. Corradini

Comment 1

The analysis of KROTOS-26 with TEXAS and IFCI is encouraging. However, the initial conditions of the test were somewhat more complex than your staff interpreted and I wanted just to clarify a couple of points. First, the actual pouring time of the jet until the gas trigger is initiated is not precisely known, because of a malfunction of the crucible opening device. In the analysis a delay/mixing time of 1.5 seconds was assumed and I think the actual value is closer to 0.35 to 0.5 seconds. This will affect the mixing process and the associated explosion propagation. I have sent Dr. Esmaili Tang's thesis and the K-26 TEXAS-III input we have used to help in his analysis.

Response 1

We have included a discussion of the Tang's results in the final report.

Comment 2

The initial conditions and boundary conditions used in the analysis generally seem reasonable. However, I am unclear why the assumed pour size from a creep rupture was 0.4 meter. Surely, it is a bounding value, but it is not clear why it can expand to this large value within a few seconds from a creep rupture breach. Since the whole mixing process would occur in a few seconds, it seems the actual pour stream size ought to be near that of the initial failure size. The ERI [draft] report gives a good argument why this might be near 0.2 meter because of the spacing between the lower head penetrations. Thus, 0.2 meter seems more defensible to me, and does not detract from the bounding nature of the calculation.

Response 2

We have chosen to select this value given the lack of consensus regarding the size of the lower head failure. If a hot spot forms in the vicinity of the instrument tube penetrations where the distance between the penetrations is greater than 0.2 m (this is the minimum spacing), then the size of the rupture would scale with the size of hot spot (see Figure 8 in the [draft] report or Figure 6 in the final report). This value further bounds the resulting explosion pressures and removes the need for additional sensitivity studies. It should be noted that a failure size of 0.2 m would not alter the final conclusions. In fact, the failure of eight instrument tube penetrations leads to high enough loads that the likelihood of the failure becomes relatively high.

Comment 3

For the dynamic water pressure propagation behavior, we have now gotten CTH to function for this problem, and I would suggest ERI (and NRC) consider using it to compare to the hand-calculations used in the ERI [draft] report. The $1/r$ dependence used to reduce the pressure magnitude at the structural wall is an estimate for a point source of pressure in an infinite medium; thus it is an estimate that should be checked. An upper bound empirical estimate would be a line source of pressure in a cylindrical geometry where the pressure would decay as $\ln(R_{\text{outer}}/R_{\text{inner}})$. Both of these additional estimates should be considered especially when the impulse approaches the structural capability of the wall.

Response 3.

We have removed the $1/r$ reduction in the point estimates of the impulse loads on the cavity wall from the final report. We have cited your CTH results as well as those by Theofanous et al. [3] as additional evidence of the pressure decay. However, our final results are based on the conservative reduction factor of 1.5-2.5 based on the IFCI calculations.